Aalto University
School of Engineering
Degree Programme in Mechanical Engineering

Mikko Haavisto

# Residual Stresses in Rotating Steel Cylinders with Composite Surface Layers

Thesis submitted in partial fulfillment of the requirements for the degree of Master of Science in Technology
Espoo, January 5, 2015

Supervisor: Professor Olli Saarela
Advisor: Mikko Kanerva D.Sc. (Tech.)

Aalto University
School of Engineering

Aalto University,
P.O. BOX 11000, 00076 AALTO
www.aalto.fi

**Abstract of master's thesis**

| | |
|---|---|
| **Author** | Mikko Haavisto |
| **Title of thesis** | Residual Stresses in Rotating Steel Cylinders with Composite Surface Layers |
| **Degree programme** | Mechanical Engineering |
| **Major** | Aeronautical Engineering |
| **Code of professorship** | Kul-34 |
| **Thesis supervisor** | Professor Olli Saarela |
| **Thesis advisor** | Mikko Kanerva D.Sc. (Tech.) |
| **Date** | 5.1.2015 |
| **Number of pages** | 71+4 |
| **Language** | English |

**Abstract**

After undergoing a manufacturing process, materials may exhibit internal stresses referred to as residual stresses. In steel-composite hybrid structures, residual stresses are typically formed due to the unequal thermal behaviour of the steel and composite. Thus, knowledge of the residual stress state is important in the assessment of the external-internal loading in steel-composite hybrid structures.

This thesis primarily focuses on estimating the criticality of the residual stress state in a paper machine roll structure consisting of a steel cylinder and glass fibre reinforced epoxy composite surface layers. Of special interest is evaluating the bond between the cylinder and surface layers with different surface layer edge geometries by studying stress and crack tip loading levels. A secondary aim is to provide an extensive overview of the physical background of residual stress formation and special characteristics of residual stress numerical simulations and related material modelling.

Numerical simulation models introduced in this study were employed to evaluate the residual stress state and its effects in the roll structure. The scope of the simulations was limited to thermal residual stresses during the cool-down phase. The emerging stress state was not found to be critical as regards the cohesive strength of surface layers. However, the bond between the cylinder and associated surface layer was evaluated as being critical in the event of an initial flaw. Thus, a crack in the bond edge may grow due to the loading induced by the residual stresses. Cylinder rotation was found to have no significant effect on the crack tip loading and a nip effect was shown not to increase the crack tip loading criticality near the nip contact area. Experimental methods could prove useful in creating more precise material models and improving simulation accuracy. In addition, the obtained simulation results for residual stress levels and crack tip loading could be validated experimentally.

**Keywords** residual stresses, steel cylinder, composite surface layers, finite element method, virtual crack closure technique, VCCT

Aalto-yliopisto
Insinööritieteiden
korkeakoulu

Aalto-yliopisto,
PL 11000, 00076 AALTO
www.aalto.fi

**Diplomityön tiivistelmä**

| | | |
|---|---|---|
| **Tekijä** Mikko Haavisto | | |
| **Työn nimi** Jäännösjännitykset komposiittipinnoitetuissa pyörivissä terästeloissa | | |
| **Koulutusohjelma** Konetekniikka | | |
| **Pääaine** Lentotekniikka | | **Professuurikoodi** Kul-34 |
| **Työn valvoja** Professori Olli Saarela | | |
| **Työn ohjaaja** Tekniikan tohtori Mikko Kanerva | | |
| **Päivämäärä** 5.1.2015 | **Sivumäärä** 71+4 | **Kieli** Englanti |

**Tiivistelmä**

Jäännösjännitykset ovat valmistusprosessin yhteydessä syntyviä materiaalin sisäisiä jännityksiä. Teräs-komposiitti-hybridirakenteissa jäännösjännityksiä muodostuu tyypillisesti materiaalien erilaisen lämpölaajenemisen johdosta. Jäännösjännitysten arviointi on välttämätöntä, jos teräs-komposiittirakenteiden kokonaiskuormittuminen halutaan arvioida tarkasti.

Tämän diplomityön päätavoitteena oli arvioida jäännösjännitysten kriittisyyttä paperikoneen telarakenteessa, joka koostuu lasikuidulla vahvistetusta epoksikomposiittipinnoitteesta ja terässylinteristä. Erityisesti komposiittikerrosten ja terässylinterin välistä liitosta haluttiin arvioida erilaisilla pinnoitteen reunageometrioilla tarkastelemalla jännitystasoja sekä mahdollisen särön kärjen kuormittumistasoja. Työn toisena tavoitteena oli tarjota laaja yleiskatsaus jäännösjännitysten muodostumisen fysikaalisiin perusteisiin ja jäännösjännitysten numeerisen simuloinnin sekä siihen liittyvän materiaalien mallintamisen erityispiirteisiin.

Tässä diplomityössä esitellään numeerisia simulaatiomalleja, joita käytettiin arvioimaan jäännösjännitysten tilaa ja vaikutuksia telarakenteessa. Simuloinnit rajattiin lämpöjäännösjännityksien analysointiin valmistuksen jäähtymisvaiheessa. Tulosten mukaan syntyvä jäännösjännitystila ei ollut kriittinen pinnoitteen lujuuden kannalta. Sylinterin ja pinnoitteen liitoksessa olevan mahdollisen särön kärjen energiatasot olivat kuitenkin tietyillä reunasärön pituuksilla kriittisiä. Liitoksen reunaan syntyvä särö saattaa siis kasvaa jäännösjännityskuormituksen johdosta. Sylinterin pyörimisen vaikutuksen todettiin olevan merkityksetön särön kärjen kuormittumisen kannalta ja nippivaikutuksen ei todettu kasvattavan särön kärjen kuormittumistason kriittisyyttä lähellä kontaktialuetta. Jatkossa voitaisiin luoda tarkempia materiaalimalleja parantamaan simulaatioiden tarkkuutta. Lisäksi saadut simulointitulokset jäännösjännitystasoista voitaisiin vahvistaa kokeellisesti.

**Avainsanat** jäännösjännitykset, terästela, komposiittipinnoite, elementtimenetelmä, virtuaalisen särön sulkemismenetelmä, VCCT

# Preface

This Master's Thesis was done in the Laboratory of Lightweight Structures at School of Engineering, Aalto University. The thesis was a part of HYBRIDS (Light Multifunctional Hybrid Structures) project funded by FIMECC (Finnish Metals and Engineering Competence Cluster).

I want to thank my supervisor, Professor Olli Saarela for the possibility to do the Thesis at the Laboratory and for the valuable comments and improvement proposals during the process. I am grateful to my instructor, D.Sc. Mikko Kanerva for the guidelines and all the help. I would also like to thank M.Sc. Jarno Jokinen for the help with the Abaqus-software, D.Sc. Heikki Kettunen from Valmet for providing valuable details about the roll structures and all my colleagues at the Laboratory for creating a good working environment.

Enormous thanks to my family and friends for all the support during my studies and when writing this Thesis. Finally, thank you Netta for always being patient and encouraging.

Espoo, January 5, 2015

Mikko Haavisto

# Nomenclature

## Abbreviations

| | |
|---|---|
| CHILE | Cure-hardening instantaneously linear-elastic |
| CME | Coefficient of moisture expansion |
| CPO | Cool-down phase only |
| CTE | Coefficient of thermal expansion |
| CVE | Coefficient of volumetric expansion |
| ECC | Entire cure cycle |
| FEM | Finite element method |
| RPM | Rounds per minute |
| SERR | Strain energy release rate |
| VCCT | Virtual crack closure technique |
| VE | Viscoelastic |

## List of Symbols

| | |
|---|---|
| $\alpha$ | Degree of cure |
| $\alpha_T$ | Shift factor |
| $\beta$ | Total volumetric shrinkage |
| $\varepsilon$ | Strain |
| $\kappa$ | Thermal conductivity |
| $\lambda_\omega$ | Discrete stress relaxation time |
| $\nu$ | Poisson's ratio |
| $\xi$ | Reduced times |
| $\rho$ | Density |
| $\sigma$ | Stress |
| $\tau$ | Time integration variable, shear stress |
| $\psi$ | Crack tip loading mode mixity |
| $\omega$ | Angular velocity |
| $A$ | Area, epoxy system constant |
| $c$ | Specific heat capacity |
| $C_p$ | Specific heat |
| $e$ | Internal energy per unit mass |
| $E$ | Young's modulus |
| $E'$ | Instantaneous elastic modulus |
| $\Delta E$ | Activation energy |
| $F$ | Centripetal force |

| | |
|---|---|
| $G$ | Shear modulus, strain energy release rate |
| $H$ | Cure reaction heat generation |
| $K$ | Cure evolution constant, stress intensity factor |
| $m$ | Mass |
| $P$ | Balancing forces |
| $q$ | Heat flux vector |
| $Q$ | Instantaneous heat generation |
| $r$ | Heat supply rate, radius from rotational axis |
| $R$ | Universal gas constant |
| $t$ | Thickness, time |
| $t'$ | Time integration variable |
| $T$ | Temperature |
| $V$ | Volume |
| $W_\omega$ | Weight factor |
| $x$ | Coordinates |

## Subscripts and superscripts

| | |
|---|---|
| $\theta, r, x, y, z$ | Coordinate direction |
| $\infty$ | Fully relaxed |
| 0 | Room temperature, initial value |
| $I, II, III$ | Fracture mode |
| $c$ | Composite, critical |
| $f$ | Final |
| $g$ | Glass transition |
| $i, j$ | Index / tensor components |
| $P$ | Balancing force |
| $R$ | Total |
| $ref$ | Reference value |
| $s$ | Chemical |
| $tc$ | Thermochemical |
| $T$ | Total value, top, thermal |
| $u$ | Unrelaxed modulus |

# Contents

# 1 Introduction

Formation of residual stresses is a manufacturing process related problem area that has received increasing attention during past decades. This type of stress is an internal stress formed during the manufacturing process of a structure due to the unequal properties of the material system constituents. These stresses are typical in composite structures and in steel-composite hybrid structures. It is imperative to know the residual stress formation in these structures in order to accurately assess the total loading due to external and internal loads. Furthermore, the residual stress magnitudes arising may influence the service life and usability of these structures. Therefore, a significant effort has been directed to evaluate the emerging residual stress state using experimental and computational methods. However, additional studies are needed to further improve the understanding of the factors behind residual stress formation and the influence of residual stresses in real-life structures, such as paper machine rolls.

The main object of this thesis is to determine the criticality and parametric sensitivity of the residual stress state after the manufacturing process in a paper machine roll structure. The roll structure is a steel-composite hybrid structure which consists of a steel cylinder with glass fibre reinforced epoxy surface layers. In addition, the loading of the bond between the cylinder and surface layers is investigated with different material parameters, surface edge parameters and after adding cylinder rotation and the nip effect. The loading state of the bond is evaluated based on the residual stresses and crack tip loading. A secondary aim is to extensively present the physical background of residual stresses, as well as special characteristics of residual stress numerical simulations and related material modelling.

This study introduces numerical finite element simulation models, which can be applied to evaluate the residual stress state and bond line loading in the roll structure. The scope of the simulations is limited only to linear thermal stresses forming during the cool-down phase of the manufacturing process. Linear-elastic temperature-independent material models are used in the simulations.

The remaining part of this thesis is divided into six chapters. Chapter 2 presents the physical background of residual stress formation in fibre-reinforced epoxy composite materials and steel-composite hybrid material systems. The essential parameters of stress formation are also introduced. Chapter 3 describes typical material models for epoxy resin and composite materials in residual stress studies. Chapter 4 introduces the special characteristics of finite element method simulations of residual stress formation and shows residual stress simulation results for two cylinder structures. Chapters 5 and 6 form the computational part of this thesis presenting and discussing the created simulation models and results obtained. Chapter 7 presents conclusions and propositions for future research.

# 2 Residual stresses

Stresses in a material system can be categorised into stresses due to external loads and residual stresses. Residual stresses are internal stresses formed during the manufacturing process of the material system. These stresses can be further divided into the stresses arising from unequal shrinkage or expansion of the materials and into the stresses arising from local plastic or viscoelastic deformations. Residual stresses caused by unequal shrinkage or expansion can be further divided into thermal stresses, hygroscopic stresses and curing stresses. [1] This stress classification is presented in Figure 2.1.

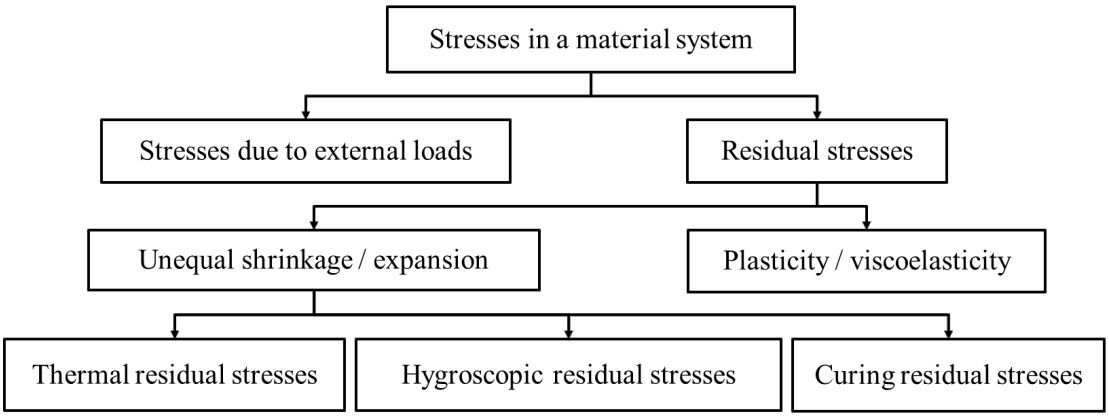


***Figure 2.1:*** *Stresses in a material system can be classified into stresses due to external loads and residual stresses. Latter can be divided into two groups according to the cause: unequal shrinkage (expansion) or plasticity (viscoelasticity). Thermal stresses, hygroscopic stresses and curing stresses are due to the unequal shrinkage (expansion). [1]*

Gradients in temperature or moisture content in a homogeneous material can cause unequal and restrained volume changes, causing thermal and hygroscopic residual stresses. For heterogeneous material systems, for example composites, this phenomenon can occur also without gradients due to different expansion coefficients of the constituent materials. [1] Composite materials are typically made of polymer matrix and reinforcing fibres of glass or carbon. The matrix and fibre materials have typically significantly different coefficients of thermal expansion (CTE) and coefficients of moisture expansion (CME). Thermal expansion coefficients are usually unequal also in hybrid material systems, where e.g. steel and composite constituents are joined together.

In addition to aforementioned stresses induced by different expansion, also chemical shrinkage and non-uniform curing during composite manufacturing process cause residual stresses, named as curing residual stresses. The polymer matrix

material typically undergoes chemical shrinkage during the polymerization reaction of curing. This volume change is restrained after the reinforcing fibres have bonded to the matrix and curing residual stresses are formed. Non-uniform curing is present for example during the manufacture of thick composite parts, as the surfaces have already cured when the centre plies are still curing. This prevents unconstrained shrinkage and causes curing residual stresses. [2]

The three main sources of unequal shrinkage and expansion causing residual stresses are thus differences in temperature, changes in moisture content and chemical reactions. These lead to thermal residual stresses, hygroscopic residual stresses and curing residual stresses, respectively. [1]

## 2.1 Thermal residual stresses

Thermal residual stresses in composites and hybrid material systems are formed due to the different thermal expansion (or contraction) of the constituent materials when the structure undergoes a temperature change. The residual stresses forming during the cool-down stage of the manufacturing process of composites are typically significant and should be included in a stress analysis. [1]

As a material is heated, the internal energy of the material increases and thus the average motion of the material particles increases and the particles maintain larger average separation. This will lead to an increase in the material volume. If the deformation of a material is unrestrained (free), no stresses are formed. However, when two dissimilar materials are joined together, as in composites or hybrid material systems, free deformation is prevented and stresses are formed under a temperature change. Deformations are also restrained when a composite part is manufactured inside a mould, as interactions between the mould and the composite part restrain free shrinkage and expansion. Thermal residual stresses can also be formed inside a homogeneous material if a temperature gradient, i.e. a non-uniform distribution of temperature, exists.

The effect of different coefficients of thermal expansion inside a material system can be studied with a simple example including two homogeneous solid materials, marked as 1 and 2, under a temperature change $\Delta T$. Temperature change $\Delta T$ is the difference between the examined temperature and reference temperature. Now $\Delta T > 0$, describing an increase in the temperature. The thermal expansion coefficients for the materials are $CTE_1$ and $CTE_2$. Now $CTE_1$ and $CTE_2$ are positive and in addition $CTE_1 > CTE_2$. Let us assume that material 2 has significantly larger thickness than the material 1, $t_2 \gg t_1$, as shown in Figure 2.2 (a), and that bending effect is negligible. Material Young's moduli, denoted as $E_1$ and $E_2$, are unequal and materials are perfectly bonded together. Thus, the strain after the temperature change in the x-direction, $\varepsilon_x$, is constant through the thickness (y-coordinate direction), as shown in Figure 2.2 (b). If the materials would not be bonded, material 1 would expand more in the x-coordinate direction than material 2 due to the CTE-mismatch. However, as the materials are joined together, this free expansion is prevented, and deformations in the thin layer of material 1 are equal to the deformations in material 2. Thus, after the temperature

change material 2 is still practically stress-free, whereas material 1 experiences a negative stress (compression) in the x-direction. Assuming Hooke's law the stress $\sigma_x$ in material 1 is:

$$\sigma_{x,1} = -\Delta T \cdot (CTE_2 - CTE_1) \cdot E_1. \tag{2.1}$$

A stress discontinuity exists at the interface between these two materials, as material 1 is under compression and material 2 is practically stress-free. The stress state is presented in Figure 2.2 (c).

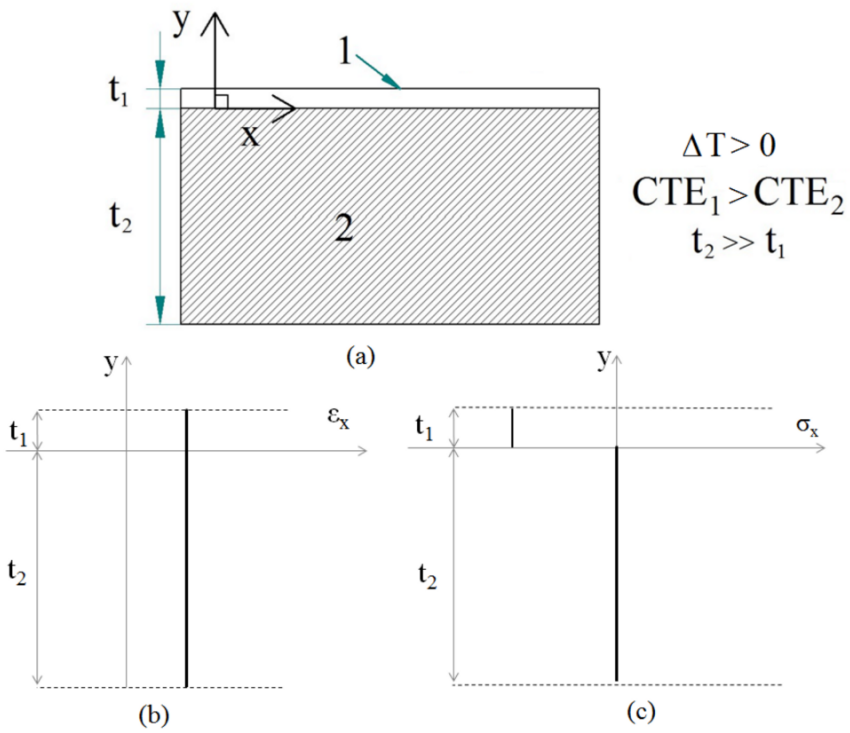


***Figure 2.2:*** *(a) Schematic example of two perfectly bonded homogeneous materials with different coefficients of thermal expansion (CTE) and significantly different thicknesses (t) under a temperature increase $\Delta T$. (b) The strain ($\varepsilon_x$) is continuous through the thickness direction. (c) However, there exists a discontinuity in the stress distribution ($\sigma_x$) through the thickness, as material 1 is under compression and material 2 is practically stress-free.*

In reality, materials go through deformations. Let us now assume that thicknesses are equal, $t_1 = t_2$. If the system is otherwise similar to the previously presented, bending will occur, as shown in Figure 2.3 (a). The bending will cause variation in strain and stress values through the material thickness. Again, the strain component in the x-coordinate direction ($\varepsilon_x$) is continuous through the interface, as the materials are joined together, see Figure 2.3 (b). The Euler beam theory can be applied to connect the deformation (strain) and the residual stress state. The stress state is discontinuous, as schematically presented in Figure 2.3 (c), because material 1 is under compression and material 2 under tension.

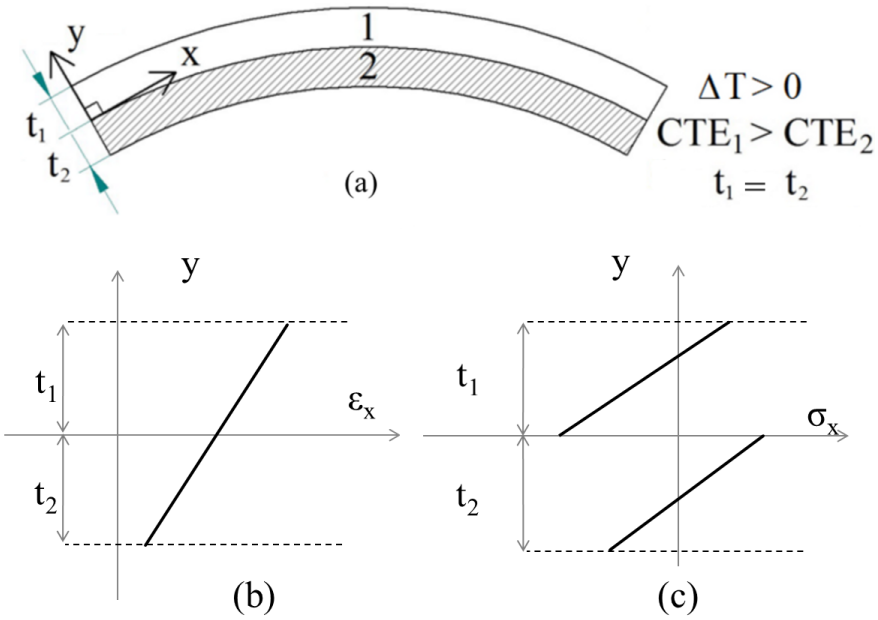


***Figure 2.3:*** *(a) Example of two homogeneous materials with different coefficients of thermal expansion (CTE) and same thicknesses (t) under a temperature increase $\Delta T$. (b) The strain ($\varepsilon_x$) is continuous through the thickness direction. (c) However, there exists a clear discontinuity in the stress ($\sigma_x$) through the thickness, as material 1 near the interface is under compression and material 2 under tension. In addition, the strain ($\varepsilon_x$) and stress ($\sigma_x$) change linearly through the thickness since bending is present.*

In fibre-matrix composites, the matrix material has typically significantly larger thermal expansion coefficient compared to the fibre material. Due to this, the (free) volumetric shrinkage in the matrix material is larger than in the fibre, if a temperature *decrease* for an unbonded system during the manufacturing process is examined. However, as the matrix and fibre are bonded together, the larger deformation of matrix is restrained by the stiffer fibre, and compressive thermal residual stresses are formed in the longitudinal direction of the fibre. Vice versa, tensional thermal residual stresses are formed in the longitudinal direction of the matrix. [2–5] This behaviour for bonded and unbonded systems is presented in Figure 2.4. The residual thermal stresses in the fibre direction are considerably greater than in the transversal direction, because fibres significantly restrain the free movement of matrix in the longitudinal fibre direction but not so much in the transversal direction. [6]

The magnitude of thermal residual stresses depends on the temperature change magnitude $\Delta T$ and difference between thermal expansion coefficients of the materials (and the magnitude of temperature gradient, if present). The temperature change refers to the difference between the so-called zero-stress temperature (or reference temperature) and the temperature of examination. The zero-stress temperature is the temperature, where the stress-free material constituents are bonded together. If only thermal residual stresses are considered, this zero-stress temper-

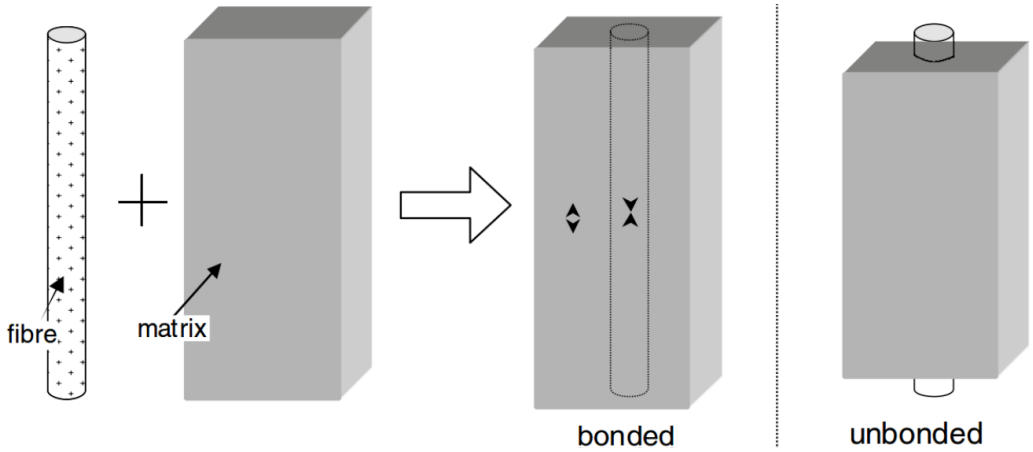


***Figure 2.4:*** *Behaviour of a single fibre and matrix material block in bonded and unbonded cases under a temperature decrease causing material shrinkage. In the bonded case tensional stresses are formed in matrix and compressive stresses are formed in the fibre, as shown with arrow heads. In the unbonded case no stresses are formed as volumetric changes are not restrained. Modified from the reference [7].*

ature for composites is usually close to the maximum temperature during the cure process. Cure process maximum temperature inside a composite consists of the external process temperature added with a possible internal temperature rise due to the exothermic resin cure reaction [8]. Cure process temperatures for composites with epoxy resins can be relatively high, between 115 °C and 250 °C [9, 10]. Thereby, a typical service temperature of 20 °C leads to a temperature difference $\Delta T$ = 95–230 °C. However, some epoxy systems are cured in a room temperature, in which case the temperature difference becomes much smaller, since the exothermic curing reaction is the main source of the temperature difference.

The thermal expansion coefficient for a fully cured epoxy polymer can be at least ten times larger than for a glass fibre. For example, the thermal expansion coefficient for an epoxy resin system Araldite LY5052/Hardener HY5052 is $71 \cdot 10^{-6}1/°C$ [11] whereas for pure E-glass fibre the value is $4.9 \cdot 10^{-6}1/°C$ [12]. The fibres dominate composite ply expansion behaviour in the longitudinal direction and the resin in the transverse direction. For a ply with Hexcel 7781-127 E-glass fibres with fibre volume fraction of 49% and epoxy system Araldite LY5052/Hardener HY5052 the thermal expansion coefficient in the longitudinal direction is $7.2 \cdot 10^{-6}1/°C$ and in the transverse direction $50.7 \cdot 10^{-6}1/°C$ [13]. Composite laminate values are dependent on ply CTE values and ply orientations. In hybrid material systems composites and metal layers are often bonded together. Metals can be considered as isotropic materials, and for example CTE for AISI 302 steel is $11 \cdot 10^{-6}1/°C$ [14].

Temperature gradients in a material during the cure will cause unequal solidification of the matrix and gradients after the cure will cause unequal thermal expansion or contraction. Especially during manufacturing of thick laminates, temperature gradients may become significant. The effects of these gradients are

studied with curing residual stresses (Chapter 2.3), as they are closely related to matrix cure process.

The fibre material properties remain approximately constant over a typical composite structure manufacture and operation temperature range. This is true also for steel and many other metal alloys. For a fully cured thermoset polymer matrix, material properties change significantly when temperature is changed around the glass transition temperature, $T_g$. Glass transition temperature is the temperature where the polymer matrix transforms from glassy, solid material into rubbery material, as temperature is increased. The volumetric change of thermoset polymer matrix around $T_g$ is presented on left in Figure 2.5. The coefficient of volumetric expansion (CVE) changes significantly around $T_g$, but has approximately constant value before and after the transition, as presented in the middle in Figure 2.5. Polymer stiffness decreases significantly after the glass transition, as presented for shear modulus $G$ on right in Figure 2.5. [15]

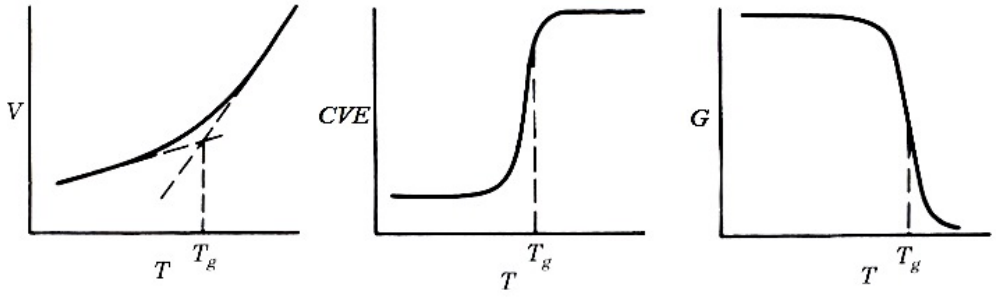


***Figure 2.5:*** *Change in thermoset polymer matrix properties as a function of temperature around $T_g$. On the left, the volumetric change is shown. In the middle the significant change in the coefficient of volumetric expansion (CVE) around $T_g$ is shown. On the right, shear modulus (G) is shown to change around $T_g$, indicating polymer stiffness change. Modified from the reference [15].*

## 2.2 Hygroscopic residual stresses

Hygroscopic residual stresses are formed due to the unequal expansion of the material system constituents as moisture is absorbed, analogous situation compared to the thermal residual stresses formation. However, effects of hygroscopic stresses should be studied more cautiously, as moisture equilibrium is reached much slower than temperature equilibrium. Thus, moisture gradients can be present more likely compared to temperature gradients. Considering the material properties, it has been noted that the modulus of the elasticity for a polymer matrix material usually decreases as moisture is absorbed. [1]

Hygroscopic absorption is generally rather slow and no significant amount of moisture is absorbed in the typical manufacturing and service environments. Thus, hygroscopic residual stresses are usually neglected. Exceptions are structures used in very moist conditions for a long time.

## 2.3 Curing residual stresses

Curing shrinkage is defined as the volume change (decrease) of a composite part during the cure. Depending on the manufacturing method, curing shrinkage may consist of chemical shrinkage of the resin, resin flow out of the composite part and/or compaction of the reinforcing fibres under a cure cycle pressure. Resin curing is a process where monomers or prepolymers form polymers (polymerization) and later these polymers link to each other (cross-linking), forming a solid matrix material with a smaller volume. This resin volume decrease during the cure is called chemical shrinkage. [16] Reinforcing fibres restrain the volume changes especially after the matrix has bonded with fibres and in some cases also the interaction between mould surface and part causes deformation constraints. Curing residual stresses are formed due to these restrains.

### 2.3.1 Physical background of curing

Large polymers are formed from monomers in the polymerization process during the cure process. Thermoset epoxy polymers undergo a step-wise polymerization process, where polymers can be formed from prepolymers (monomers or systems of monomers with intermediate molecular weight) with the help of a curing agent to catalyst the process in a room temperature or in an elevated temperature. The situation before the start of the cure reaction including prepolymer and curing agent is presented in Figure 2.6 (A). The molecular size of the components increase during the curing process as molecules first form chains and then grow linearly through branching, as shown in Figure 2.6 (B). Formed molecular chains further cross-link with each other. Figure 2.6 (C) shows gelation (gel point), which is the moment when the first continuous three-dimensional molecular network is formed. Eventually full cure is reached, cross-linking ends and material has vitrified, as presented in Figure 2.6 (D). [17, 18]

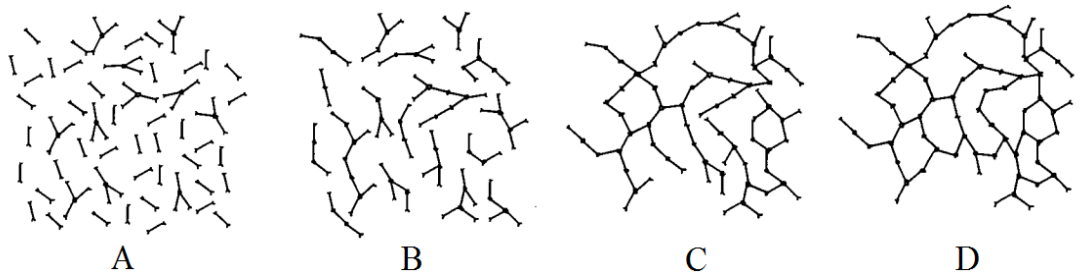


***Figure 2.6:*** *A step-wise polymerization cure reaction. A: prepolymers and curing agent before the reaction starts. B: The cure reaction has started and molecular size is increasing as molecules form chains and grow through branching. C: First continuous molecular network is created, denoted as gelation or gel point. D: Cure process has ended as cross-linking has stopped and material has vitrified. [19]*

In the initial part of the curing process, uncured resin behaves as a viscous fluid. The monomer molecules can be described as separate chemical entities, which each

take a unit volume, as shown in Figure 2.7 on the left. The size of this unit volume is governed by Van der Waals volume and the thermal energy of the molecule. [20] After polymerization the previously separate monomers are constrained together into tightly packed polymers, as thermal energy storage degrees of freedom are reduced, as shown in Figure 2.7 on the right. In addition, the bonds between molecules are transformed from Van der Waals bonds into shorter but stronger covalent bonds. The resin volume decreases, denoted as chemical shrinkage. [8, 17, 21]

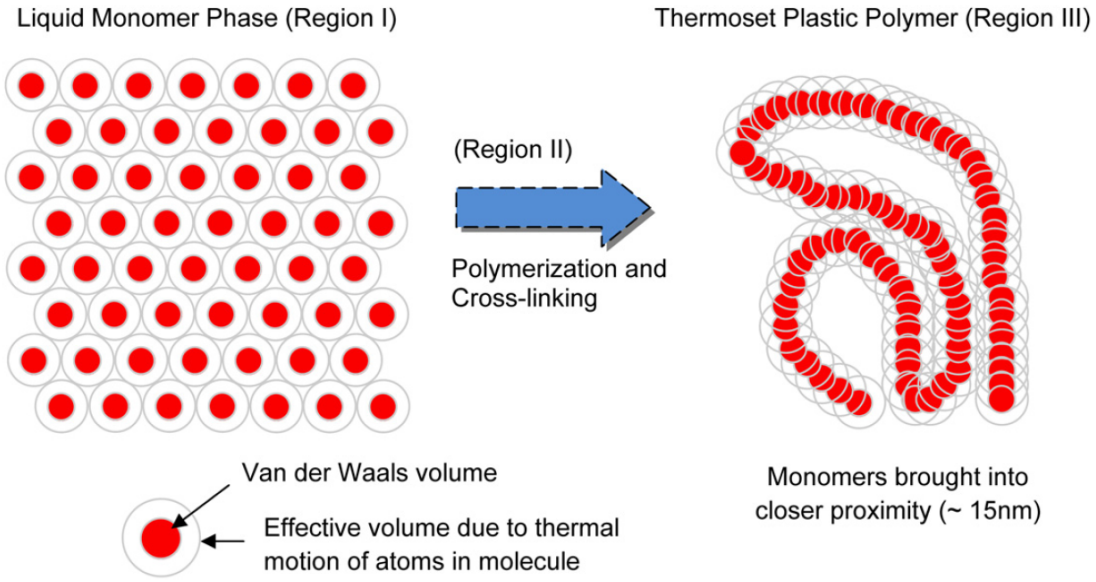


***Figure 2.7:*** *On the left: liquid monomer molecules before curing process, occupying separate effective volumes. On the right: Tightly packed monomers forming polymers with shorter covalent bonds, decreasing the resin volume. As a result, chemical shrinkage is observed. [17]*

Volumetric changes during epoxy resin curing process are schematically presented in Figure 2.8, taking into account thermal expansion/shrinkage and chemical shrinkage. First, the resin volume increases due to thermal expansion when temperature is increased from reference (room) temperature $T_0$ to the curing temperature $T_{cure}$ (stage a–b). No chemical shrinkage occurs during this stage, because curing has not started. The volume decreases due to the chemical shrinkage when a constant cure temperature $T_{cure}$ is reached (stage b–c). After resin has cured, the temperature is decreased towards reference temperature and resin volume decreases due to this temperature decrease. The thermal expansion coefficient of the epoxy changes (decreases) significantly around the glass transition temperature $T_g$ (point d), as previously presented in Figure 2.5. Finally, when the reference (room) temperature is reached again, an external shrinkage in the resin volume can be observed (volume difference between points a and e). However, the volumetric shrinkage between points a and e does not equal the total chemical shrinkage (change between b and c), as the resin thermal expansion behaviour has changed during the cure process. [22]

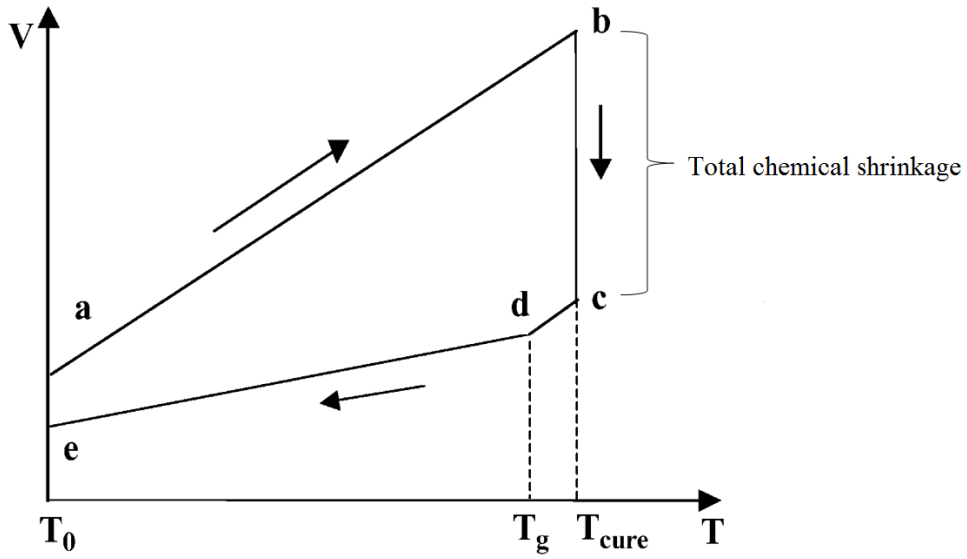


***Figure 2.8:*** *Volumetric changes of epoxy resin during the cure process. First, volume increases as temperature is increased (a–b). Then, due to the chemical shrinkage during curing the resin volume decreases (b–c). After resin has cured, temperature is decreased and also volume decreases (c–d). At the glass transition temperature $T_g$ the resin CTE value changes significantly (d). Resin volume decreases as temperature is further decreased (d–e). The difference in the final and initial resin volume (points a and e) does not equal the total chemical shrinkage due to property changes during the cure process. Modified from the reference [22].*

The magnitude of the chemical shrinkage depends on the material, but for example the following values have been reported: epoxy resins 1–6.9% [23], unsaturated polyester resins 6–9% and urethane methacrylates 10–12.5% [21]. The shrinkage in a unidirectional composite ply is restricted by the non-reacting fibres, and due to this the shrinkage strain in the transverse direction is larger than in the longitudinal direction. Curing residual stresses are formed due to these restrictions. To counteract the shrinkage, thermoplastic polymers or inorganic fillers may be added. These additives either do not react during curing, holding their original volume, or they expand due to the exothermic process. [21]

The evolution of the curing process is often described with a parameter called degree of cure, $\alpha$. The degree of cure is defined as [24]:

$$\alpha = \frac{H}{H_R} \tag{2.2}$$

where $H$ is the heat generated up to the time $t$ and $H_R$ is the total amount of heat generated during the whole reaction (up to the total time $t_f$). $H$ and $H_R$ can be further defined as [24]:

$$H = \int_0^t \frac{dQ}{dt} dt \quad \text{and} \quad H_R = \int_0^{t_f} \frac{dQ}{dt} dt \tag{2.3}$$

where $dQ/dt$ is the heat generation rate of the reaction and $t$ is the time. In the beginning of the cure, the process is controlled by the chemical reactivity of the functional groups, but after gelation the diffusion of these groups inside the polymer network starts to control the process [25].

Typical autoclave cure cycle for a composite part with epoxy resin is presented in Figure 2.9. In Figure 2.9, the autoclave temperature, composite part temperature, resin instantaneous glass transition temperature and resin degree of cure are presented as a function of time. The cure cycle can be divided into three phases, denoted as I, II and III. During the phase I, resin behaves as viscous fluid, it is unable to support shear loads and due to this internal stresses are not formed. During the phase II, after gelation but before vitrification, resin behaviour is viscoelastic. Some of the stresses formed during this phase relax, but this phase is important concerning the final residual stress state. During the phase III, after vitrification, resin behaviour can be described elastic. [8]

Figure 2.9 shows that the composite part temperature follows autoclave temperature with a small lag. The exothermic cure reaction evolves rapidly in the beginning of the second temperature hold period and the part temperature rises over the autoclave temperature. Gelation occurs at the point A, at a certain degree of cure. Vitrification happens later at the point B, when the instantaneous glass transition temperature of the resin reaches the part temperature. The degree of cure does not change significantly after vitrification. As the cure process proceeds, the elastic modulus and viscosity of the resin material increase. The autoclave temperature is decreased in the end of the cycle as the composite part is wanted to cool-down to room temperature. Typically a pressure is also applied through the autoclave cycle — its magnitude depends on the materials and manufacturing method in question. [8]

### 2.3.2 Generalized effects of curing residual stresses

Cure shrinkage strains increase with the degree of cure and residual stresses in a fibre-reinforced composite accumulate as the transition from liquid to glassy state proceeds. This is due to the interaction between fibres and the resin: Resin is not adhered to the fibres in the beginning of the cure process. No significant stresses are typically formed as cure shrinkage happens in matrix at this stage. [6] As the cure process proceeds, resin adheres to the fibres and the load due to the curing shrinkage is transferred to the fibres. Thus, especially the events after the gel point, when matrix is adhered to the fibres, greatly affect residual stress development. [26, 27]

Significant stress relaxation happens during the curing process, as matrix changes from liquid to solid state. Stress relaxation means that the formed stresses may relieve in partly cured matrix under a high temperature as some of the matrix is still in liquid form and deformation is not restrained. Due to this, ignoring the stress relaxation during the curing will lead to too large curing stress estimates. The amount of stress relaxation is hard to determine. Thus, two methods have been created for assessing the emerging curing stress state: it can be assumed that the relaxation stops after certain degree of cure (gelation) or it can be assumed

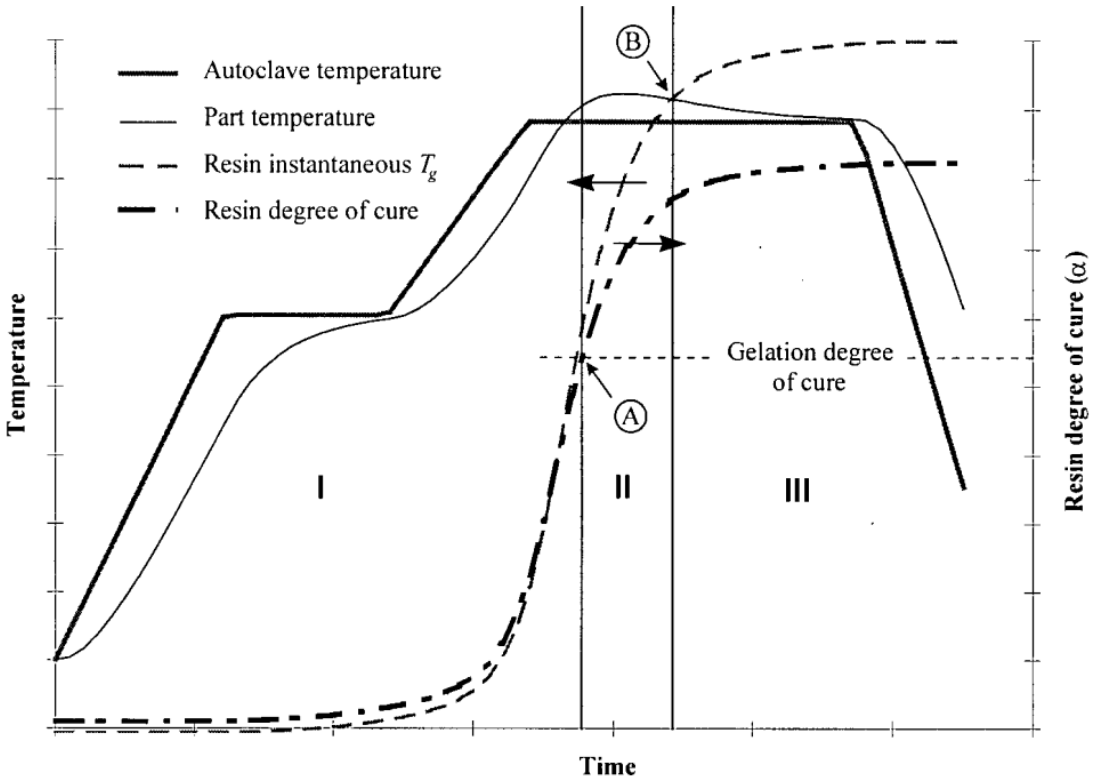


***Figure 2.9:*** *Typical autoclave cure process of a composite part with epoxy resin. Autoclave temperature, part temperature, resin instantaneous glass transition temperature and resin degree of cure are presented as a function of time. Resin properties can be divided into three phases during the process: in phase I resin is viscous liquid, in phase II viscoelastic and in phase III elastic solid. Autoclave temperature profile has two holding steps, and part temperature follows the same profile with a small lag. Due to the exothermic cure process the part temperature rises momentarily higher than the autoclave temperature. Glass transition temperature evolves during the process, and vitrification happens when glass transition temperature equals to the part temperature (point B). Gelation happens earlier at a certain degree of cure (point A). Modified from the reference [8].*

that the forming curing stresses are negligible compared to other forms of residual stresses and to stresses due to external loads. [1] Studies done with bi-material strip specimens have shown that the thermal residual stresses in the room temperature after cool-down have been notably larger than the curing residual stresses [14, 28]. However, a study for a cross-ply laminate with a lay-up $[0_4/90_4]$ showed, that curing residual stresses were notable compared to the thermal residual stresses formed during the cool-down phase, and should not be ignored in analysis [29]. Thus it may be proposed, that the proportional magnitude of curing stresses is case-dependent, and no general conclusion of the negligibility can be done.

Yu et al. [1] investigated the stress-free temperature of bi-material strips after curing by heating the strip again from the service temperature towards curing temperature and by observing when deformations vanish. They found out that

the stress-free temperature was slightly higher than the initial curing temperature, indicating that reheating slightly increased the degree of cure. Curing residual stresses and the increase in degree of cure after reheating can be included in thermal residual stress analyses by using this experimentally defined stress-free temperature as the curing temperature when determining the temperature difference. [1] Post-curing may cause additional curing residual stresses due to further shrinkage and loss of volatiles or moisture [6].

In thick laminates, it is likely that temperature and also degree of cure gradients are present. As the temperature is brought outside the laminate and the thermal conduction of the materials is comparatively low, areas near the surfaces of laminates have higher temperature than inside the laminate. Consequently, the top and bottom parts of the composite cure and solidify before the centre area. When the centre area starts to cure and shrink, solid outer layers restrain the shrinkage, and compressive curing residual stresses are formed in the outer layers and tensile curing residual stresses in the inner layers. Often the distribution of these stresses through the thickness of the laminate is parabolic, as presented in Figure 2.10. [30, 31]

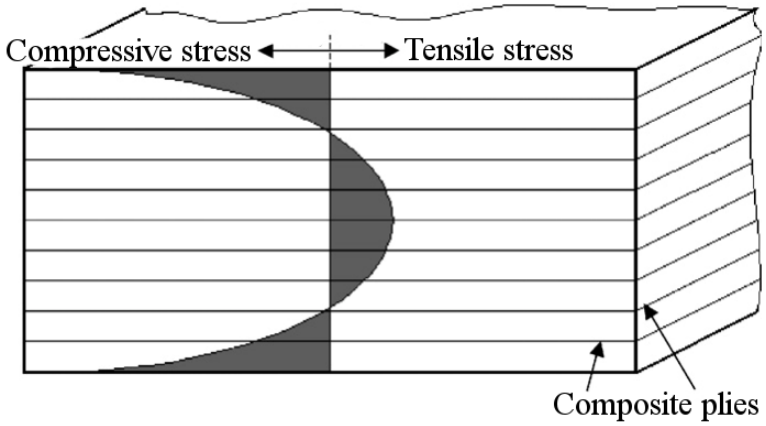


***Figure 2.10:*** *Formation of chemical residual stresses in a thick laminate, as the outer layers of the laminate cure before the inner layers. Thus, solid outer layers prevent the shrinkage of the inner layers as they shrink during the cure. As a result, compressive curing residual stresses are formed in the outer plies and tensile curing residual stresses in the inner plies. [32]*

Above, mainly factors related to chemical shrinkage and chemical residual stresses have been studied. Resin flow effects, compaction and part-tool interaction also induce curing residual stresses. Resin flow during initial stages of the cure process can cause composite part to deform and shrink, as excess resin flows out from the part. In addition, this causes non-uniform distribution in the fibre volume fraction and thus also in material properties, which leads to uneven thermal and shrinkage strains causing residual stresses. [8] Compaction effect is typically non-uniform in the part thickness direction, contributing most on the outer layers. Thus, top plies become thin and bottom plies thick. Part dimensions change

and lead to residual stresses. [16] Curing residual stresses due to part-tool interaction are formed through the following process: The tool has a different, typically larger coefficient of thermal expansion than the fibres. As temperature ramps and pressure are applied during the cure process, a shear interaction is formed in the interface of the fibre tows and the tool. Due to the CTE-mismatch, the fibre tows located near the tool surface become in tension, as the tool expands more than the fibres and the shear interaction prevents the free movement of the fibre tows. This phenomenon takes place in early parts of the cure cycle, when resin has not cured and it has a low modulus of elasticity. Tensile stress distribution is formed and "locked in" to the part as the curing proceeds. [33]

# 3 Continuum material models

Material constituents in a steel-composite hybrid material system with glass-fibre reinforced epoxy behave completely differently during the cure process. Epoxy behaviour is highly viscoelastic and rheologically complex throughout the cure process and the material properties change significantly as a function of the degree of cure and temperature. For steel and reinforcing fibres the material parameters stay relatively constant during the entire cure process including the cool-down phase. Thus, interest is in modelling the epoxy behaviour, and composite material values can be derived with micromechanical models.

Different types of models are needed to describe the whole cure process. A thermo-chemical process model is needed if temperature distributions inside the composite part during the exothermic cure process are wanted to assess accurately. Constitutive mechanical models define material behaviour and mechanism behind stress formation. Both relatively simple elastic constitutive models and complex viscoelastic constitutive models have been developed and utilised in the residual stress analyses of composite materials. More complex material models offer more accurate results with the cost of heavier computational load and need for broader material characterization. [34] Models that combine both viscoelastic and purely elastic characteristics (e.g. CHILE, cure-hardening instantaneously linear-elastic model) have also been presented. These yield accurate results with good computational efficiency and without the need for extensive material characterization [35]. In orded to utilize the process and constitutive models, adequate characterization for epoxy and composite material properties are also needed.

## 3.1 Curing composite thermo-chemical process model

The curing process of a composite includes both local heat generation of the curing resin and heat conduction due to external surfaces or along fibres. The thermo-chemical process model can be derived from the local form of the first law of thermodynamics (conservation of energy) [23]:

$$\rho \frac{\mathrm{d}e}{\mathrm{d}t} = -\frac{\partial q_i}{\partial x_i} + \rho r + \sigma_{ij} \frac{\mathrm{d}}{\mathrm{d}t} \varepsilon_{ij} \quad \text{in } V(i,j=1,2,3) \tag{3.1}$$

where $e$ is the internal energy per unit mass, $\rho$ is the current mass density of the composite, $q_i$ are the components of the heat flux vector, $r$ is the rate of heat supply per unit mass, $\sigma_{ij}$ are the stress tensor components and $\varepsilon_{ij}$ are the infinitesimal strain tensor components, $x_i$ are the coordinates, $t$ is the time and $V$ is the examined volume. Now, the mechanical work rate, i.e. the last term of

Equation (3.1) can be assumed negligible and the internal energy to be dependant of temperature with relation $e = cT$, where $c$ is the specific heat capacity of the composite material and $T$ temperature. According to the Fourier law of heat conduction, the heat flux vector $q_i$ and temperature gradient $\partial T/(\partial x_i)$ are related through equation [23]:

$$q_i = -\kappa \frac{\partial T}{\partial x_i} \tag{3.2}$$

where $\kappa = \kappa(T, \alpha)$ is the thermal conductivity of the composite depending on the temperature $T$ and the degree of cure $\alpha$. With these assumptions, we can write the thermo-chemical process model for curing composite as [23]:

$$\rho c \frac{\mathrm{d}T}{\mathrm{d}t} = \frac{\partial}{\partial x_i}\left(\kappa(\alpha, T)\frac{\partial T}{\partial x_i}\right) + \rho H_{R,c}\frac{\partial \alpha}{\partial t} \tag{3.3}$$

where $\rho$ is mass density of the composite, $c$ is the specific heat capacity of the composite, $T$ is the temperature, $t$ is the time, $x_i$ are the coordinates, $\kappa$ is the thermal conductivity of the composite, $\alpha$ is the degree of cure and $H_{R,c}$ is the total heat generated by the cure reaction per mass unit for the whole composite. [23] In Equation 3.3 the convective terms resulting from resin flow are excluded, due to the extremely low flow rate and thus negligible contribution to the internal convective heat transfer. [8] Equation 3.3 should be adopted especially with thick specimens and when targeting the accurate modelling of temperature distribution throughout the part. In thin parts, the temperature distribution is rather uniform everywhere and often a uniform process temperature inside the part is approximated, neglecting epoxy exothermic curing. [36–38]

## 3.2 Curing composite constitutive mechanical models

A proper constitutive model is needed in order to accurately describe the material mechanical behaviour during cure, under temperature changes and degree of cure evolution. Even though epoxy resin has been noted to behave in a viscoelastic manner during the cure, also elastic constitutive models have been utilized due to simpler mathematical modelling, material characterization and as in many cases they still produce usable results [34]. This is true especially in cases when residual stresses are mainly relaxed before cool-down due to a high-temperature hold period. Elastic models have also been applied to study the stress state throughout the whole cycle, but residual stresses are in this case often over-predicted, as no stress relaxation is included in the analysis. [8] Cure-hardening instantaneously linear-elastic (CHILE) models, where the elastic modulus of the resin material is changed as a function of the instantaneous temperature and cure degree, have also been found to give good results [35, 39].

Viscoelastic material behaviour can be described with the so-called Boltzmann superposition principle [40]. For a one-dimensional case, the constitutive equation

for stress under constant temperature and degree of cure for homogeneous viscoelastic material can be written in an integral form as [39]:

$$\sigma(t) = \int_0^t E(t-\tau)\frac{\mathrm{d}\varepsilon}{\mathrm{d}\tau}\,\mathrm{d}\tau \tag{3.4}$$

where $\sigma$ is the stress, $E$ is the relaxation modulus, $\varepsilon$ is the mechanical strain, $t$ is the current time and $\tau$ is the time integration variable.

In order to account temperature change and degree of cure evolution, time-temperature superposition method is typically applied. The base assumption is that the effect of temperature and time in polymer materials are interchangeable, meaning that behaviour of material at an increased temperature corresponds the behaviour at the original temperature after a longer time. [39, 41, 42] The degree of cure has been combined with temperature and time with the same assumption [29], and thus in one-dimensional case the stress in linear-viscoelastic material can be expressed as [29]:

$$\sigma(t) = \int_0^t E(\alpha, T, t-\tau)\frac{\mathrm{d}}{\mathrm{d}\tau}\left(\varepsilon^{total}(\tau) - \varepsilon^{tc}(\tau)\right)\,\mathrm{d}\tau \tag{3.5}$$

where $\sigma$ is the stress, $E$ is the relaxation modulus, $\varepsilon^{total}$ is the total strain, $t$ is the current time and $\tau$ is the time integration variable, $\alpha$ is the degree of cure, $T$ is the temperature and $\varepsilon^{tc}$ is the so-called free thermochemical strain, which combines the strains resulting both from thermal expansion due to temperature changes and cure shrinkage as degree of cure changes. Further, by assuming that the material can be described with thermorheologically simple behaviour, meaning that material behaviour between different temperatures can be converted only with a shift in time [42], the previous equation may be written as:

$$\sigma(t) = \int_0^t E\left[\xi(t) - \xi'(\tau)\right]\frac{\mathrm{d}}{\mathrm{d}\tau}\left(\varepsilon^{total}(\tau) - \varepsilon^{tc}(\tau)\right)\,\mathrm{d}\tau \tag{3.6}$$

where $\sigma$ is the stress, $E$ is the relaxation modulus, $\varepsilon^{total}$ is the total strain, $t$ is the current time and $\tau$ is the time integration variable, $\varepsilon^{tc}$ is the so-called free thermochemical strain, and $\xi$(t) and $\xi$' ($\tau$) are the reduced times to combine time with degree of cure and temperature. Reduced times can be defined as [39]:

$$\xi(t) = \int_0^t \frac{1}{a_T(\alpha, T)}\mathrm{d}t' \;; \quad \xi'(\tau) = \int_0^\tau \frac{1}{a_T(\alpha, T)}\mathrm{d}t' \tag{3.7}$$

where $t$ is the current time, $a_T$ is the shift factor for time-temperature superposition, $\alpha$ is the degree of cure, $T$ is the temperature and $t'$ is another time integration variable. For example for Hercules 3501-6 epoxy the shift factor function is of form [43]:

$$\log a_T = \left[-1.4\exp\frac{1}{1-\alpha} - 0.0712\right](T - 30°\mathrm{C}) \tag{3.8}$$

where $\alpha$ is the degree of cure and $T$ is the current temperature.

Also cure-hardening instantaneously linear-elastic (CHILE) models have been utilized to describe the material behaviour during the cure. These models are based on the following assumptions:

- The resin modulus can be assumed to be constant at each instant of time during the cure cycle.
- This constant resin modulus value is a function of temperature and degree of cure.

The modulus values are based on experiments. In the simplest form, only two constant values of the modulus, one for the rubbery state and one for the glassy state, can be defined [13, 44]. For more accurate results, modulus needs to be defined with small enough time increments. The constitutive equation for these models in one dimension can be expressed in the integral form as [35]:

$$\sigma(t) = \int_0^t E'(T, \alpha) \frac{\mathrm{d}\varepsilon}{\mathrm{d}\tau} \, \mathrm{d}\tau \tag{3.9}$$

where $\sigma$ is the stress, $E'$ is the instantaneous elastic modulus as a function of temperature $T$ and degree of cure $\alpha$ obtained with testing, $\varepsilon$ is the mechanical strain, $t$ is the current time and $\tau$ is the time integration variable.

## 3.3 Models for epoxy and composite material properties

### 3.3.1 Degree of cure models

Different degree of cure models describing the evolution of curing have been developed, based on purely chemical reaction mechanics, purely on empirical data or combining features of both, which are so-called semi-empirical models.

Typically degree of cure models express the reaction rate (time derivative of degree of cure, $\frac{\mathrm{d}\alpha}{\mathrm{d}t}$) as a function of degree of cure and temperature. Often applied semi-empirical model of this type for amine-cured autocatalytic epoxy systems, in which the reaction products catalyse the ongoing reaction, is [8, 23]:

$$\frac{\mathrm{d}\alpha}{\mathrm{d}t} = (K_1 + K_2 \alpha^m)(1 - \alpha)^n \tag{3.10}$$

where $\alpha$ is the degree of cure, $t$ is the time and $m$ and $n$ are experimentally determined constants for the specific epoxy system. Parameters $K_i$ are defined as [8, 23]:

$$K_i = A_i \exp \frac{\Delta E_i}{RT} \tag{3.11}$$

where $A_i$ is experimentally determined constant for the specific epoxy system, $\Delta E_i$ is the activation energy, $R$ is the universal gas constant and $T$ is the temperature. For non-autocatalytic reactions, an empirical model (which can be derived from Equation 3.10 by assuming that $K_2$ equals zero) is usually of form [8]:

$$\frac{\mathrm{d}\alpha}{\mathrm{d}t} = K_1 (1 - \alpha)^n \tag{3.12}$$

where $\alpha$ is the degree of cure, $t$ is the time, $n$ is the experimentally determined constant for a specific epoxy system and $K_1$ is defined according to Equation (3.11). Table 3.1 presents experimental parameters $m, n, K_1$ and $K_2$ for multiple different epoxy systems and the total heat generated by the cure process $H_R$ [23].

***Table 3.1:*** *Curing equation parameters and the total heat generated by the cure process $H_R$ for multiple different epoxy systems. For Epon 862 -epoxy hardener systems different results are obtained in different studies. $R$ is the universal gas constant and $T$ is the temperature. [23]*

| Material | $H_r$ [J/g] | $m$ | $n$ | $K_1$ and $K_2$ |
|---|---|---|---|---|
| Epon 862 and Epikure W | 341 | 0 | 0 | $K_1 = 1.76 \cdot 10^7 \exp(\frac{-75000}{RT})/s$ <br> $K_2 = 0$ |
| Epon 862 and Epikure W | 399 | 0.39 | 1.67 | $K_1 = 0$ <br> $K_2 = 6488 \exp(\frac{-53326}{RT})/s$ |
| Epon 862 and Epikure 9553 | - | 0 | 1 | $K_1 = 3.62 \cdot 10^{11} \exp(\frac{-88500}{RT})/s$ <br> $K_2 = 0$ |
| Epon 815 and Epikure 3274 | 384 | 0.25 | 1.7 | $K_1 = 0$ <br> $K_2 = 4.18^5 \exp(\frac{-55920}{RT})/s$ |

The above expressions assume, that the degree of cure rate is controlled by the kinetics of the molecular bond formation. This is typically a valid assumption in the early stage of the cure, but at later stage the control mechanism shifts from kinetics to diffusion as molecular mobility is restricted due to vitrification. To take this into account, previously presented models can be combined. [8] For example, the degree of cure rate for Hercules 3501-6 epoxy resin including vitrification effect can be expressed as [24]:

$$\frac{\mathrm{d}\alpha}{\mathrm{d}t} = \begin{cases} (K_1 + K_2\alpha)(1-\alpha)(0.47-\alpha) & (\alpha \leq 0.3) \\ K_3(1-\alpha) & (\alpha \geq 0.3) \end{cases} \tag{3.13}$$

where $K_i$ are as presented in Equation (3.11), $\alpha$ is the degree of cure and $t$ is the time. Table 3.2 presents the cure kinetic constants for calculating the parameters $K_i$ for Hercules 3501-6 epoxy resin.

### 3.3.2 Epoxy modulus models

Sham *et al.* [45] studied experimentally material behavior of a glass slide (strip) and different fully cured epoxy resins near the glass transition temperature. As a result, they obtained flexural modulus values for the glass slide (strip) and different types of epoxies as a function of temperature, which are presented in Figure 3.1. It can be noted from Figure 3.1 that the epoxy modulus decreases rapidly after the glass transition temperature has been reached. The flexural modulus for the

***Table 3.2:*** *Cure kinetic constants for Hercules 3501-6 epoxy resin. [24]*

| Constant | Value |
|---|---|
| $A_1$ [$\text{min}^{-1}$] | 2.101 $\cdot 10^9$ |
| $A_2$ [$\text{min}^{-1}$] | -2.014 $\cdot 10^9$ |
| $A_3$ [$\text{min}^{-1}$] | 1.960 $\cdot 10^5$ |
| $\Delta E_1$ [J/mol] | 8.07 $\cdot 10^4$ |
| $\Delta E_2$ [J/mol] | 7.78 $\cdot 10^4$ |
| $\Delta E_3$ [J/mol] | 5.66 $\cdot 10^4$ |

glass slide (strip) stays approximately constant during the studied temperature range.

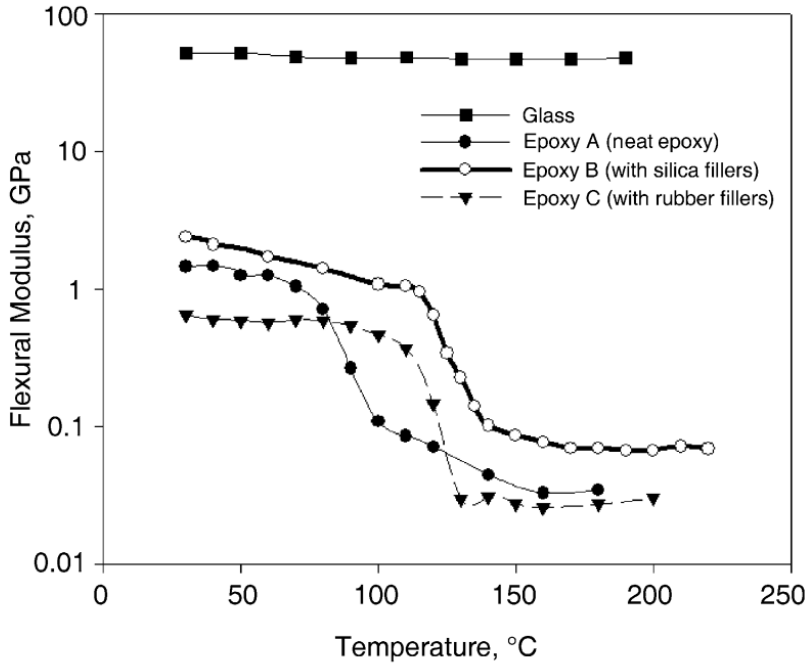


***Figure 3.1:*** *Experimentally measured flexural modulus values as a function of temperature for different epoxies and glass. Epoxy flexural modulus values change rapidly around the glass transition temperature (now approximately between 80–140 °C). Before and after the glass transition temperature flexural modulus is approximately constant. [45]*

During the cure, the epoxy modulus value has been described with one or two constant values, changing either instantaneously [13, 44] or linearly in between a defined degree of cure range [26]. For Hercules 3501-6 resin the linear change has been expressed with equation [26]:

$$E(\alpha) = \begin{cases} E_0 & (0 \leq \alpha \leq 0.3) \\ E_0 + K_E(\alpha - 0.3) & (0.3 \leq \alpha \leq 0.8) \\ E_f & (0.8 \leq \alpha \leq 1) \end{cases} \tag{3.14}$$

where $E$ is the epoxy modulus, $\alpha$ is the degree of cure, $E_0$ is the modulus of uncured resin, $K_E$ is the parameter taking into account the effect of developing degree of cure and $E_f$ is the modulus of fully cured resin. These parameters for Hercules 3501-6 resin are $E_0 = 5.0$ GPa, $E_f = 9.0$ GPa, $K_E = 8.0$GPa [23].

For viscoelastic material models the modulus (including stress relaxation) for a thermorheologically simple material, taking into account the curing state, can be approximated by $M$-number of Maxwell elements, often called as Prony-series [39]:

$$E(\alpha, \xi) = E^{\infty}(\alpha) + E^{*}(\alpha) \sum_{\omega=1}^{M} W_{\omega}(\alpha) \exp\left(-\frac{\xi(\alpha, T)}{\lambda_{\omega}(\alpha)}\right) \tag{3.15}$$

where $E$ is the epoxy modulus, $\alpha$ is the degree of cure, $\xi$ is the reduced time defined by Equation (3.7), $E^{*} = E^{u}\ (\alpha)$-$E^{\infty}\ (\alpha)$ is a material constant, $E^{\infty}$ is the fully relaxed modulus, $E^{u}$ is the unrelaxed modulus, $W_{\omega}$ are the weight factors, $\lambda_{\omega}$ are the discrete stress relaxation times and $T$ is the temperature. [29, 39] It has been assumed that $E^{u}\ (\alpha)$ and $E^{\infty}\ (\alpha)$ are constant and independent of temperature and degree of cure and that $W_{\omega}$ is independent of degree of cure [43]. Thus, the equation simplifies to the form:

$$E(\alpha, \xi) = E^{\infty} + E^{*} \sum_{\omega=1}^{M} W_{\omega} \exp\left(-\frac{\xi(\alpha, T)}{\lambda_{\omega}(\alpha)}\right). \tag{3.16}$$

Prony-series parameters defining the stress relaxation modulus in the viscoelastic constitutive model for Hercules 3501-6 epoxy are as presented in Table 3.3.

***Table 3.3:*** *Prony series parameters for Hercules 3501-6 epoxy. $W_{\omega}$ are the weight factors and $\lambda_{\omega}$ the discrete stress relaxation times. [43]*

| $\omega$ | $\lambda_{\omega}$ [min] | $W_{\omega}$ |
|---|---|---|
| 1 | 29.2 | 0.059 |
| 2 | $2.92 \cdot 10^{3}$ | 0.066 |
| 3 | $1.82 \cdot 10^{5}$ | 0.083 |
| 4 | $1.10 \cdot 10^{7}$ | 0.112 |
| 5 | $2.83 \cdot 10^{8}$ | 0.154 |
| 6 | $7.94 \cdot 10^{9}$ | 0.262 |
| 7 | $1.95 \cdot 10^{11}$ | 0.184 |
| 8 | $3.32 \cdot 10^{12}$ | 0.049 |
| 9 | $4.92 \cdot 10^{14}$ | 0.025 |

### 3.3.3 Chemical shrinkage models

Chemical shrinkage evolution during the cure process has been studied experimentally by Li *et al.* [22]. They found out that for the MY750 epoxy resin system chemical shrinkage during curing could be defined with a bilinear model and that the model was independent of the cure temperature. Figure 3.2 presents the obtained shrinkage evolution. Total cure shrinkage of 6.9% was determined at the 100% degree of cure. This kind of bilinear shrinkage model has been applied also in full cure cycle simulations.

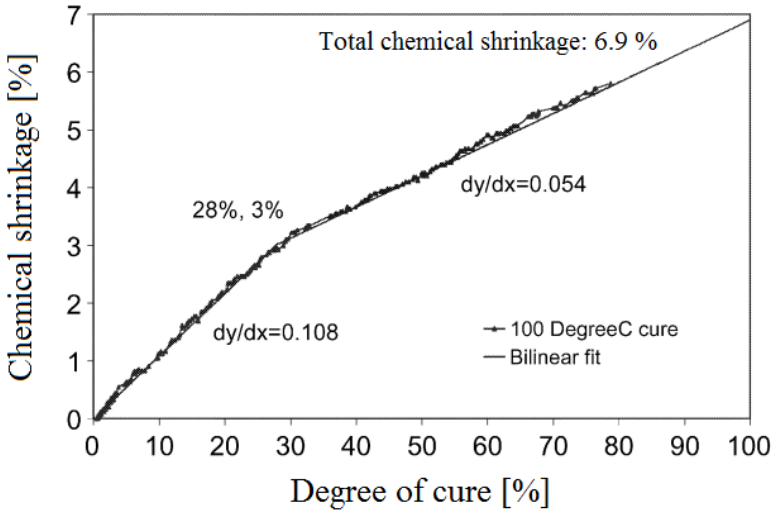


***Figure 3.2:*** *Experimentally determined chemical shrinkage evolution as a function of degree of cure for the MY750 epoxy resin system. Chemical shrinkage can be expressed with a bilinear model. Total chemical shrinkage of 6.9% was obtained. [22]*

Total chemical shrinkage values obtained experimentally for multiple epoxy resin systems are presented in Table 3.4.

***Table 3.4:*** *Experimentally determined total chemical shrinkage values for different epoxy systems. [23]*

| Epoxy system | Chemical shrinkage |
|---|---|
| MY750 | 6.9% |
| DGEBA/MCDEA | 4.5% |
| Epon 828/DEA | $> 1\%$ |
| Bisphenol F | 2.75% after gelation |
| Epikote 828/MNA/BDMA | $< 2\%$ |
| Epon 862/Epikure 9553 | 2% |

Most simple chemical shrinkage models for epoxy assume that cure shrinkage is equal in each direction and changes linearly with the degree of cure. This can be presented with the equation [46]:

$$\varepsilon_i^s = (\sqrt[3]{1+\beta\alpha}) - 1 \tag{3.17}$$

where $\varepsilon_i^s$ is the chemical strain (shrinkage) in direction $i$, $\beta$ is the total volumetric shrinkage value and $\alpha$ is the degree of cure.

### 3.3.4 Coefficient of thermal expansion models

Sham *et al.* [45] studied experimentally changes in a bi-material strip dimensions as a function of temperature. The thermal expansion coefficient for neat epoxy was found to be adequately described with two constant values, above and below the glass transition temperature value (see also Figure 2.5). The same step-change approach was used by Svanberg *et al.* [13], who used an experimentally defined ratio of these values. For example, Araldite LY5052/Hardener HY5052 epoxy system CTE above $T_g$ was found to be 2.5 times the CTE below $T_g$ [47]. System's CTE value below $T_g$ is $71 \cdot 10^{-6}/°\text{C}$ [11].

Rabearison *et al.* [10] used the rule of mixture for resin and matrix weighted by the degree of cure to define the material properties during the cure. CTE was defined with the equation:

$$CTE(t) = [1-\alpha(t)] \cdot CTE_0 + \alpha(t) \cdot CTE_f(t, T_g) \tag{3.18}$$

where $CTE_0$ is the CTE for the uncured part of epoxy resin and $CTE_f$ is the CTE for fully cured epoxy resin, $t$ is the time, $\alpha$ is the degree of cure and $T_g$ is the glass transition temperature. The CTE for fully cured resin is changing as a function of temperature. For the LY556 epoxy system glass transition temperature for a fully cured matrix is $T_g = 136$ °C and CTE values are:

- $CTE_0 = 500 \cdot 10^{-6} 1/°\text{C}$ for a vitrified matrix ($T < T_g$)
- $CTE_f = 450 \cdot 10^{-6} 1/°\text{C}$ for a vitrified matrix ($T < T_g$)
- $CTE_f = 450 \cdot 10^{-6} + 4.1 \cdot 10^{-6}(T - T_g) 1/°\text{C}$ for a rubbery matrix ($T > T_g$).

Jumbo *et al.* [14] used a constant CTE value, measured using a dilatometer, for the thermal expansion coefficient of epoxy resin in a residual stress analysis. Only the cool-down phase of bi-material strips was analysed, and temperature was under the glass transition temperature. Constant CTE values have also been used for the whole cure cycle.

### 3.3.5 Specific heat capacity models and thermal conductivity models

Material specific heat capacity $c$ and thermal conductivity $\kappa$ are needed when the whole cure cycle is simulated with a thermo-chemical model of curing composite. A

strong discontinuity for specific heat capacity has been observed experimentally at the vitrification point for uncured AS4/8552 carbon fibre/epoxy composite. Values before and after vitrification stay approximately the same. For cured composite the behaviour was found to be linear as a function of temperature. Figure 3.3 presentes this behaviour. [8]

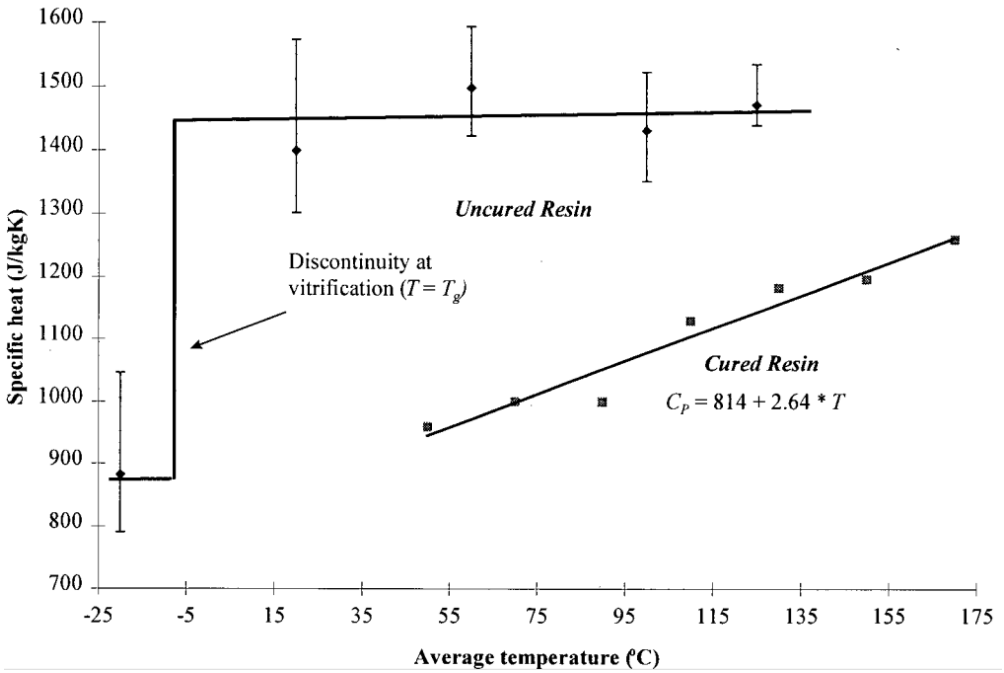


***Figure 3.3:*** *Experimentally determined specific heat capacity as a function of temperature for cured and uncured resin (composite). [8]*

Constant but orthotropic values or rule of mixtures values have been used for resin conductivity [10]:

$$\kappa(\alpha, T) = (1 - \alpha) \cdot \kappa(0, T) + \alpha\kappa(1, T) \tag{3.19}$$

where $\kappa(0, T)$ and $\kappa(1, T)$ are the temperature dependent thermal conductivities of uncured resin and fully cured matrix, $\alpha$ is the degree of cure and $T$ is the temperature.

### 3.3.6 Interface interaction models

The interface between fibres and epoxy can be modelled with a shear layer. The epoxy behaviour during the cure process can be divided into two parts: before the gel point the behaviour is as viscous liquid, and after the gel point behaviour is rubber-like. During the first part, chemical shrinkage does not form any interaction as no adhesion has been formed between fibres and matrix. Over the second part the adhesion in the interface of these two components opposes the slippage of the epoxy on the fibre. This resisting shear stress $\tau$ can be modelled to increase with

the degree of cure near the gel point, and described as:

$$\tau = \begin{cases} \tau_0 & (0 \leq \alpha \leq 0.3) \\ \tau_0 + K_\tau(\alpha - 0.3) & (0.3 \leq \alpha \leq 0.8) \\ \tau_f & (0.8 \leq \alpha \leq 1) \end{cases} \tag{3.20}$$

where $\tau_0$ is the initial resisting shear stress value, $K_\tau$ is a parameter taking into account shear stress evolution with the degree of cure evolution, $\alpha$ is the degree of cure and $\tau_f$ is the final value of the resisting shear stress. For the T800 carbon fibre and Hercules 3501-6 epoxy resin interface these parameters are $\tau_0$=0 MPa, $\tau_f$= 100 MPa and $K_\tau = 2\ \tau_f$. [26]

For the interface between a tool and a composite part, resisting shear stress values have been noted to change during the cure. For example, between an aluminium mould treated with a release agent and the Hexcel AS4/8552 carbon-fibre-epoxy prepreg the resisting shear stress values of 0.006 MPa before and 0.06 MPa after the gel point have been observed. [33]

# 4 Finite element simulations of residual stress formation

In general, most finite element analysis methods used for analysing specific part manufacture processes are constructed on the macroscopic scale. This means that homogenised composite properties can be calculated using micromechanical modelling of fibres and matrix. However, models describing the interaction between single fibres and resin have also been utilised in order to study micro-scale behaviour. [34] A finite element model by Nishikawa *et al.* [26] was used to describe the curing and adhesion behaviour of a specimen with a single carbon fibre and an epoxy droplet.

The simulation of the residual stress formation during the whole cure process is complicated and computationally time-consuming, as the material behaviour of resin during the process is highly viscoelastic and rheologically complex. Viscoelastic and rheologically complex material models are highly dependent of time, temperature and degree of cure. Finite element simulations of residual stresses taking into account only the unequal thermal contraction of material system constituents during the cool-down phase of the process is the simplest method to study residual stresses [14], and has been the most common analysis method [34]. This method is based on the assumption that the part is free of stresses before the cool-down due to the stress relaxation behaviour of a highly viscoelastic material at cure temperature, and that significant residual stresses start to develop during the cool-down phase. Often elastic constitutive models are used in these cool-down phase simulations. Depending on analysis dimensions, part shape, geometrical restrictions and manufacturing process parameters, simulations with this assumption have sometimes offered applicable results. [34] However, it has also been stated that the assumption is questionable: the stress-free temperature is usually elevated above the cure temperature and fully relaxed modulus is not negligibly small due to the reinforcing fibres in the resin, leading to only partial stress relaxation. Thus, in some cases three-dimensional analysis of the full cure cycle with viscoelastic constitutive equation is needed to capture all the important mechanisms that produce residual stresses during the process. [36]

Maybe the most extensive incorporation of these different mechanisms producing residual stresses is made in a study by Tavakol *et al.* [16], where included are cure kinetics (also exothermic curing), nonlinear orthotropic chemical cure shrinkage, uniform through-thickness compaction, uniform orthotropic resin flow, changes in nonlinear orthotropic thermal and mechanical material properties due to curing, nonlinear mechanical and thermal contact at tool-part interface and different nonlinear orthotropic thermal expansion coefficient changes during and after the cure [16].

The process flow chart for this simulation is presented in Figure 4.1. In the start of simulation, the needed initial values are temperature, degree of cure and stress in the material. Cure kinetics model is then used to obtain cure rate which tells the heat flux due to the exothermal curing. Specific heat and thermal conductivity are approximated and the thermal analysis is done by taking into account the heat transfer due to the heat flux from curing and thermal contact between part and tool. Thermal analysis gives the temperature and degree of cure for the time increment analysed. Then, the mechanical properties of the materials are approximated, and used for mechanical analysis part including modules for calculation of cure shrinkage, thermal strain, mechanical contact and mechanical strains. Resin chemical shrinkage, resin flow and compaction behaviour are included in the cure shrinkage analysis, whereas strain due to the temperature change and change of CTE with respect of temperature and degree of cure are calculated in the thermal strain analysis. Tool-part mechanical interaction is taken into account in mechanical contact analysis and mechanical strains are approximated in the fourth module of the mechanical analysis. The strains and distortions in the part are obtained as the output of the mechanical analysis. These steps are repeated until the wanted process time is simulated. [16]

## 4.1 Dimensional context

Residual stress simulations have been done both with two-dimensional and three-dimensional models for the whole cure cycle as well as for the cool-down phase alone. Two-dimensional models are used in order to make simulations computationally faster. Using a two-dimensional analysis involves some kind of simplifications in order to describe the real three-dimensional problem only in two dimensions. The typical approximations assume plane-strain or plane-stress state. In plane-strain state there is no strain in one main material direction, whereas in plane-stress state the stress component in one main material direction and the shear stress components related to this direction are zero. A generalised plane-strain state is an extension to the plane-strain state, allowing uniform straining in the out-of-plane direction.

The suitability of different simplifications is case-dependent, as shown in the study by Jumbo *et al.* [14], where different simulation cases were compared. Two bi-material strips, made of epoxy adhesive FM300-2 and AISI 312 steel (high length-to-width ratio) and epoxy adhesive FM73 and 1050-H18 aluminium (low length-to-width ratio), were studied under a temperature change describing the cool-down phase of epoxy cure process. As a result, it was found out that plane-stress state was accurate predicting the deflection and stresses in a specimen with a high length-to-width ratio, but that the results were not as accurate with a low length-to-width ratio. Plane-strain state derived more accurate results with the latter type of specimens. In addition, a generalised plane-strain state and a three-dimensional model were used. Especially three-dimensional simulations provided accurate results. Table 4.1 describes the differences in deflection, when temperature dependant material properties and geometrical nonlinearity are in-

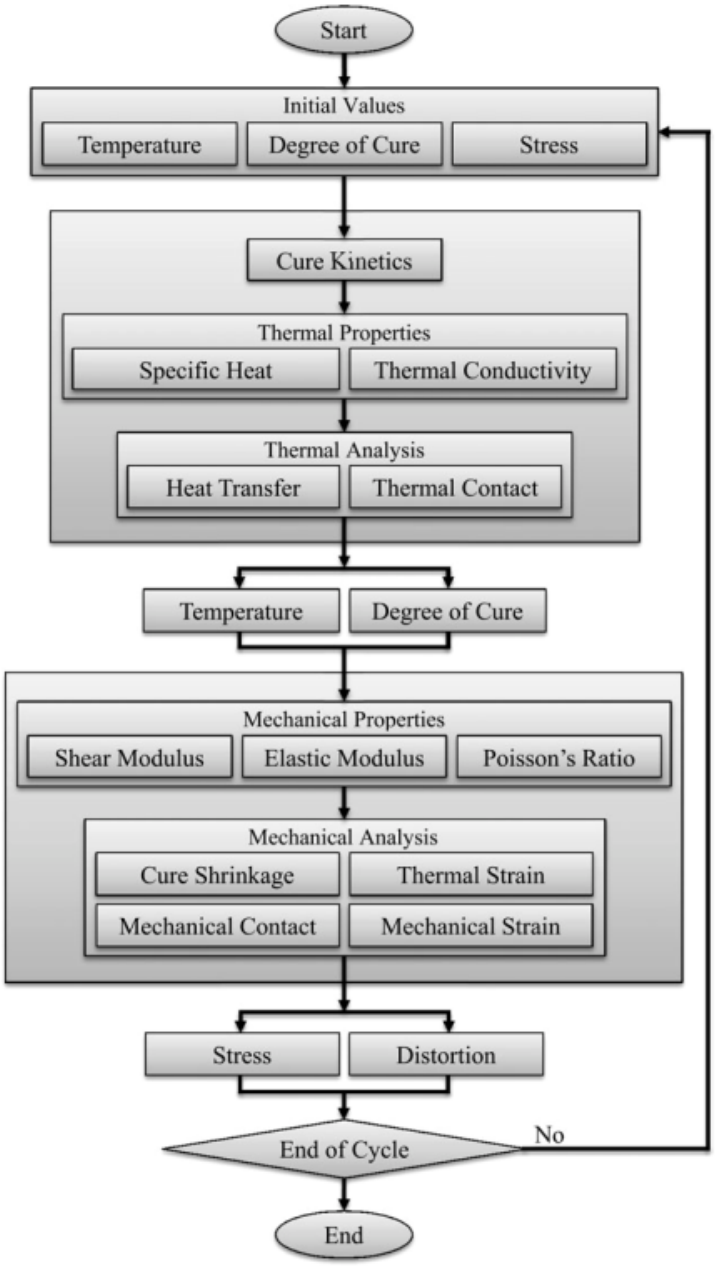


***Figure 4.1:*** *Finite element residual stress simulation flow chart for the whole cure cycle. Presented simulation method takes into account cure kinetics, chemical cure shrinkage, compaction, resin flow, non-linear thermal and mechanical material property changes, mechanical and tool-part interface and thermal expansion coefficient changes during and after the cure. [16]*

cluded in the analysis and an experimentally determined value can be used as a reference. In addition to previous results, it has been shown that in some cases two-dimensional finite element analysis can be misleading, as it does not fully express the real three-dimensional stress field, e.g. close to the free edges of the material body [48, 49].

***Table 4.1:*** *Displacements in two different bi-material strips with two-dimensional and three-dimensional finite element simulations and experimentally. FM300-2 / AISI 312 steel specimen had high length-to-width ratio and FM73 / 1050-H18 aluminium specimen low length-to-width ratio. [14]*

| Method | Displacement [mm] | |
|---|---|---|
| | FM300-2 adhesive and AISI 312 steel | FM73 adhesive and 1050-H18 aluminium |
| Experimental | 29.93 | 39.09 |
| Plane-strain model | 41.52 | 41.56 |
| Generalised plane-strain model | 40.80 | 40.57 |
| Plane-stress model | 30.00 | 33.13 |
| 3D solid model | 27.15 | 39.75 |
| 3D shell model | 30.20 | 38.99 |

## 4.2 Boundary conditions and interfaces

The mechanical interface between a composite part and a tool or between hybrid material system constituents has been defined according to the simulation case. Typically the interface interaction is defined as a coupled interaction, meaning that no movement between the components is allowed. However, in some cases movement (slipping) is allowed between parts in specific directions with special conditions, for example when cure-dependent shear stress value is exceeded between part and tool. When no movement is allowed, a hard, non-penetrating behaviour in the normal direction and non-sliding behaviour in the tangential direction of the surfaces is assigned. This kind of contact between the constituents can be assumed when the focus is on simulating the cool-down phase after the matrix has cured [14]. Using the elastic shear layer enables to alter the amount of shifted stress between the part and the tool.

The cool-down phase residual stresses can be simulated with linear thermal expansion by preventing only the rigid body motion of the object (free deformation) and by applying a constant temperature difference $\Delta T$ throughout the model. This describes situation of free uniform cooling, when no thermal gradients or mechanical constraints are present.

When simulating the full cure cycle, a typical temperature boundary condition is to apply the changing cure cycle temperature (autoclave process temperature or experimentally measured temperature) for the part boundaries to describe the mould/autoclave temperature. If the mould is included in the simulation, the cure cycle temperature is applied to the mould, and adequate heat transfer interfaces are defined for heat conduction from the mould to the part. Heat transfer through convection between the mould or composite part and autoclave environment can be simulated with a convective interface. The heat generation due to the exothermic

cure process can be simulated, but often a simplifying assumption of a uniform cure cycle temperature throughout the part is made especially with thin parts. To describe the manufacturing process accurately, also the cure cycle pressure can be applied to the part surfaces as a pressure boundary condition.

## 4.3 Example cases from literature

Formation and magnitude of residual stresses in cylindrical composites have been studied with different laminate lay-ups and constitutive models (elastic and viscoelastic), by concidering the effect of mandrel or liner inside the cylinder and by simulating only the cool-down phase or the whole cure cycle. [36, 37] All of these are found to affect the obtained estimate of residual stress values.

### 4.3.1 Effect of composite lay-up and constitutive models

Hwang *et al.* [38] studied hollow composite-aluminium hybrid cylinders made from AS4/3501-6 carbon fibre epoxy prepreg composite with 6061-T6 aluminium liner inside the composite cylinder. Material properties for these materials are presented in Table 4.2. Elastic and viscoelastic constitutive models and different composite lay-ups were used in finite element simulations. The used viscoelastic material model equations including the shift factor for AS4/3501-6 prepreg are those presented in Section 3.2. The applied epoxy modulus model and parameters are those presented in Section 3.3.2. The cylinder geometry, dimensions and used coordinate system are shown in Figure 4.2. Finite element simulation model consisted of 4-node isoparametric ring elements.

***Table 4.2:*** *Material properties for AS4 fibre, 3501-6 epoxy resin and 6061-T6 aluminium. [36, 38].*

| Material property | AS4 graphite fibre | 3501-6 epoxy matrix | 6061-T6 aluminium |
|---|---|---|---|
| $E_1$ [GPa] | 207.0 | 3.2 | 69.5 |
| $E_2 = E_3$ [GPa] | 20.7 | 3.2 | - |
| $G_{12} = G_{13}$ [GPa] | 27.6 | 1.19 | - |
| $G_{23}$ [GPa] | 6.89 | 1.19 | - |
| $\nu_{12} = \nu_{13}$ [-] | 0.2 | 0.35 | 0.3 |
| $\nu_{23}$ [-] | 0.3 | 0.35 | 0.3 |
| $CTE_1$ [$10^{-6}$/°C] | -0.9 | 57.6 | 23.6 |
| $CTE_2 = CTE_3$ [$10^{-6}$/°C] | 7.2 | 57.6 | - |
| $\varepsilon_1^s = \varepsilon_2^s = \varepsilon_3^s$ [-] | 0 | -0.01695 | 0 |

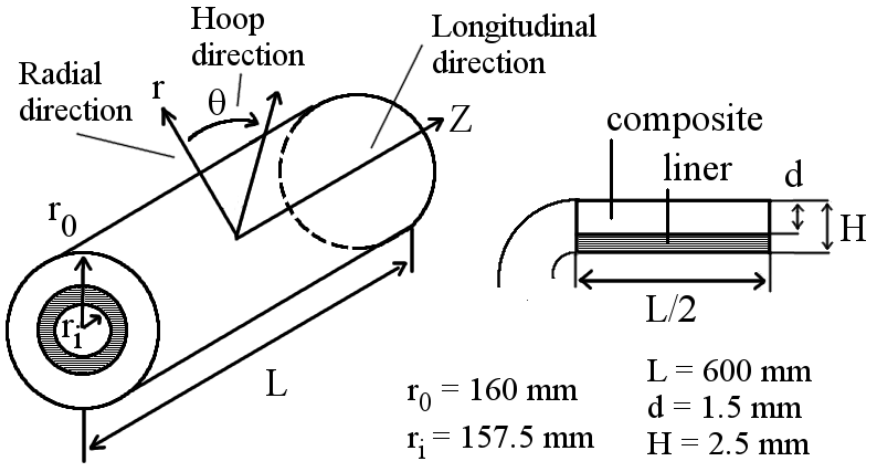


***Figure 4.2:*** *Dimensions of the hollow composite-aluminium hybrid cylinder made from AS4/3501-6 carbon-fibre epoxy prepreg with aluminium liner inside the cylinder. Composite layer consists of different lay-ups. [38]*

The studied composite material lay-ups were $[(15/\text{-}15)_{2s}/90_4]$, $[(30/\text{-}30)_{2s}/90_4]$ and $[(45/\text{-}45)_{3s}/90_4]$, where 0-direction is the longitudinal direction of the cylinder and 90-direction is the hoop direction of the cylinder. Viscoelastic constitutive model and simulation of the full cure cycle including cool-down phase was used and compared with an elastic constitutive model and simulation of the cool-down phase alone. Resin heat generation during the cure was not considered, temperature at cylinder boundaries was defined to correspond the cure cycle temperature. Linear resin chemical shrinkage was also included in the analysis, corresponding to the total volumetric shrinkage of 5%. The studied cure cycle and corresponding degree of cure evolution for AS4/3501-6 prepreg are presented in Figure 4.3. The cure cycle consisted of hold periods at temperature of 115 °C for 60 minutes and at temperature of 177 °C for 120 minutes, temperature increase periods between the hold periods and a cool-down phase from 177 °C to 25 °C, resulting in total temperature change $\Delta T = -152$ °C. Epoxy cure evolution was modelled according to equations presented in Section 3.3.1 for the 3501-6 epoxy.

Cylinder ends were allowed to move freely. Hoop residual stresses with different lay-ups and with viscoelastic analysis of entire cure cycle and elastic analysis of the cool-down phase alone through the thickness of the tube are presented in Figure 4.4. From Figure 4.4 the stress discontinuities can be observed in the interfaces of aluminium liner and first composite layers (at wall thickness 0.4) and between varying directed and 90° plies (wall thickness 0.8).

Figure 4.4 shows that elastic cool-down phase model over-predicts the residual stress state with all analysed lay-ups compared to the corresponding viscoelastic models simulating the whole cure cycle. The same behaviour was also noted in the longitudinal and radial residual stress components with different lay-ups. Differences between stess components obtained with the elastic cool-down phase

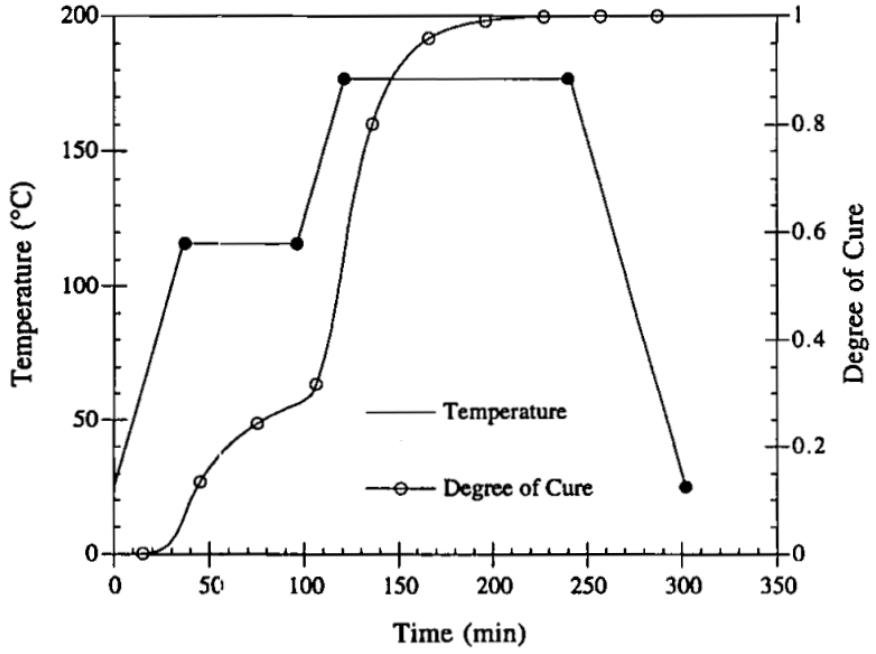


***Figure 4.3:*** *Cure cycle temperature and degree of cure evolution for AS4/3501-6 carbon fibre epoxy prepreg. The temperature change during the cool-down phase is* $\Delta T = -152\,^{\circ}C$. *[38]*

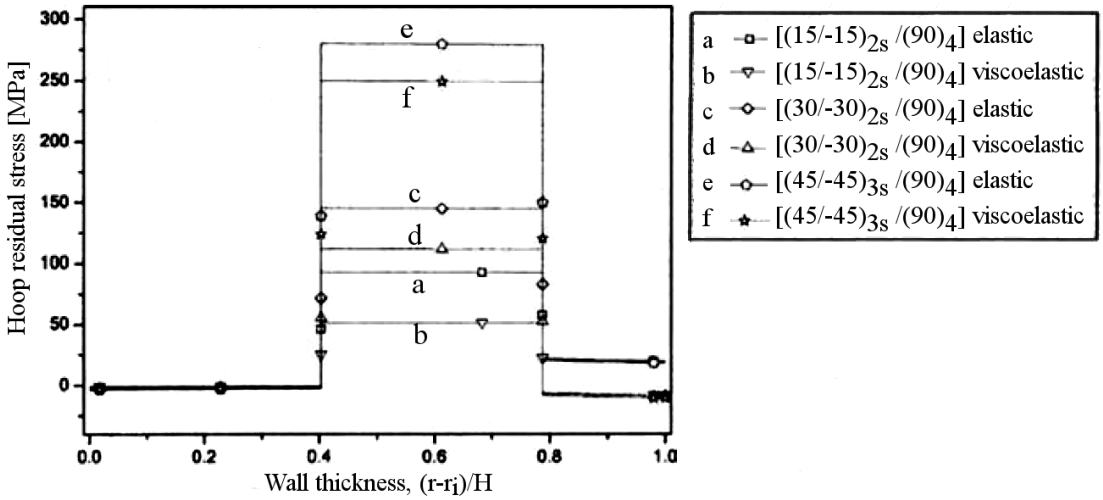


***Figure 4.4:*** *Hoop residual stresses for composite cylinder with aluminium liner inside with different AS4/3501-6 prepreg composite lay-ups. In elastic models only cool-down phase of the manufacturing cycle was studied whereas for viscoelastic models the whole cure cycle was studied. Elastic cool-down phase analyses over-predict the residual stress state with every lay-up compared to the viscoelastic full cure-cycle models, as elastic cool-down phase models neglect stress relaxation and chemical shrinkage. [38]*

model and viscoelastic full cure cycle model are presented in Table 4.3. It should be noted that for the radial stresses the actual stress values were only between 0 and -1.0 MPa, even though percentual differences were noted to be large. For longitudinal and hoop stresses the values varied between 0 and 300 MPa. Based on these results it can be said that for the studied case the use of viscoelastic stress models is necessary, if accurate results are wanted with all lay-ups. [38]

***Table 4.3:*** *Differences from the stress analysis for elastic models for cool-down phase alone and viscoelastic models for the whole cure cycle with different lay-ups. Elastic cool-down phase simulations predicted larger stresses with all lay-ups. The actual stress values for longitudinal and hoop stresses vary between 0 and 300 MPa, whereas for radial stresses only between 0 and -1.0 MPa. [38]*

| | Difference between viscoelastic and elastic analyses | | |
|---|---|---|---|
| Lay-up | Hoop stress | Longitudinal stress | Radial stress |
| $[(15/\text{-}15)_{2s}/90_4]$ | 80% | 29% | 110% |
| $[(30/\text{-}30)_{2s}/90_4]$ | 20% | 11% | 50% |
| $[(45/\text{-}45)_{3s}/90_4]$ | 10% | 10% | 20% |

Kim *et al.* [37] have also studied residual stress formation in filament wound composite cylinders using a viscoelastic constitutive model with the entire cure cycle, with cool-down phase alone and using an elastic constitutive model with cool-down phase alone. As the composite was considered thin, uniform temperature distribution throughout the cylinder corresponding the cure cycle temperature was assumed, and resin heat generation was neglected. The studied cure cycle was similar to the previously presented: hold periods at temperature of 115 °C for 60 minutes and at temperature of 177 °C for 120 minutes and a cool-down phase resulting in total temperature change of $\Delta T = -152$ °C (see figure 4.3). Also similar model for the degree of cure of the 3501-6 epoxy resin was used (see Section 3.3.1). A cross-ply $[0/90]_T$ laminate, where 0-direction is the longitudinal direction and 90-direction is the hoop direction and subscript $T$ denotes top location, from AS4/3501-6 carbon fibre/epoxy resin prepreg was simulated to be manufactured on an aluminium mandrel. Material properties for the AS4/3501-6 carbon fibre epoxy resin prepreg were as previously presented (see Table 4.2). For separation of the components after curing, a thin Teflon film was used between composite and mandrel. The behaviour due to the film was modelled between composite and mandrel, allowing slipping in the longitudinal ($z$-axis) direction. In addition, if the radial stress became positive during the analysis, separation was simulated. Used material properties for the aluminium mandrel and Teflon film are presented in Table 4.4. Due to the axisymmetry, only a cross-section in the $rz$-plane of the cylinder was modelled, as presented in Figure 4.5, with total number of 400 isoparametric ring elements.

Stress results for analysis with the elastic model for cool-down phase alone and for analysis with the viscoelastic models for different cases in radial ($\sigma_r$),

***Table 4.4:*** *Aluminium mandrel and Teflon film material properties. [37]*

| Material property | Aluminium mandrel | Teflon film |
|---|---|---|
| $E$ [GPa] | 72.4 | 0.312 |
| $\nu$ [-] | 0.3 | 0.35 |
| $CTE$ [$10^{-6}$/°C] | 23.6 | 23.6 |

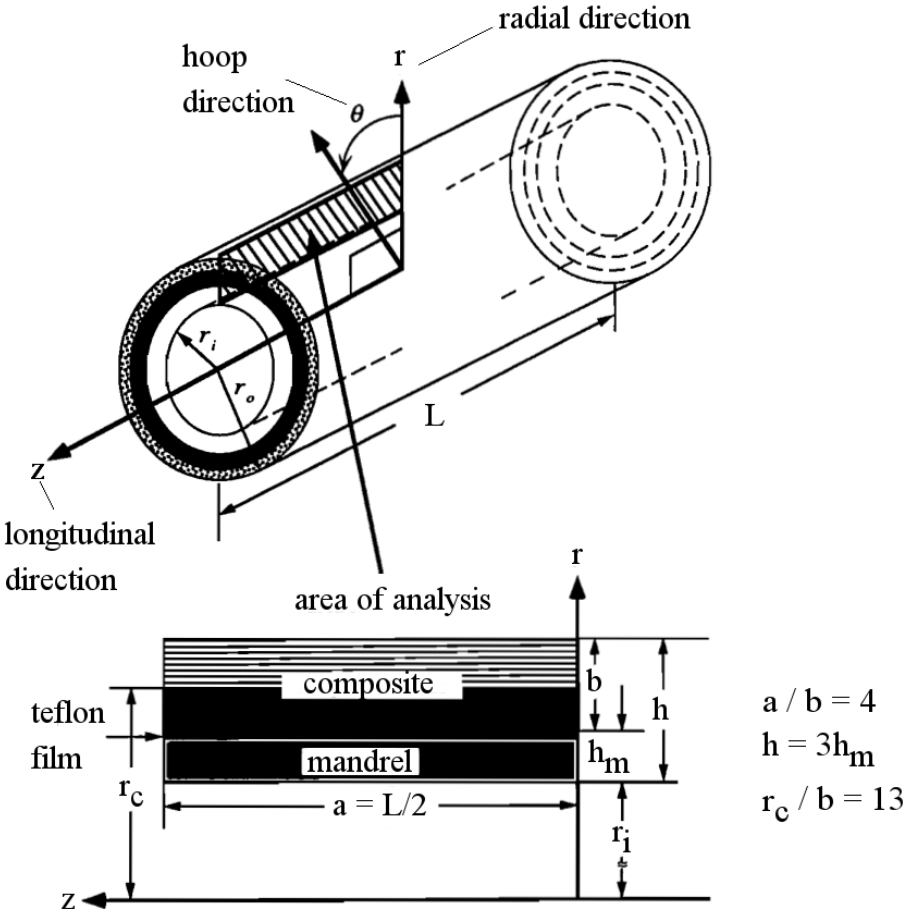


***Figure 4.5:*** *Analysis area for axisymmetric cylinder with cross-ply composite manufactured on mandrel. Thin teflon film separates composite and mandrel. Only half of the cylinder cross section was modelled in the length direction due to symmetry. [37]*

longitudinal ($\sigma_z$) and hoop ($\sigma_\theta$) directions in the middle of the cylinder in the longitudinal direction are presented in Table 4.5. The presented radial stresses are the maximum radial stresses, located approximately at the interface of 0°/90° layers in the thickness direction. The presented longitudinal and hoop stresses are calculated at the inner radius of the composite (in the analysis with mandrel this is the interface between composite 0° layer and Teflon film).

The obtained radial residual stresses are small compared to the longitudinal and hoop stresses. For the cool-down phase alone, differences between simulations with the elastic and viscoelastic models are approximately 20% for every stress component. Simulations with the elastic model give larger values, following the previously presented trend, as stress relaxation is not included. When the whole cure cycle is taken into account and the viscoelastic constitutive model is used, but mandrel restrictions and resin shrinkage are excluded, obtained residual stress values are further smaller, differences to the cool-down residual stresses with the elastic model being about 35%. Including resin shrinkage without mandrel, obtained radial stress is larger, only 8.3% different from the elastic solution for cool-down. Thus it can be said that cure shrinkage increases the total residual stresses formed during the manufacturing process. Introducing the restrictive effect of the mandrel but ignoring shrinkage, differences increase between 35% and 50%, indicating how the use of mandrel actually decreases residual stresses compared to the situation without mandrel. Finally, taking into account the whole cure cycle with mandrel effects and cure shrinkage, obtained residual stress values with viscoelastic constitutive model differ from 8.6% to 25% compared to results analysing the cool-down phase only with an elastic constitutive model. [37]

***Table 4.5:*** *Residual stress results for a filament wound composite cylinder with elastic (E) and viscoelastic (VE) models for cool-down phase only (CPO) and for entire cure cycle (ECC). Stresses are calculated with and without resin chemical shrinkage and mandrel. Longitudinal stress ($\sigma_z$) and hoop stress ($\sigma_\theta$) values are maximum values obtained at the inner radius of the cylinder, whereas radial stress ($\sigma_r$) is the maximum value obtained at the interface between 0° and 90° plies. "Diff." indicates the percentual difference when stress values with viscoelastic model are compared to the values with cool-down phase simulation using elastic model. [37]*

| Case | Mandrel / Shrinkage | $\sigma_\theta$ [MPa] | Diff. [%] | $\sigma_z$ [MPa] | Diff. [%] | $\sigma_r$ [MPa] | Diff. [%] |
|---|---|---|---|---|---|---|---|
| E, CPO | -/- | 40.0 | - | -38.3 | - | 1.45 | - |
| VE, CPO | -/- | 32.0 | -20.0 | -30.5 | -20.4 | 1.15 | -20.7 |
| VE, ECC | -/- | 26.0 | -35.0 | -25.4 | -33.7 | 0.94 | -35.2 |
| VE, ECC | -/x | - | - | - | - | 1.33 | -8.3 |
| VE, ECC | x/- | 20.3 | -49.3 | -25.0 | -34.7 | 0.74 | -49.0 |
| VE, ECC | x/x | 30.0 | -25.0 | -35.0 | -8.6 | 1.17 | -19.3 |

Obtained differences for the simulation of the cool-down phase alone with elastic constitutive model and full cure cycle simulation with viscoelastic model are approximately around the same magnitude, 10–30%, than in the study by Hwan *et al*. (see Table 4.3) with few exceptions. Differences result from unequal composite lay-ups, constraints between different material layers and mandrel/liner material parameters. However, for every case the analysis of cool-down phase alone

with elastic constitutive model gave larger residual stresses than the analysis of the full cure cycle with a viscoelastic constitutive model.

CHILE models have shown to give accurate results in multiple comparison cases when set against viscoelastic models. For example when comparing the residual stress state after multiple cure cycles for pure Hercules 8551-7 resin, maximum difference of 8% was found when results with a CHILE constitutive model were compared to the solutions obtained with viscoelastic models. [35] However, no comparison of viscoelastic and CHILE models for whole fibre reinforced composite parts was found from the literature.

### 4.3.2 Residual stress formation during cure cycle

Hwang *et al.* [38] studied also the residual stress evolution during the cure cycle for the presented AS4/3506-1 composite/aluminium liner hybrid cylinder with composite lay-up of $[(45/\text{-}45)_{3s}/90_4]$ (see Figure 4.2). Simulations were done with the previously presented simulation model using the viscoelastic constitutive model for the whole cure cycle (see Figure 4.3). Figure 4.6 presents the evolution of residual stresses during the curing and cool-down phase in the hoop direction as a function of cylinder wall thickness. Residual stresses are presented during the first temperature hold period (66 min, curve a), during the second temperature hold period (180 min, curve b), at the start of the cool-down phase (240 min, curve c), during the cool-down phase (280 min, curve d) and after the cool-down phase (300 min, curve e). The maximum stress value in the composite layers is reached during

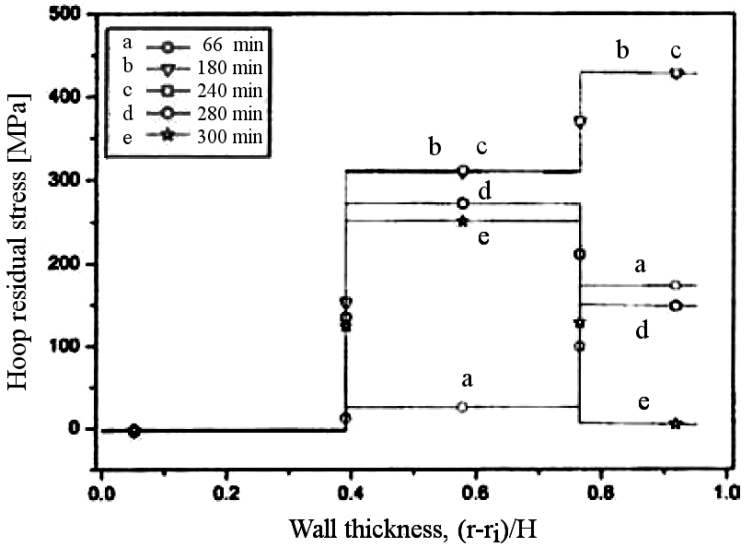


***Figure 4.6:*** *Hoop residual stress evolution during curing through the thickness of aluminium liner (wall thickness 0–0.4) and composite cylinder (wall thickness 0.4–1.0) with lay-up $[(45/\text{-}45)_{3s}/90_4]$. Final residual stress values are lower than the maximum values during curing. In aluminium liner and top composite layers (oriented in the 90-direction) final stress value is close to zero. [38]*

the second temperature hold period (curve b) and stays constant until the start of the cool-down phase (curve c). During the second temperature hold period, at 180 minutes, the degree of cure reaches value 0.98 and evolves to 1.00 before the start of the cool down phase. After this, the temperature starts to decrease from the cure temperature and also stress values decrease (curves d and e). The final residual stress values are smaller than these maximum values during curing: The hoop stress in the outer layer plies has maximum value around 430 MPa during cure (curves b and c) and after cool-down around 10 MPa (curve e). For inner plies, the difference is only from 310 MPa to 250 MPa. Largest stress discontinuity is in the interface of the aluminium liner and inner composite plies, at wall thickness 0.4. Behaviour of other residual stress components was found to be similar: largest stress values were obtained between times 180 minutes and 240 minutes and final residual stress values were significantly smaller.

Kim *et al.* [37] studied the residual stress formation with the previously presented composite cylinder manufactured from AS4/3501-6 prepreg with a lay-up $[0/90]_T$ on an aluminium mandrel (see Figure 4.5). Taking into account the mandrel interaction and cure shrinkage, the evolution of residual stresses during the curing and cool-down phase in the hoop direction is presented in Figure 4.7.

From Figure 4.7 it can be noted, how residual stresses may significantly evolve and also change from compressive to tensile or vice versa during the full cure cycle. For example, the hoop stress around relative thickness of 0.8 is during the cure approximately 140 MPa, but after cool-down -20 MPa. Largest stresses in the mandrel are formed in the hoop direction with the magnitude around -150 MPa before the cool-down starts, but decrease close to zero after the cool-down phase. Obtained results are in line with results presented by Hwang *et al.*: significantly larger residual stresses may evolve during the cure process when compared to final residual stresses after the cool-down phase. Reasons for this are restrictions from the cylinder itself (espescially if layers oriented in the hoop direction are used) and from the mandrel. Hoop-oriented fibres in the composite layers and the mandrel restrict the epoxy expansion during the temperature increases and the chemical shrinkage at the cure temperature and thus significant residual stresses are formed during the cure. [37]

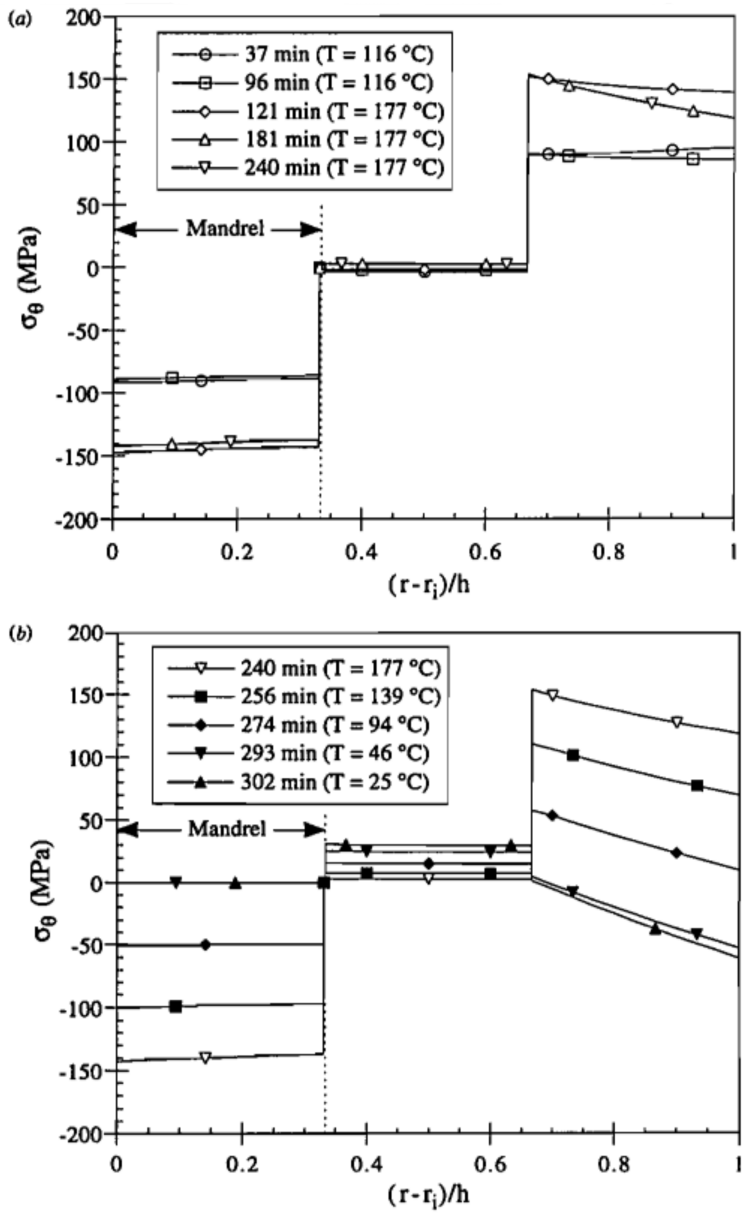


***Figure 4.7:*** *Hoop residual stress development in a cylindrical composite with lay-up [0/90] manufactured on an aluminium mandrel. (a): Stresses during curing. (b): Stresses during the cool-down phase. Very large stresses may occur during the cure before or during the cool-down compared to the final stress values. [37]*

# 5 Residual stress analysis of a roll structure

Residual stress formation in a paper machine roll structure is studied in the following chapters. As no detailed information about resin material viscoelastic behaviour or cure reaction parameters are known, only thermal residual stresses due to a temperature decrease in the cool-down phase of the manufacturing process are studied with a linear-elastic constitutive model. The roll structure is made of a steel cylinder coated with two glass fibre reinforced epoxy resin layers. In addition to the global residual stresses, the loading in the bond between the cylinder and bottom surface layer is studied with different surface layer edge geometries and loading conditions: (1) after residual stresses, (2) with rotational inertia and (3) in contact with another cylinder.

The total length of the steel cylinder is 15.4 metres and diameter is 0.8 metres. In order to simplify the simulation models, the cylinder is modelled as a solid part. The steel cylinder is coated with two layers of glass fibre composite: bottom layer, wound on the top of cylinder, is 5 millimetres thick. Second layer, called top layer, is 10 millimetres thick, and made of epoxy reinforced with non-woven glass fibre fabric. Dimensions and layers of the roll structure, marked with 1 (cylinder), 2 (bottom layer) and 3 (top layer) are presented in Figure 5.1.

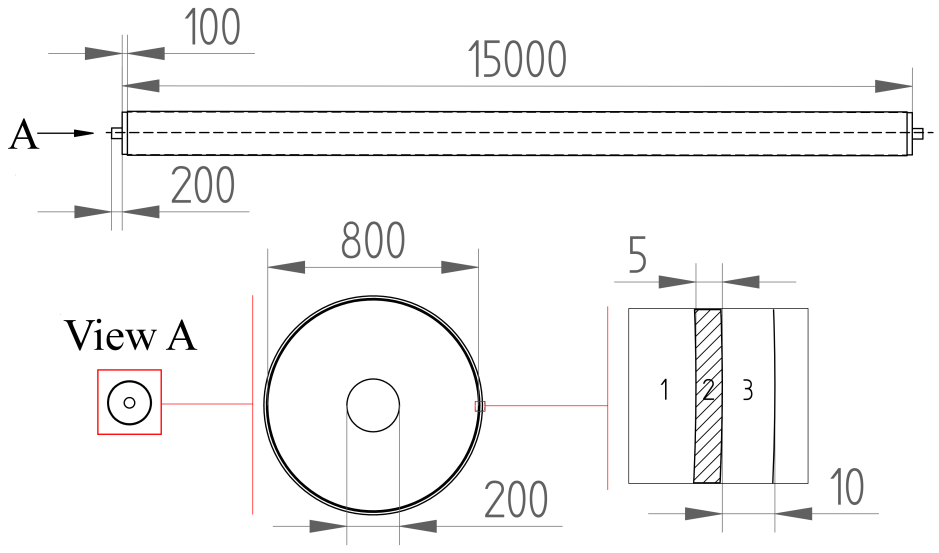


***Figure 5.1:*** *Roll structure dimensions and material layers. Cylinder is marked with number 1, bottom surface layer with number 2 and top surface layer with number 3. Dimensions are in millimetres.*

## 5.1 Analytical calculation

Longitudinal global thermal residual stresses in a simplified one dimensional roll structure model are first studied analytically. These analytical results can be compared with numerical results for validation purposes. Figure 5.2 on left presents a roll structure consisting of three different materials: cylinder material is marked with number 1, bottom layer material with number 2 and top layer material with number 3. In the middle in Figure 5.2, free material deformations after a temperature decrease $\Delta T < 0$ are shown. In order to satisfy deformation compatibility in the material interfaces, balancing forces $P_1$, $P_2$ and $P_3$ are applied to material layers, as presented in Figure 5.2 on right. Due to these balancing forces, a longitudinal stress component exists in each layer. Applied temperature difference, structure dimensions and one-dimensional material parameters for analytical calculation are presented in Table 5.1.

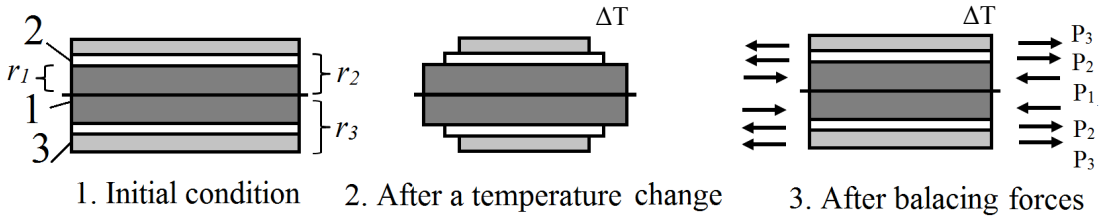


***Figure 5.2:*** *One-dimensional simplified analysis model for longitudinal residual stresses in a roll structure. Cylinder is marked with number 1, bottom surface layer with number 2, top surface layer with number 3 and layer radius values with r. 1. Initial stress-free condition. 2. Free deformations when temperature decreases and outer layers contract more than the cylinder due to larger CTE-values. 3. Balancing forces P applied to layers to balance the deformations.*

The free thermal strain after a temperature change in each layer can be expressed with equation:

$$\varepsilon_{T,i} = \Delta T \cdot CTE_i \tag{5.1}$$

where $\Delta T$ is the temperature change and $CTE_i$ is the one-dimensional thermal expansion coefficient in the layer. The strain due to the balancing forces, using Hooke's law, can be expressed as:

$$\varepsilon_{P,i} = \frac{P_i}{A_i E_i} \tag{5.2}$$

where $P_i$ is the balancing force, $A_i$ is the area of the layer cross-section and $E_i$ is the Young's modulus. Cross-section areas for circular cross-sections are now:

$$A_1 = \pi r_1^2, \qquad A_2 = \pi(r_2 - r_1)^2, \qquad A_3 = \pi(r_3 - r_2)^2 \tag{5.3}$$

where $r_i$ is the outer radius of each layer. The total strain in layer $i$ is the sum of thermal strain and balancing force strain:

$$\varepsilon_{Total,i} = \varepsilon_{T,i} + \varepsilon_{P,i}. \tag{5.4}$$

***Table 5.1:*** *Parameters for one-dimensional analytical calculation.*

| Parameter | Value |
|---|---|
| $\Delta T$ [°C] | -100 |
| $CTE_1$ [$10^{-6}$ 1/°C] | 12 [50] |
| $CTE_2$ [$10^{-6}$ 1/°C] | 25 [51] |
| $CTE_3$ [$10^{-6}$ 1/°C] | 50 [51] |
| $E_1$ [GPa] | 200 [52] |
| $E_2$ [GPa] | 12 [51] |
| $E_3$ [GPa] | 5 [51] |
| $r_1$ [m] | 0.400 |
| $r_2$ [m] | 0.405 |
| $r_3$ [m] | 0.415 |

Strain compatibility can be used to solve the unknown balancing forces. The total strains between the layers 1 and 2 and between the layers 2 and 3 are equal, and in addition the balancing forces are in balance in the longitudinal direction:

$$\begin{cases} \varepsilon_{Total,1} &= \varepsilon_{Total,2} \\ \varepsilon_{Total,2} &= \varepsilon_{Total,3} \\ P_1 &= P_2 + P_3 \end{cases}$$

$$\Leftrightarrow \begin{cases} \Delta T \cdot CTE_1 + \frac{P_1}{A_1 E_1} &= \Delta T \cdot CTE_2 + \frac{P_2}{A_2 E_2} \\ \Delta T \cdot CTE_1 + \frac{P_2}{A_2 E_2} &= \Delta T \cdot CTE_3 + \frac{P_3}{A_3 E_3} \\ P_1 &= P_2 + P_3 \end{cases} . \tag{5.5}$$

This equation group can be expressed in matrix format, where the balancing forces can be solved from:

$$\begin{Bmatrix} P_1 \\ P_2 \\ P_3 \end{Bmatrix} = \begin{bmatrix} \frac{-1}{A_1 E_1} & \frac{-1}{A_2 E_2} & 0 \\ 0 & \frac{1}{A_2 E_2} \frac{-1}{A_3 E_3} & \\ 1 & 1 & 1 \end{bmatrix}^{-1} \cdot \begin{Bmatrix} \Delta T \cdot (CTE_2 - CTE_1) \\ \Delta T \cdot (CTE_3 - CTE_2) \\ 0 \end{Bmatrix} . \tag{5.6}$$

Longitudinal stress in each layer can be calculated by using stress-force relation after knowing the balancing forces and layer areas:

$$\sigma_{z,i} = \frac{P_i}{A_i}. \tag{5.7}$$

## 5.2 Numerical calculation

The residual stress formation during the cool-down phase of the manufacturing process in the presented roll structure is simulated with Finite Element Method,

using commercial FEM-code Abaqus Standard 6.13-3. Linear-elastic material behaviour and temperature-independent material parameters are used in the simulations. Roll structure is assumed to be stress-free at the high cure temperature. The used coordinate system is presented in Figure 5.3. In text, $r$-direction is called radial direction, $z$-direction is called longitudinal (or axial) direction and $\theta$-direction is called circumferential (or hoop) direction.

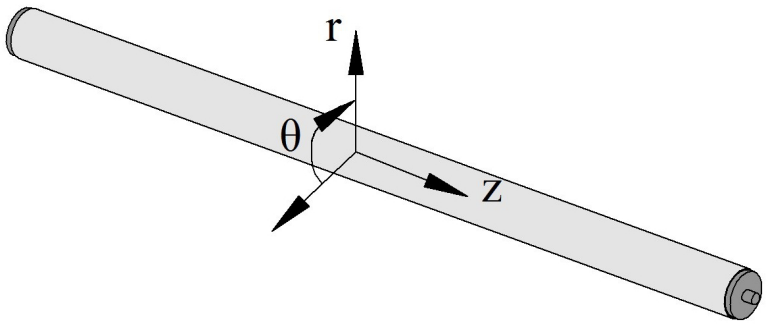


***Figure 5.3:*** *Coordinate system used in the numerical simulations. Shown r-direction is called radial direction, z-direction longitudinal (axial) direction and θ-direction circumferential (hoop) direction.*

Table 5.2 presents material property values including Young's moduli, Poisson's ratios, shear moduli and CTE values in different coordinate directions for structural steel and used glass fibre reinforced epoxy layers. Structural steel is isotropic material, whereas coating layers are orthotropic materials. Circumferential ($\theta$) and longitudinal ($z$) directions form the orthotropic plane in the surface layers.

***Table 5.2:*** *Material properties for structural steel cylinder and glass fibre/epoxy composite surface layers.*

| Material property | Cylinder: Structural steel | Bottom layer: Wound glass fibre / epoxy | Top layer: Glass fibre fabric / epoxy |
|---|---|---|---|
| $E_\theta, E_z$ [GPa] | 200 [52] | 12 [51] | 5 [51] |
| $E_r$ [GPa] | - | 3 [51] | 3 [51] |
| $\nu_{\theta z}$ [-] | 0.26 [52] | 0.1 | 0.1 |
| $\nu_{\theta r}$, $\nu_{rz}$ [-] | - | 0.3 | 0.3 |
| $G_{\theta z}$ [GPa] | - | 2 | 2 |
| $G_{\theta r}$, $G_{rz}$ [GPa] | - | 1.5 | 1.5 |
| $CTE_\theta$, $CTE_z$ [$10^{-6}$/°C] | 12 [50] | 25 [51] | 50 [51] |
| $CTE_r$ [$10^{-6}$/°C] | - | 70 [51] | 50 [51] |

A uniform temperature decrease in the roll structure from a stress-free manufacturing temperature of 150 °C to a service temperature of 50 °C is studied, leading to a temperature change $\Delta T$ = -100 °C. During the manufacturing process the roll structure is free to deform, and thus only the rigid body motion of the structure is prevented in the simulations. Cylinder and surface layers are perfectly bonded together. Basic information about the used simulation models are presented in this chapter. Appendix A presents further details about the models.

### 5.2.1 Case I: Global residual stresses

Three finite element models are created to simulate the residual stress formation in the longitudinal direction. The stress distribution near the structure end differs from the stress state at a longer distance from the end due to the cylinder and coating edge. An adequate distance for calculating global residual stress values, unaffected by the coating and cylinder edge, is studied with these models. First model, denoted as "full model", describes full three-dimensional geometry of the roll structure. The second model, denoted as "1/8 model", describes only one eighth of the full geometry by using longitudinal and transverse direction symmetry. The third model, denoted as "axisymmetric model", describes only one cross-section of the 1/8 model in a two-dimensional plane. Figure 5.4 shows schematically the geometries of these models (a) and how in Abaqus a three-dimensional axisymmetric model can be modelled in a two-dimensional plane, which is then rotated around the symmetry axis (b). With the help of symmetry, the same geometry can be presented with smaller amount of same-size elements, decreasing the amount of unknown variables and thus making simulations faster.

Figures 5.5, 5.6 and 5.7 present the element meshes and boundary conditions of the full model, 1/8 model and axisymmetric model, respectively.

Residual stresses with different longitudinal distances from the coating edge are calculated in the middle of top layer, in the middle of bottom layer and in the middle of half cylinder ($r_1/2$). Based on these results, global residual stress components in the circumferential ($\sigma_\theta$), longitudinal ($\sigma_z$) and radial ($\sigma_r$) direction are calculated in the constant stress area.

The global residual stress sensitivity to coating material CTE values and cylinder material is studied with the previously presented axisymmetric model (Figure 5.7). The maximum values of global residual stress components of the two surface layers are calculated at the constant residual stress area using 50% and 150% values of original CTE for bottom and top layers. CTE values are changed both simultaneously and individually for the top and bottom layers. Table 5.3 presents the original and modified CTE values for surface layers.

In addition to the different surface layer CTE values, global residual stresses between structural steel cylinder and cast iron cylinder are compared. Table 5.4 shows the material properties of these two materials.

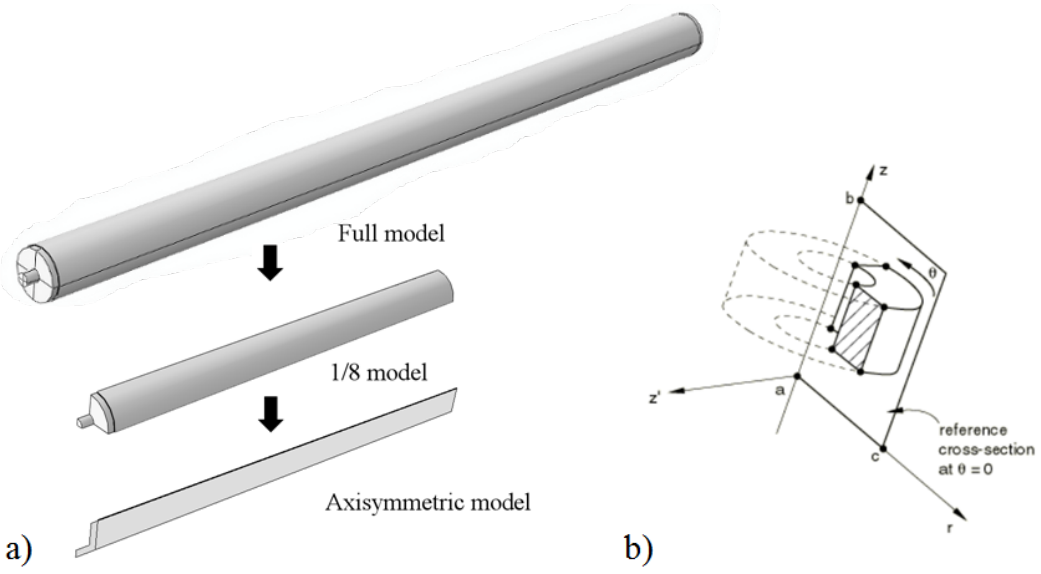


***Figure 5.4:*** *a) Full model, 1/8 model and axisymmetric model used in the simulations. By using symmetry the number of unknown variables can be decreased and simulations made faster. b) Axisymmetric modelling of a three-dimensional model in a two-dimensional plane which is rotated around the symmetry axis [53].*

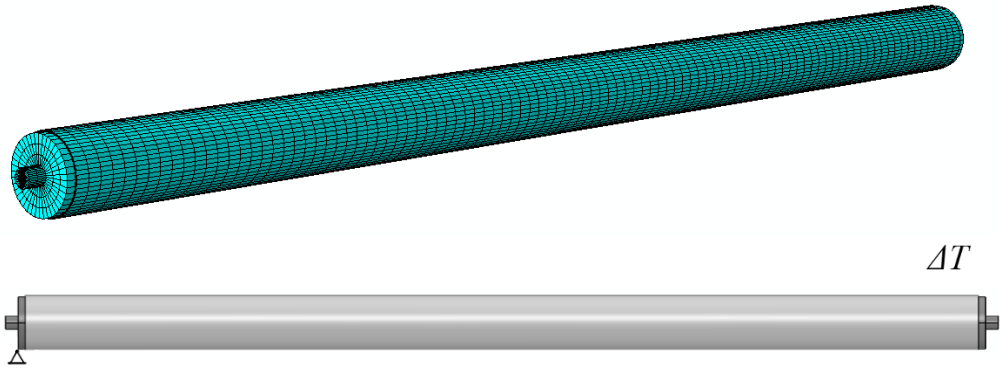


***Figure 5.5:*** *Element mesh (above) and used boundary conditions (below) of the full model describing the whole roll structure. Temperature difference $\Delta T$ is applied to the model and only rigid body motion of the model is prevented by binding one corner node.*

### 5.2.2 Case II: Coating bond loading

The shear stress distribution at the bond of the cylinder and bottom surface layer is studied with three different edge geometries: straight edge, chamfered edge with 45-degree angle and curved edge with radius of 17.5 mm, as shown in Figure 5.8. Cylinder is marked with number 1, bottom surface layer with number 2 and top surface layer with number 3, respectively. The edge area and bond shear stresses are studied in order to estimate the applicability of the three edge geometries.

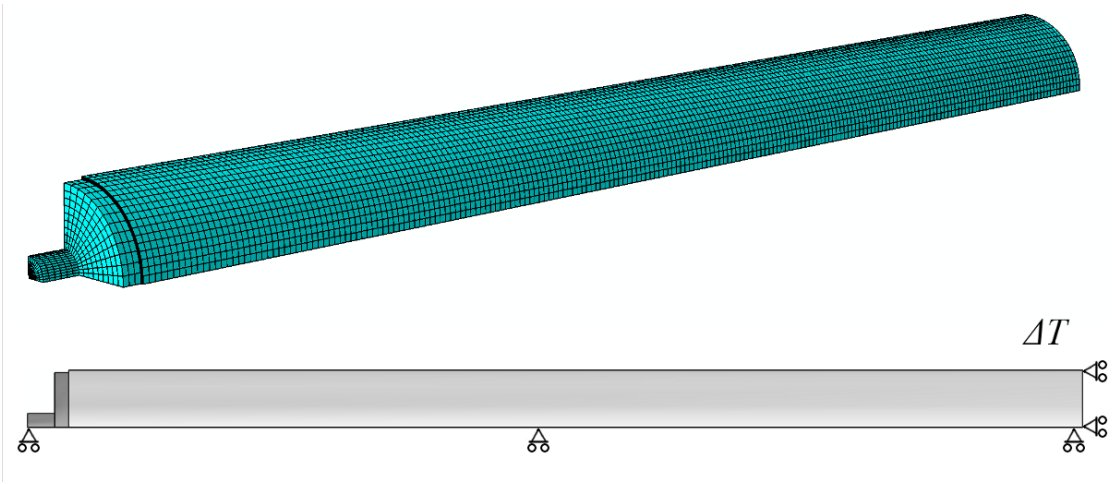


***Figure 5.6:*** *Element mesh (above) and used symmetry boundary conditions (below) of the 1/8 model describing one eighth of the full structure. Temperature difference $\Delta T$ is applied to the model.*

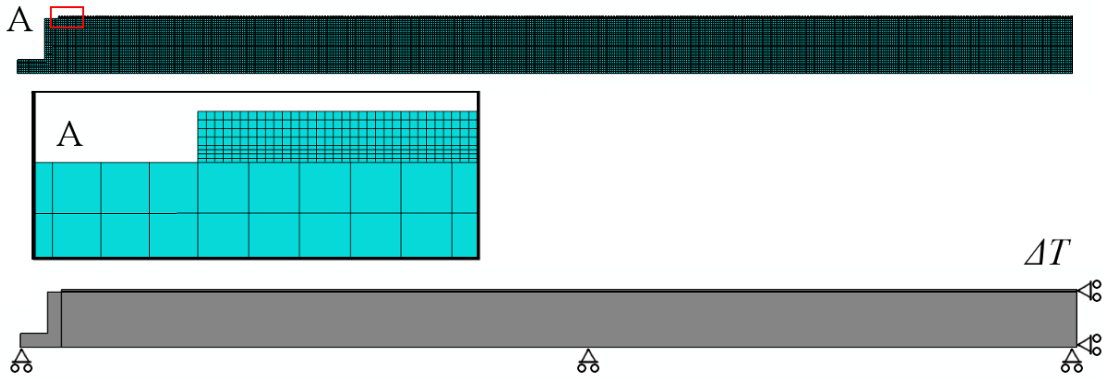


***Figure 5.7:*** *Element mesh (above) and used symmetry boundary conditions (below) of the axisymmetric model describing one cross-section of the 1/8 model. Temperature difference $\Delta T$ is applied to the model. Detail A shows the element mesh in the surface layers.*

***Table 5.3:*** *Original and modified surface layer CTE values for parametric study.*

| | Bottom layer | | Top layer |
|---|---|---|---|
| | $CTE_\theta$, $CTE_z$ | $CTE_r$ | $CTE_\theta$, $CTE_z$, $CTE_r$ |
| 50% of original [$10^{-6}$/°C] | 12.5 | 35 | 25 |
| Original value [$10^{-6}$/°C] | 25 | 70 | 50 |
| 150% of original [$10^{-6}$/°C] | 37.5 | 105 | 75 |

***Table 5.4:*** *Structural steel and cast iron material properties.*

| Material parameter | Structural Steel | Cast Iron |
|---|---|---|
| $E$ [GPa] | 200 [52] | 110 [54] |
| $\nu$ [-] | 0.26 [52] | 0.26 [54] |
| $CTE$ [$10^{-6}$/°C] | 12 [50] | 11 [50] |

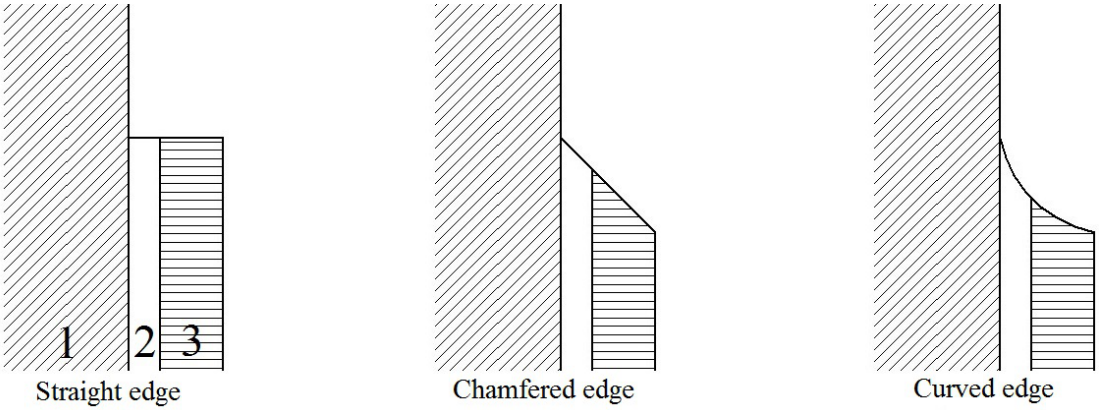


***Figure 5.8:*** *Studied three different edge geometries: straight edge, chamfered edge with 45-degree angle and curved edge with radius of 17.5 mm. Cylinder material is marked with number 1, bottom surface layer with number 2 and top surface layer with number 3.*

Axisymmetric finite element models with presented edge geometries are used for the simulations. 1.0 metres from the cylinder end is modelled, as the interest is to study the behaviour near the coating edge and as comparable meshes as possible are used. Figure 5.9 (a) shows the chamfered edge model boundary conditions and used mesh. Shear stress values are defined from 0.1 mm distance until 50 mm distance from the edge, as there exists mesh-sensitive shear stress peak right at the edge. In addition, the shear stress distributions at the region of coating edge are calculated to qualitatively compare stress distributions with different edge geometries.

Two types of cracks are studied in further analyses: edge and internal cracks in the cylinder and bottom surface layer bond with different lengths. These cracks simulate possible manufacturing defects or effects of bond corrosion, situations where the bottom surface layer is not bonded with the steel cylinder. The two crack types are shown in Figure 5.9 (b).

### Crack tip loading

Stress intensity factor $K$ is a parameter used to characterize the stress state near a crack tip. For each material and fracture mode, there exists a critical stress intensity factor, $K_c$, which can be determined experimentally. Crack propagates

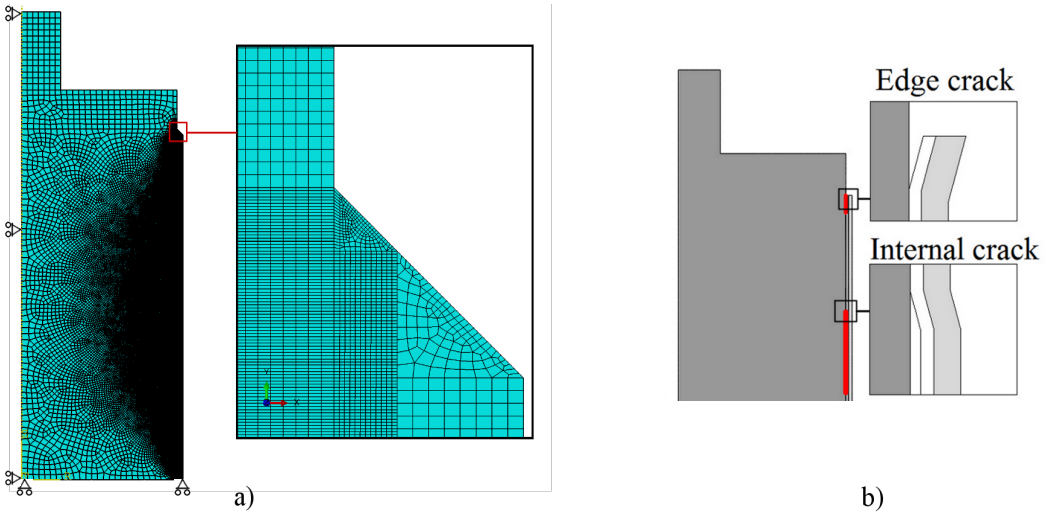


***Figure 5.9:*** *a) Chamfered edge geometry FE-model mesh and boundary conditions. b) Edge and internal cracks in the cylinder and bottom surface layer bond with exaggerated deformations near crack tips.*

when the stress intensity factor $K$ due to some loading state exceeds the material's critical stress intensity factor value $K_c$ in the corresponding loading state. Energy-based parameter for determining the loading state at the crack tip is called as strain energy release rate (SERR) $G$, which can be calculated from the stress intensity factor values. Similarly as with the stress intensity factors, crack grows when the SERR value due to a loading in material exceeds the material's critical SERR value $G_C$ in the corresponding loading. The strain energy release rate can be considered as a stored energy, which is released when the crack grows and critical SERR value as the energy needed to create a new crack surface. In this study, the loading state due to the residual stresses at a crack tip are estimated with total strain energy release rate, $G_T$. Total strain energy release rate can be calculated with equation:

$$G_T = G_I + G_{II} + G_{III} \tag{5.8}$$

where $G_I$ is the crack opening mode SERR value, $G_{II}$ is the in-plane shear mode SERR value and $G_{III}$ is the out-of-plane shear mode SERR value. These three modes are presented in Figure 5.10. In two-dimensional cases $G_{III} = 0$. The criticality of the crack tip loading depends on the proportional magnitude of different loading modes: experiments have shown that typically material's $G_C$ value under pure mode I loading is lower than under pure mode II loading. In mixed-mode loading the criticality depends on the mode ratio.

Virtual crack closure technique (VCCT) is a method to define the energy release rate with different crack situations. VCCT is based on the assumption that the energy released in the small crack extension process equals the work required to close the crack into the original length. With this assumption, the components of the strain energy release rate ($G_I$, $G_{II}$ and $G_{III}$) can be computed with finite element simulations giving the nodal forces and displacements at the crack area. [56]

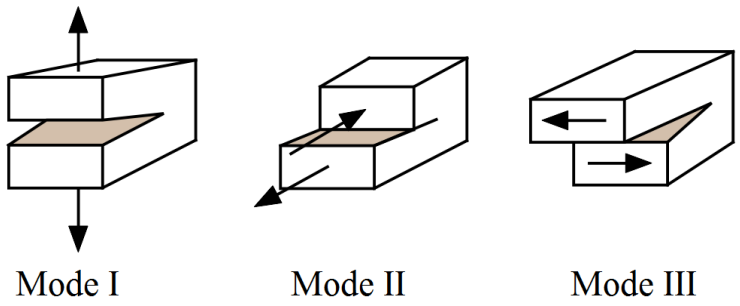


***Figure 5.10:*** *Fracture modes. Mode I: Crack opening mode. II: In-plane shear mode. Mode III: Out-of-plane shear mode. [55]*

In this study, only SERR-values for an initial crack (due to a manufacturing defect) are investigated, and crack propagation is prevented by using very high critical SERR values for the investigated bond. Also other techniques besides VCCT exist to evaluate strain energy release rate values, but VCCT was chosen due to the computational efficiency of the approach [56] and straightforward implementation in the Abaqus FEM-code.

First, the effect of initial crack size to the strain energy release rate value is studied by comparing the three different edge geometries and by changing initial crack length in the cylinder and bottom coating layer bond between 1–70 mm. Previously presented axisymmetric finite element models are modified to employ VCCT with different initial crack lengths. It should be noted that the initial crack is continuous through the whole circumferential length of the bond.

Crack tip loading mode mixity $\psi$, presenting the relative magnitude between the opening mode ($G_I$) and the in-plane shear mode ($G_{II}$) magnitude, can be expressed as:

$$\psi = atan\left(\frac{G_{II}}{G_I}\right). \tag{5.9}$$

Parameter $\psi$ gets the value 0° when only mode I loading is present, the value 45° when mode values are equal and reaches the value 90° when only mode II loading is present. The mode mixity value is studied as a function of initial crack length for different edge geometries.

For comparison of two- and three-dimensional crack cases and assessing the magnitude of mode III loading, total strain energy release rate values and individual components are also calculated by using three-dimensional model. A model with the same geometry as the axisymmetric model used for VCCT analyses is created with three-dimensional continuum elements using different edge cracks lengths.

### Rotational inertia effect

The roll structure rotates in a paper machine with a high angular velocity, typically 300–600 rounds per minute (RPM), corresponding to the velocity of 31–63 radians

per second. Due to the rotation, a centripetal force $F$ affects to the structure:

$$F = m\omega^2 r \tag{5.10}$$

where $m$ is the mass of the rotating part, $\omega$ is the angular velocity and $r$ is the radius from the rotation axis. The mass of roll structure components can be defined with the material density and volume. Typical density for structural steel is 7850 kg/m$^3$ [50] and for glass fibre reinforced epoxy 1750 kg/m$^3$ [57].

Centripetal force changes the loading state at the crack tip compared to the case where only residual stresses are present. This effect of rotational inertia to SERR values is studied with edge and internal cracks. Two edge cracks of lengths 8 mm and 40 mm and an internal crack with length 200 mm at a distance 300 mm from the coating edge are studied with angular velocities ranging from 0 to 2000 RPM (0–200 radians per second). The previously presented axisymmetric model with chamfered edge is used in the analysis, with two modifications: rotational body force is applied for the whole model and deformations at cylinder axis ends are restricted to describe the situation when the roll structure is installed to a paper machine. Mode mixity values are also calculated using the parameter $\psi$. For comparison of two- and three-dimensional modelling methods, total strain energy release rate values with a 40 mm crack are calculated also using previously described three-dimensional model by applying different angular velocities.

### Surface layer CTE effect

Strain energy release rate value sensitivity to different surface layer CTE values is studied by changing the top and bottom layer CTEs to 50 % and 150 % of the original value (see Table 5.3). 8 mm and 40 mm long edge cracks with chamfered edge geometry were studied with the presented axisymmetric model with VCCT.

### Nip effect

During the paper making process paper is compressed between two rolls. The effect of this part of the process is studied by pressing second cylinder (nip cylinder) against the roll structure (nip effect). The real paper making process is simplified by excluding dynamic effects and the paper and felts between the rolls from the simulations. The change in SERR values due to this nip effect in a roll structure loaded with residual stresses ($\Delta T$ = -100°C) and rotational inertia (600 RPM) is analysed. Half of three-dimensional roll structure end of length 2.2 metres and equal length quarter of a steel cylinder (diameter 0.80 metres), pressed against the roll structure, are modelled. Internal and edge cracks in roll structure with lengths 40 mm and 200 mm, respectively, are studied with chamfered edge geometry. For both cases the cracked surface goes around the whole cylinder circumference. SERR components and the total SERR value are computed around the cylinder circumference at the crack tip.

Transformations of the roll structure axis ends are prevented during the pressing. Nip roll movement is allowed only to the pressing direction and the contact between cylinders is defined ideal, i.e. frictionless behaviour in the tangential

direction and "hard" contact in the normal direction of the surfaces. Typical nip contact pressure is highly dependable on the nip type and position in the paper machine. However, for these analyses contact pressure is assumed to be between 1.8–3.5 MPa [58]. Six different pressing pressures (10 kPa, 20 kPa, 30 kPa, 40 kPa, 50 kPa and 100 kPa), denoted as cases I-VI, are applied to the nip roll upper surface to press the nip roll against the roll structure. The pressing pressure producing the assumed contact pressure value in the roll structure is used in the following analyses to calculate the SERR values at the crack tip and to compare these to the values without the nip effect. Figure 5.11 shows the finite element model mesh, boundary conditions and pressing direction used in the nip effect simulations.

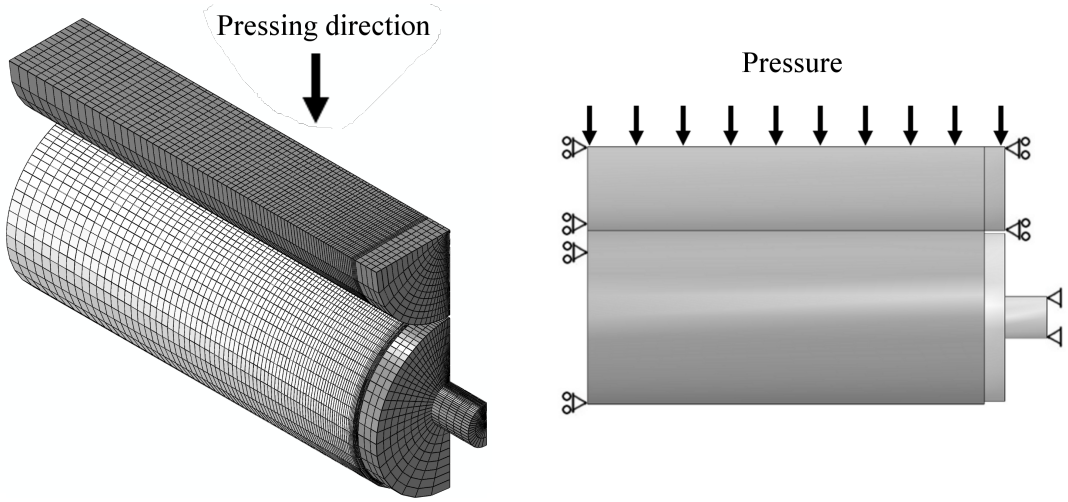


***Figure 5.11:*** *Finite element simulation model mesh and boundary conditions of the three-dimensional roll structure and nip roll. Only half of the roll structure end and one quarter of nip roll end are modelled with the help of symmetry. Pressure is applied to the upper surface of the nip roll to cause the nip effect.*

# 6 Results and discussion

## 6.1 Global residual stresses

### 6.1.1 Analytical calculation results

Layer balancing forces in one-dimensional analytical calculation (see Figure 5.2) are:

$$\begin{Bmatrix} P_1 \\ P_2 \\ P_3 \end{Bmatrix} = \begin{bmatrix} \frac{-1}{A_1E_1} & \frac{-1}{A_2E_2} & 0 \\ 0 & \frac{1}{A_2E_2}\frac{-1}{A_3E_3} & \\ 1 & 1 & 1 \end{bmatrix}^{-1} \cdot \begin{Bmatrix} \Delta T \cdot (CTE_2 - CTE_1) \\ \Delta T \cdot (CTE_3 - CTE_2) \\ 0 \end{Bmatrix}$$

$$= \begin{bmatrix} \frac{-1}{\pi(0.4\text{m})^2 \cdot 200\text{GPa}} & \frac{-1}{\pi(0.405\text{m}-0.4\text{m})^2 \cdot 12\text{GPa}} & 0 \\ 0 & \frac{-1}{\pi(0.405\text{m}-0.4\text{m})^2 \cdot 12\text{GPa}} & \frac{-1}{\pi(0.415\text{m}-0.4\text{m})^2 \cdot 5\text{GPa}} \\ 1 & 1 & 1 \end{bmatrix}^{-1}$$

$$\cdot \begin{Bmatrix} 100°\text{C} \cdot (25-12) \cdot 10^{-6} 1/°\text{C} \\ 100°\text{C} \cdot (50-25) \cdot 10^{-6} 1/°\text{C} \\ 0 \end{Bmatrix}$$

$$\approx \begin{Bmatrix} -7194 \\ 1225 \\ 5969 \end{Bmatrix} \text{N}.$$

Corresponding longitudinal residual stresses in different structure parts are:

$$\begin{Bmatrix} \sigma_{z,1} \\ \sigma_{z,2} \\ \sigma_{z,3} \end{Bmatrix} = \begin{Bmatrix} \frac{P_1}{A_1} \\ \frac{P_2}{A_2} \\ \frac{P_3}{A_3} \end{Bmatrix}$$

$$= \begin{Bmatrix} \frac{-7194\text{N}}{\pi \cdot (0.4\text{m})^2} \\ \frac{1225\text{N}}{\pi \cdot (0.405\text{m}-0.4\text{m})^2} \\ \frac{5969\text{N}}{\pi \cdot (0.415\text{m}-0.405\text{m})^2} \end{Bmatrix} \approx \begin{Bmatrix} -0.014 \\ 15.6 \\ 19.0 \end{Bmatrix} \text{MPa}.$$

The cylinder stress ($\sigma_{z,1}$) is compressive and close to zero, whereas for bottom ($\sigma_{z,2}$) and top ($\sigma_{z,3}$) surface layers the stresses are tensile and significantly larger. CTE values for surface layers are larger than for the cylinder, so surface layers try to contract more than the cylinder. However, larger and stiffer cylinder opposes the surface layer contraction, and higher tensile stresses are formed in the surface layers and smaller compressive stress in the cylinder.

### 6.1.2 Finite element simulation results

Figure 6.1 presents the circumferential residual stress component in different roll structure components as a function of longitudinal distance from the coating edge calculated with the full model, 1/8 model and axisymmetric model. Figure 6.2 presents corresponding longitudinal stresses and Figure 6.3 radial stresses. The presented stresses are calculated in the middle of each layer in the thickness direction. There exists variation in stress values in different models due to different elements and mesh refinement level. However, all stress values reach approximately the same level, but in full and 1/8 models after a longer distance than in the axisymmetric model with more refined mesh, as clearly seen in Figure 6.2. According to these Figures, residual stress values stabilise after a distance of 0.30 metres from the coating edge with axisymmetric models, where mesh is most refined. Thus, global residual stress values neglecting edge effects can be defined by using at least 30 cm distance from the coating edge with approriate mesh refinement level.

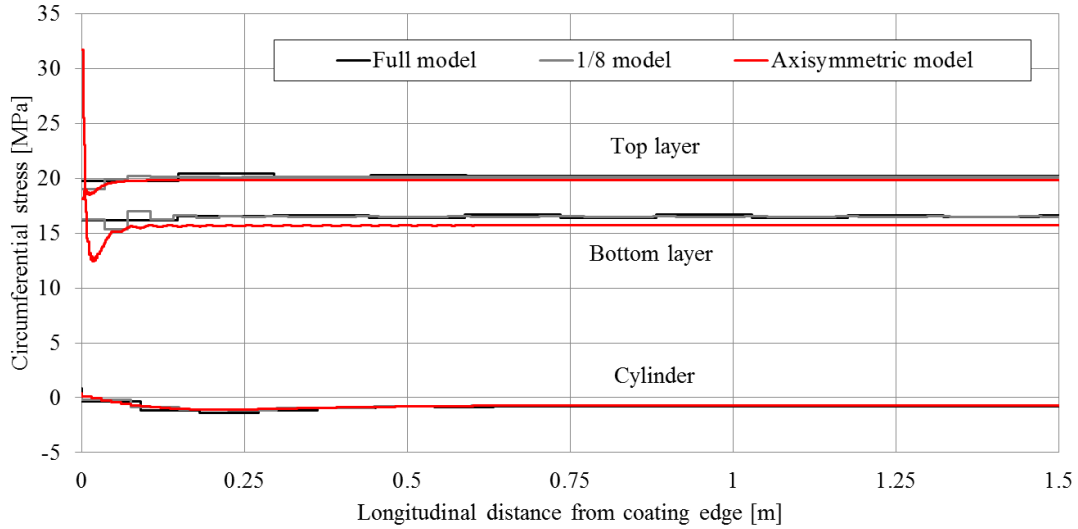


***Figure 6.1:*** *Residual stress in the circumferential direction as a function of the longitudinal distance from the coating edge in different roll structure parts.*

Figures 6.4, 6.5 and 6.6 present global residual stress components in the circumferential, longitudinal and radial direction at the distance of 0.5 metres from the coating edge. Stresses are elemental stresses presented as a function of the radial coordinate of the roll structure. A good agreement between the global residual stress results with different simulation models is shown in the figures. Thus, representative modelling can be done with a two-dimensional axisymmetric model, which provides the fastest computation. Differences can be explained with different mesh densities (and element types).

Table 6.1 summarises the maximum values of global residual stress components in the roll structure parts. Circumferential and longitudinal stresses in the surface layers are tensile and in the cylinder compressive. Radial stresses in all parts and all cylinder stress components are small.

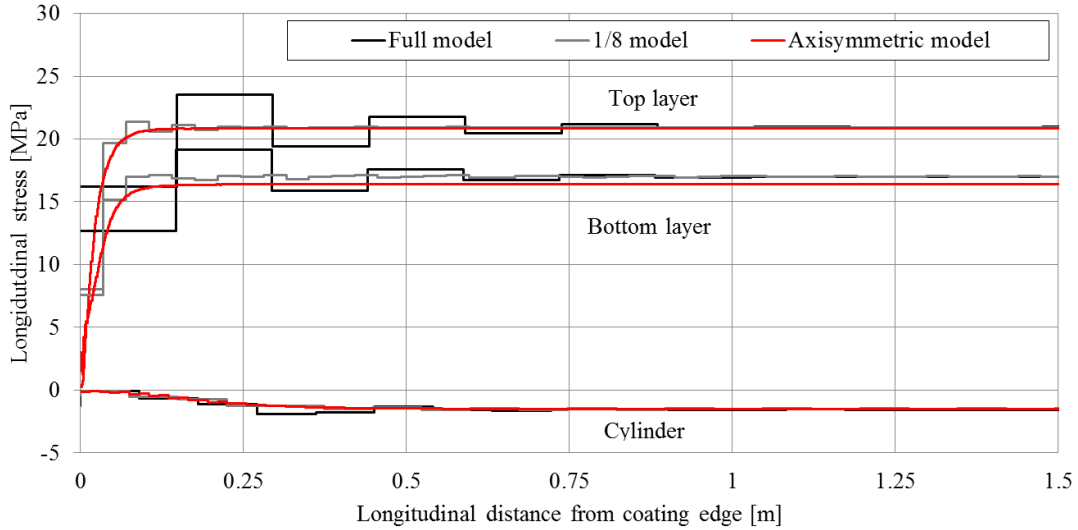


***Figure 6.2:*** *Residual stress in the longitudinal direction as a function of the longitudinal distance from the coating edge in different roll structure parts.*

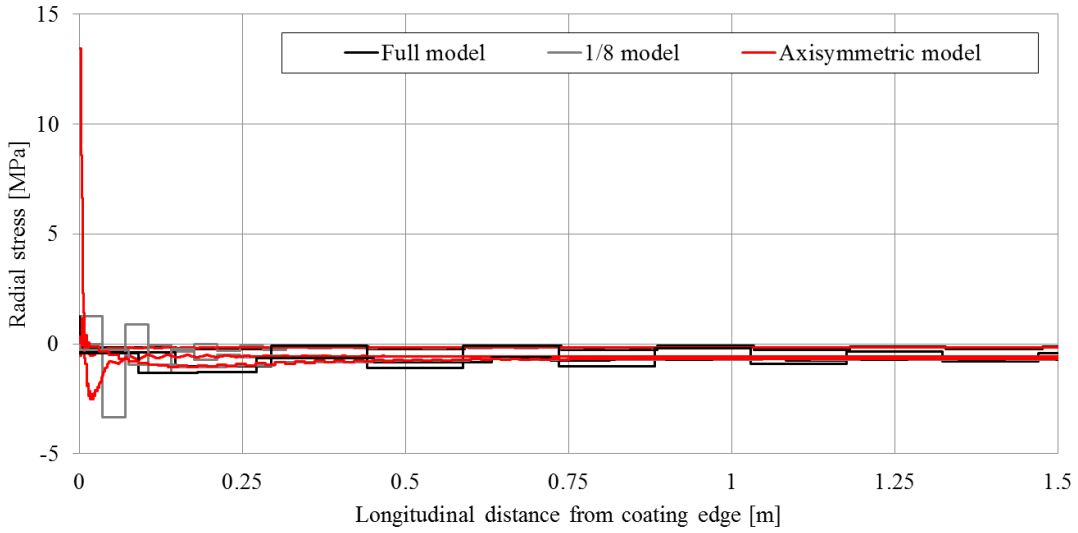


***Figure 6.3:*** *Residual stress in the radial direction as a function of the longitudinal distance from the coating edge in different roll structure parts.*

***Table 6.1:*** *Global residual stress values in surface layers and cylinder.*

| Stress component | Cylinder (1) | Bottom layer (2) | Top layer (3) |
|---|---|---|---|
| Circumferential stress $\sigma_\theta$ [MPa] | -0.83 | 16.25 | 20.17 |
| Longitudinal stress $\sigma_z$ [MPa] | -1.60 | 17.22 | 21.17 |
| Radial stress $\sigma_r$ [MPa] | -0.72 | -0.58 | -0.33 |

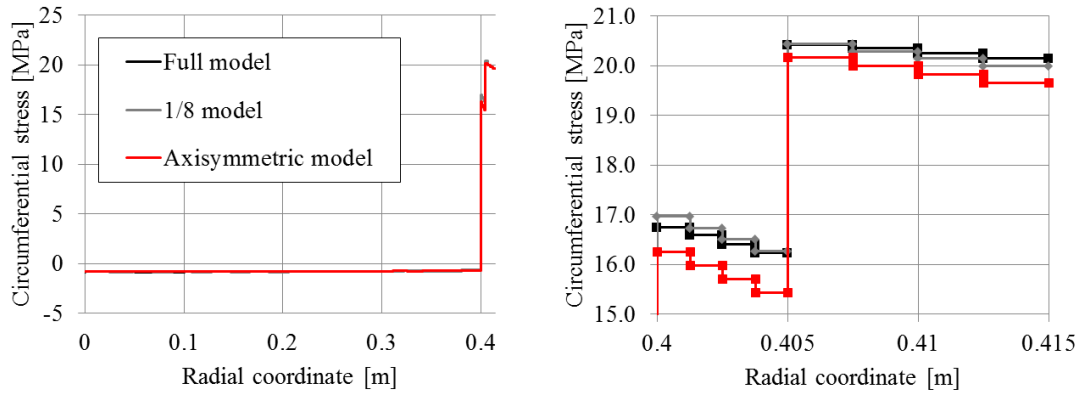


***Figure 6.4:*** *Circumferential residual stress at distance of 0.5 from the coating edge with different simulation models as a function of radial coordinate.*

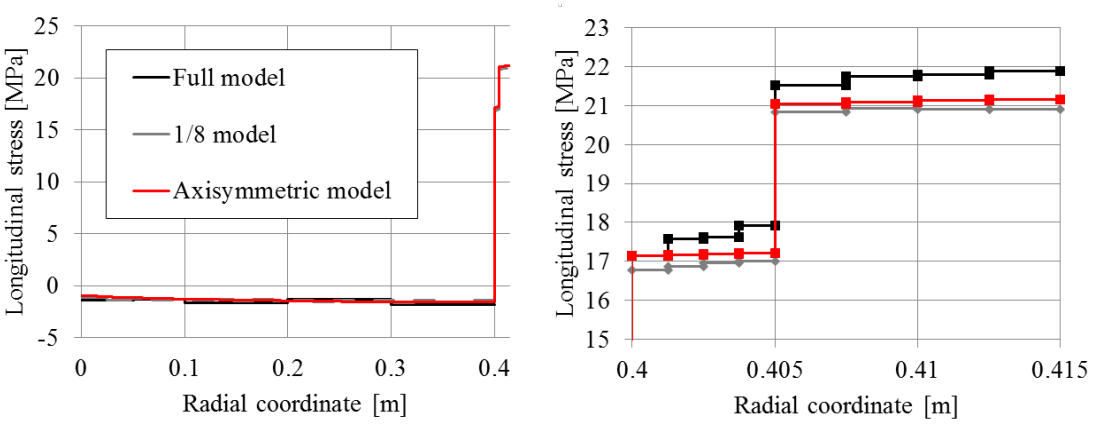


***Figure 6.5:*** *Longitudinal residual stress at distance of 0.5 from the coating edge with different simulation models as a function of radial coordinate.*

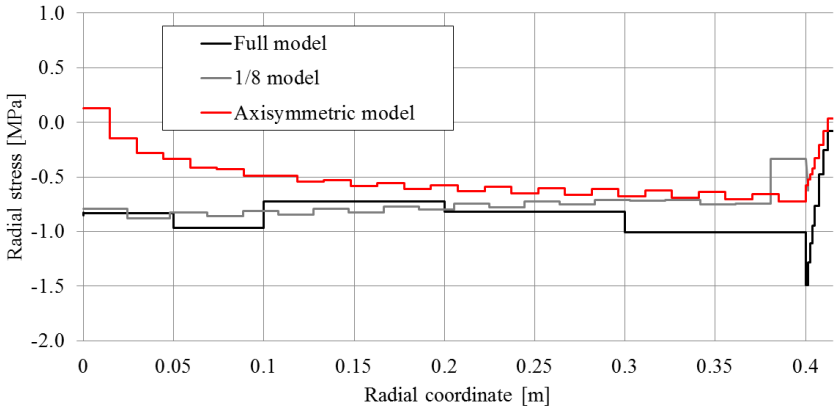


***Figure 6.6:*** *Radial residual stress at distance of 0.5 from the coating edge with different simulation models as a function of radial coordinate.*

The difference between longitudinal residual stress component in analytical calculation and presented numerical simulation in cylinder ($\sigma_{z,1}$), bottom layer ($\sigma_{z,2}$) and top layer ($\sigma_{z,3}$) are:

$$\begin{Bmatrix} \sigma_{z,1} \\ \sigma_{z,2} \\ \sigma_{z,3} \end{Bmatrix} = \begin{Bmatrix} 99.1 \\ 9.40 \\ 10.2 \end{Bmatrix} \%.$$

The difference in bottom and top surface layer stress values between analytical and numerical calculations is approximately 10%, verifying that same mechanical phenomenon is analysed in both cases. However, the difference between cylinder stress values is significant. Reason for this difference is considered to rise from the simplifications related to the one-dimensional analysis, which exclude three-dimensional Poisson's effects making the cylinder stiffer in numerical analyses. The $\sigma_{z,1}$ is constant for the analytical analysis. The absolute value of the cylinder stress component is negligible compared to the surface layer stress components.

The magnitude of residual stresses in surface layers seems not critical. A typical ultimate tensile strength value for a cured epoxy or polyester is 50–70 MPa and for E-glass fibre reinforced polyester mat laminates with fibre mass fraction of 25% around 83 MPa. [57] The tensile strengths of used materials are not known, but the presented typical values can be used as reference values. The obtained residual stress values around 20 MPa are well below these reference ultimate values.

### 6.1.3 Parametric study

Figure 6.7 presents residual stress components with two cylinder materials, cast iron and structural steel. Cylinder material has only a small influence on the residual stress state in the surface layers: stresses are smaller with the steel cylinder than with the cast iron cylinder, but differences are around 0.5–1.0 MPa in the top layer for axial and circumferential stress components. In the bottom surface layer the differences are approximately 1.0–2.0 MPa.

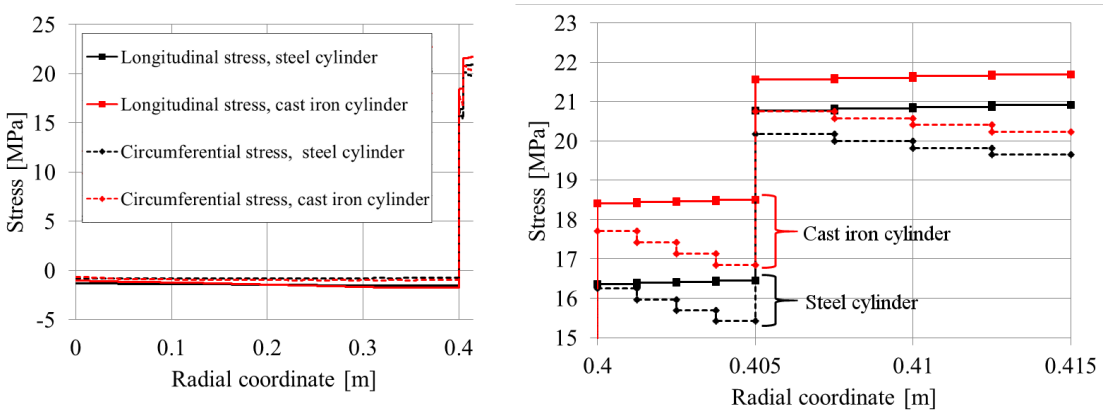


***Figure 6.7:*** *Global residual stress components with structural steel and cast iron cylinders.*

The longitudinal and circumferential stress values as a function of coefficient of thermal expansion for top and bottom layers is presented in Figure 6.8. Results are shown for the case where CTEs of both layers are changed simultaneously. If only one layer CTE is changed, behaviour in this layer is similar as presented in Figure 6.8, and the stress state in the other layer does not significantly change from the original value. Stress in the cylinder was not affected by changing CTE of the surface layers. Results show that increasing surface layer CTE values further increases the residual stress values, as the difference between cylinder and surface layer CTE values becomes larger. Residual stresses change linearly with the CTE values. However, critical stress levels are not reached even with using the 150% values of original layer CTE values.

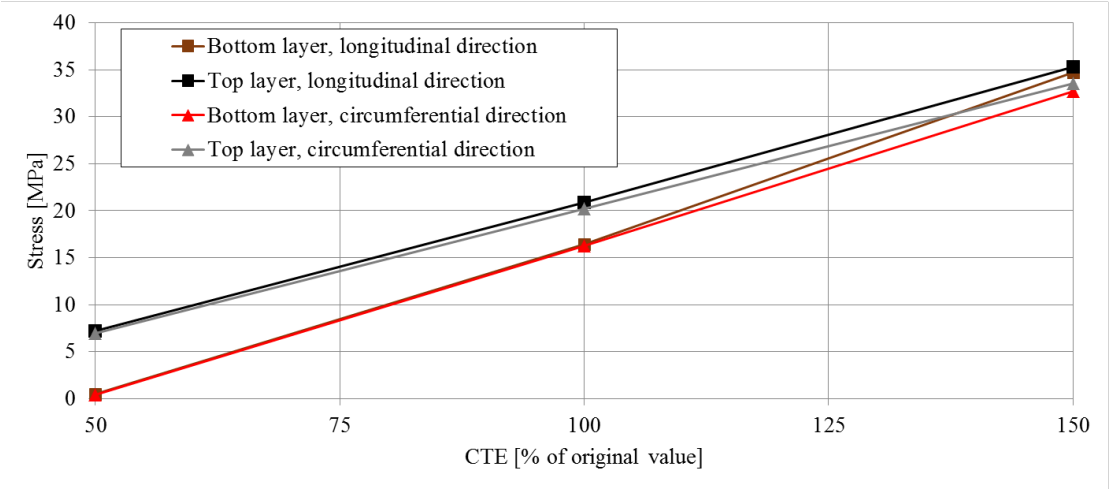


***Figure 6.8:*** *Stress in the longitudinal and circumferential direction as a function of layer CTE values. CTE values for both layers are changed simultaneously.*

## 6.2 Coating bond analysis results

### 6.2.1 Shear stress distribution

Figure 6.9 shows the shear stress absolute value distribution near the coating edge with different edge geometries. With the straight and chamfered edge a peak shear stress value is located at the edge of the cylinder and bottom surface layer bond, whereas for the curved edge the peak value, smaller in magnitude, is located in the bond of the two surface layers.

Figure 6.10 shows shear stress values in the bond line, starting from distance 0.5 mm from the edge until distance of 50 mm. Defining the shear stress peak value right at the coating edge is difficult, as shear stress values were found to be mesh-dependent due to local stress singularity at the sharp edge. The straight edge geometry has the largest absolute shear stress value near the edge. Edge geometry effects diminish rather quickly as the distance from edge is increased, and after a distance of 20 mm shear stress values are approximately same with

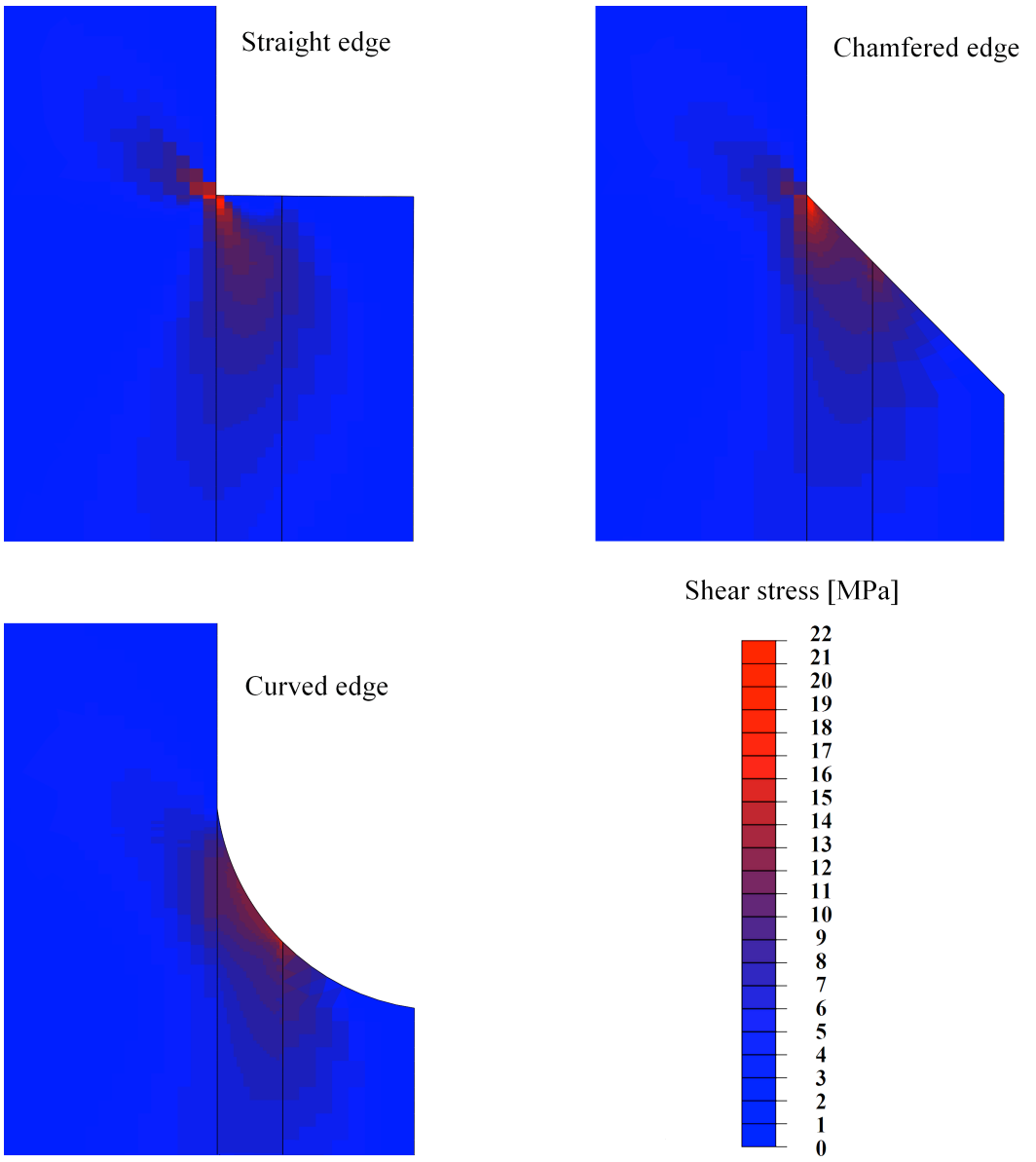


***Figure 6.9:*** *Absolute shear stress distribution near the coating edge with the three different edge geometries. With straight and chamfered edge the peak value is located at cylinder and bottom surface layer bond, whereas for curved edge at the bond of bottom and top surface layers.*

each edge geometry. Straight edge has the largest stress peak value, chamfered edge the second largest value and curved edge the smallest value. If possible, rounding should be used when the surface layer edge is finished, as this decreases the shear stress level in the bond line.

The shear strength value for the studied bond is not known. Therefore, reference values from the literature are used: joint strength for Araldite Standard epoxy adhesive and AISI 304 stainless steel adherends is reported to be 20–30 MPa [59] and for Araldite 2015 epoxy and low carbon steel joints around 15–30 MPa [60],

but also smaller values have been reported for epoxy/steel joints. The obtained bond shear stress values with straight and chamfered edge are close or in the area of these typical critical values. Thus, fracture mechanics based approach is used to further evaluate the criticality of the bond between the cylinder and bottom surface layer.

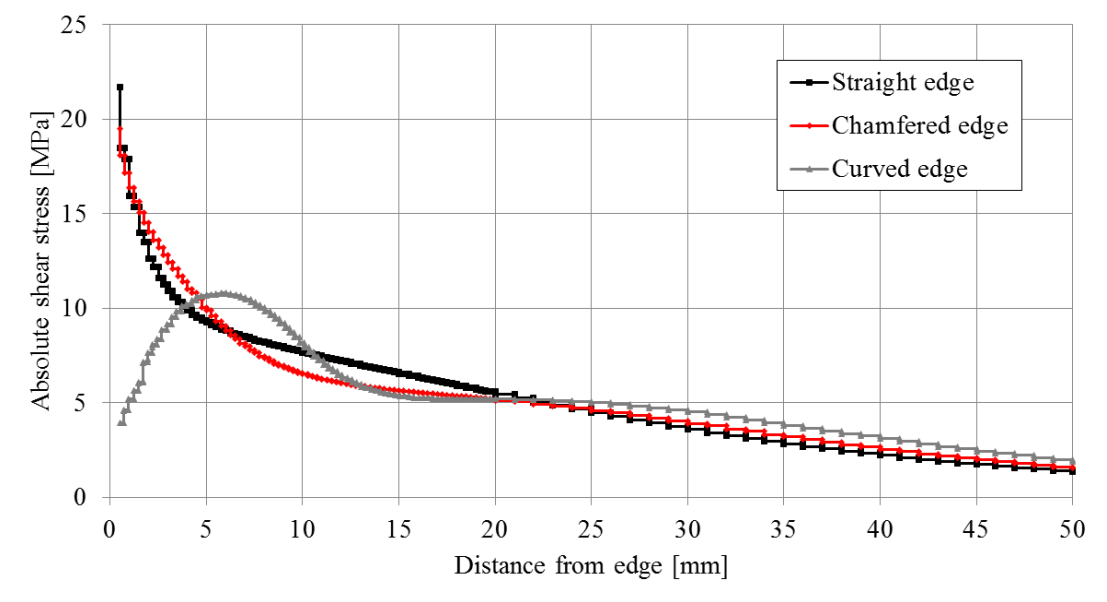


***Figure 6.10:*** *Shear stress absolute values along the cylinder and bottom surface layer bond line with different edge geometries.*

### 6.2.2 Bond fracture

Total strain energy release rate values ($G_T$) with the three different edge geometries and different initial crack lengths are presented in Figure 6.11. For each edge geometries $G_T$ reaches approximately the same largest value, around 460 J/m$^2$, but with different crack lengths. For straight edge geometry this crack length is around 2 mm, for chamfered edge geometry 8 mm and for curved edge geometry 12 mm. After the maximum value, total strain energy release rate values decrease close to the value 280 J/m$^2$ and start then to increase again with longer crack lengths towards the value 400 J/m$^2$.

Figure 6.12 shows the fracture mode mixity $\psi$ as a function of crack length with different edge geometries. All edge geometries follow the same trend: as the initial edge crack length is increased, mode II loading becomes more dominating, until around crack length of 60 mm loading is almost pure mode II for all geometries. Maximum SERR value is reached with mode mixity of approximately 6° with every edge geometry.

Material system's critical strain energy release rate value depends on the mode mixity ratio. The critical value for the studied material system is not known. However, a glass fibre reinforced epoxy laminate with a lay-up of +45/-45 bonded

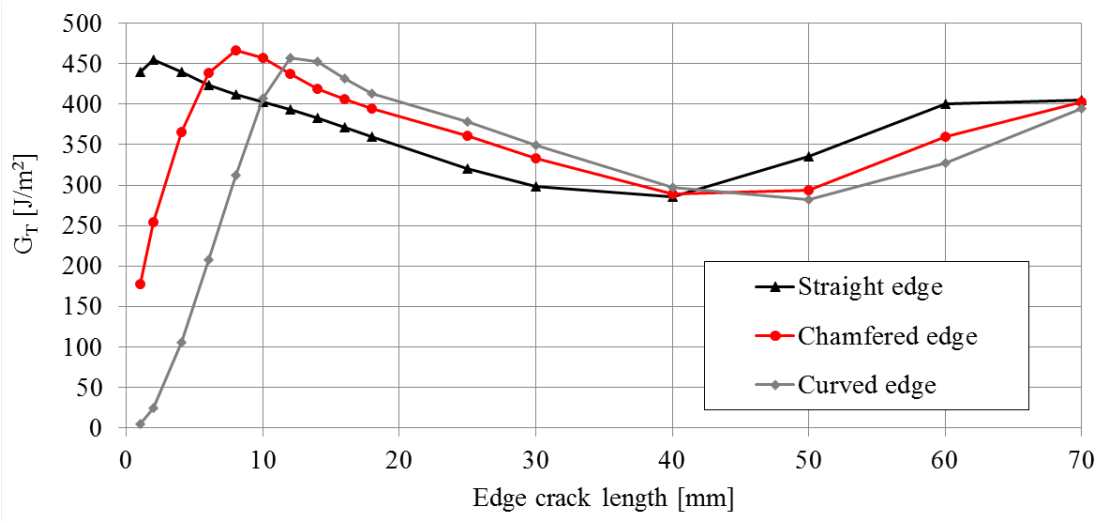


***Figure 6.11:*** *Total strain energy release rate values $G_T$ with different edge geometries and initial crack lengths.*

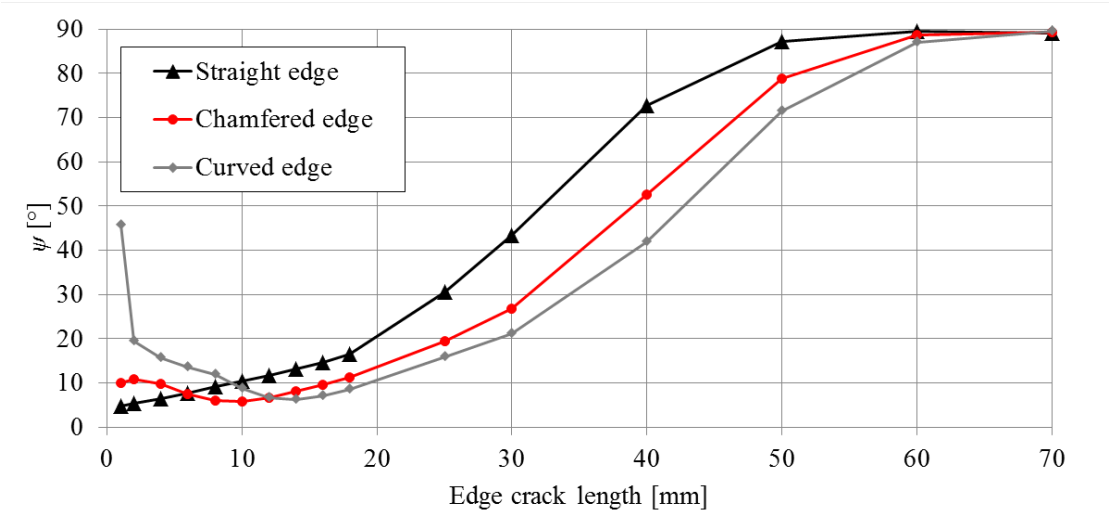


***Figure 6.12:*** *Mode mixity $\psi$ with different edge geometries and edge crack lengths.*

to a steel plate with epoxy adhesive has been studied experimentally by Gong *et al.* [61]. Experimentally determined average critical SERR value with mode mixity ratio corresponding of 6° was around 400 J/m$^2$ [61]. Based on the made study, obtained total strain energy release rate values with all edge geometries are over the typical critical value of the corresponding material system. An initial crack with adequate length will thus grow due to the loading by the residual stress state.

Figure 6.13 shows the differences in total strain energy release rate values and individual components with two- and three-dimensional models. Total SERR-values are very close to each other, even though mode I values are slightly smaller

and mode II values slightly larger with two-dimensional models for every case. Unequal mesh refinement and different elements are believed to be the reason for variation in the SERR component values. However, results show that two-dimensional and three-dimensional models provide approximately equal strain energy release rate values and that mode III component is not significant in the studied case.

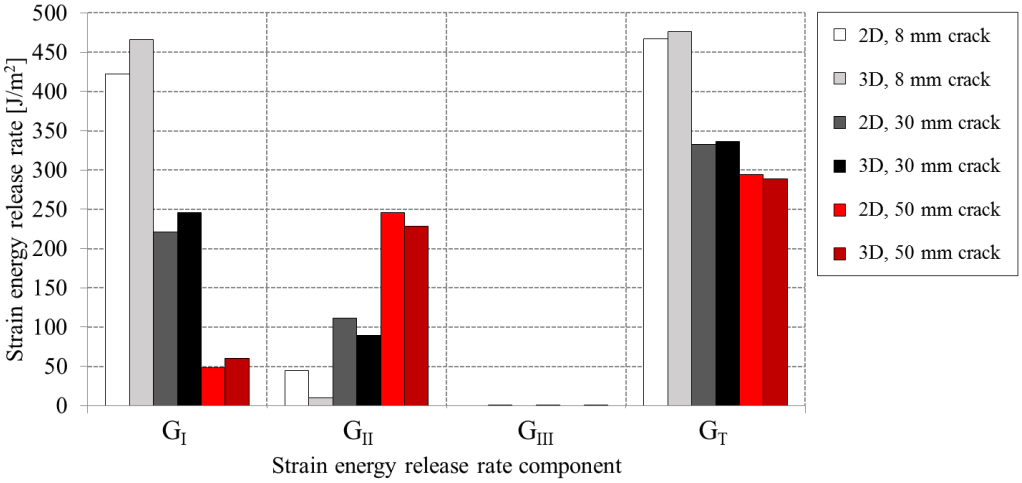


***Figure 6.13:*** *Differences of two- and three-dimensional strain energy release rate components and total values.*

### 6.2.3 Rotational inertia effect

Figure 6.14 shows the effect of rotational inertia to the strain energy release rate values with two edge cracks and by using two-dimensional and three-dimensional models with the chamfered edge geometry. Two- and three-dimensional simulations show that increasing angular velocity also increases the edge crack total strain energy release rate values. However, the rotational inertia effect is greater with a longer crack. Corresponding analysis was performed also with a 200 mm long internal crack, which showed that total SERR values even with high angular velocities were negligible. The increase in the total SERR value is insignificant in the typical roll structure rotation speed of 31–63 radians per second (300–600 RPM) with both edge and internal cracks.

Mode mixity obtained with the axisymmetric model as a function of angular velocity is presented in Figure 6.15. With the longer crack mode I comes more dominant when the angular velocity is increased. The direction of the centripetal force is outwards from the rotation axis, and thus it tends to open the crack tip, increasing mode I dominance. With the shorter crack this effect is negligible, as the loading is already governed by mode I.

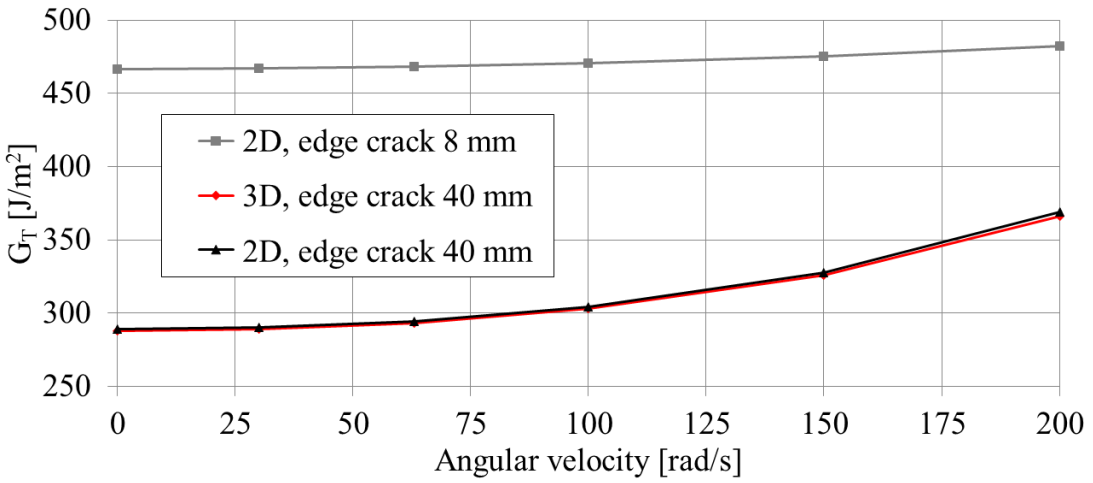


***Figure 6.14:*** *Effect of rotational inertia to total SERR values with 8 mm and 40 mm edge cracks and chamfered edge geometry using two-dimensional and three-dimensional models.*

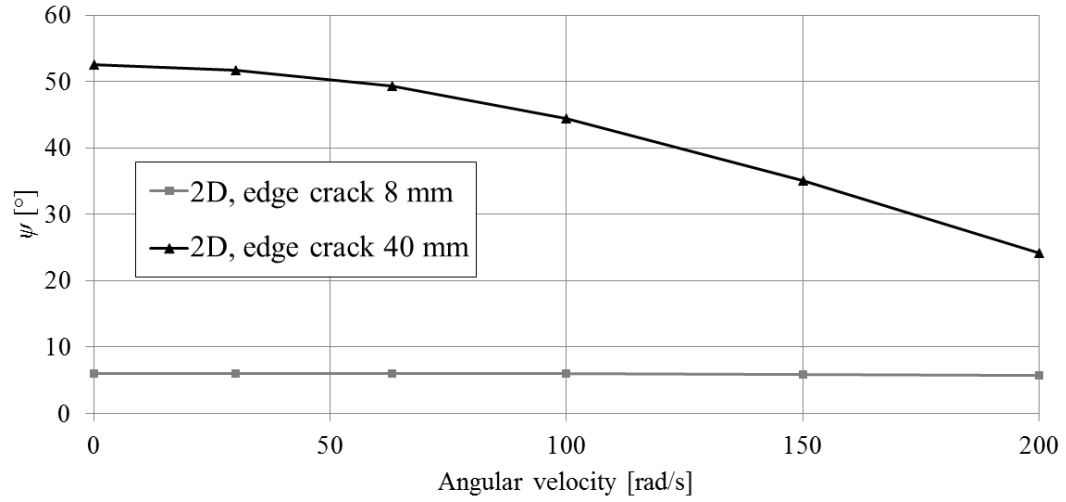


***Figure 6.15:*** *Angular velocity effect to mode mixity $\psi$. As angular velocity increases, mode I (crack tip opening) becomes more dominating with the longer crack due to the opening centripetal force.*

### 6.2.4 CTE sensitivity

Figure 6.16 shows the effect of different top and bottom layer CTE values to the total strain energy release rate values and the individual components, when the two-dimensional model with 8 mm and 40 mm edge cracks and chamfered edge geometry is used. Changing CTE values greatly affects the SERR values: For example, when the CTE of both layers is increased to 150% of original value, total strain energy release rate value triples with both crack lengths. Respectively, when CTE values are decreased to 50% of original value, total SERR is only one sixth of

the original value with longer crack and one tenth with shorther crack. Residual stress components were found to change linearly with surface layer CTE values, but effect to SERR values is stronger.

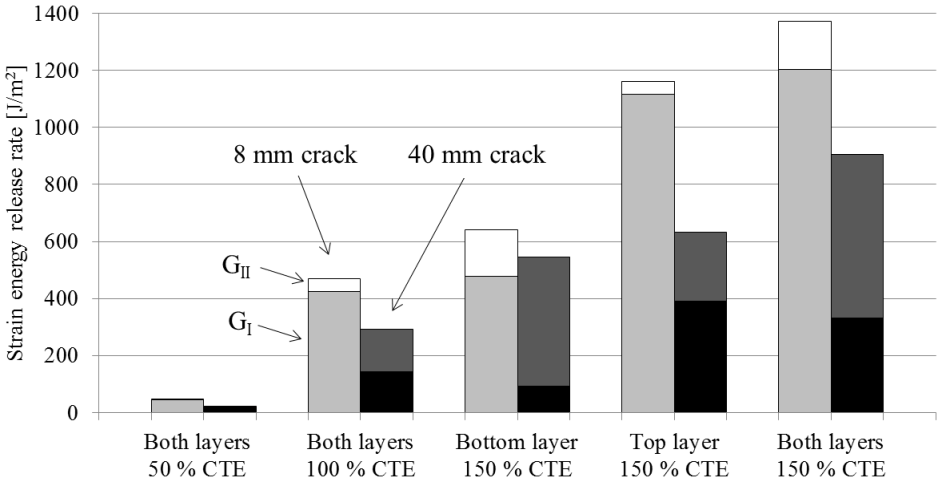


***Figure 6.16:*** *Effect of bottom and top layer coefficient of thermal expansion to strain energy release rate values with 8 mm and 40 mm edge cracks and chamfered edge geometry.*

Figure 6.16 also shows how the ratio of the individual SERR components changes in different cases. When the bottom layer CTE value is changed, proportional mode II loading increases, whereas when increasing the top layer CTE value proportional mode I loading becomes larger. When a single layer CTE value is increased, the corresponding layer tries to contract more than previously. As the bottom layer is bonded to the cylinder, this contraction is mode II loading. When the top layer contracts, it induces bending to the bottom layer which in the crack tip acts as an opening mode I loading. Figure 6.17 shows schematically this behaviour.

### 6.2.5 Nip effect

Figure 6.18 shows the contact pressure distribution along the roll structure contact surface with different pressures affecting to the nip roll. Pressure distributions were approximately similar with both 8 mm and 40 mm edge cracks. Contact pressure with nip was assumed to be 1.8-3.5 MPa [58], which is produced with case III loading. Thus, case III loading was used in the following analyses. Figure 6.18 also shows how a contact pressure peak exists in the coating edge area (when $\zeta/L$ is close to zero), as the nip surface first presses against the opened surface layers before contact is formed to the whole cylinder length.

The strain energy release rate total values are presented in Figure 6.19. Values are presented around one quarter of the three-dimensional cylinder circumference of the roll structure with 8 mm and 40 mm edge cracks. $G_T$ due to residual stresses and rotational inertia (600 RPM) is marked with red lines and after adding nip

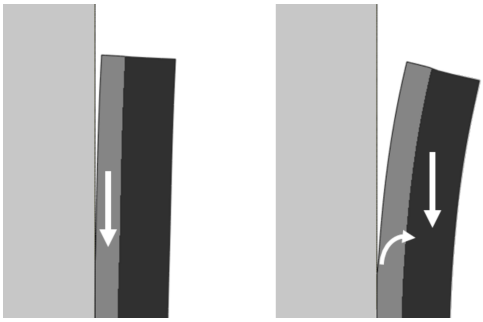

***Figure 6.17:*** *Different crack loading behaviour when changing bottom or top layer CTE values. After bottom layer CTE value is increased the layer contracts more and surface layers bend only slightly (shown on left). After top layer CTE value is increased the layer contracts more and due to this also bottom layer bends more (shown on right), icreasing mode II loading in the crack tip.*

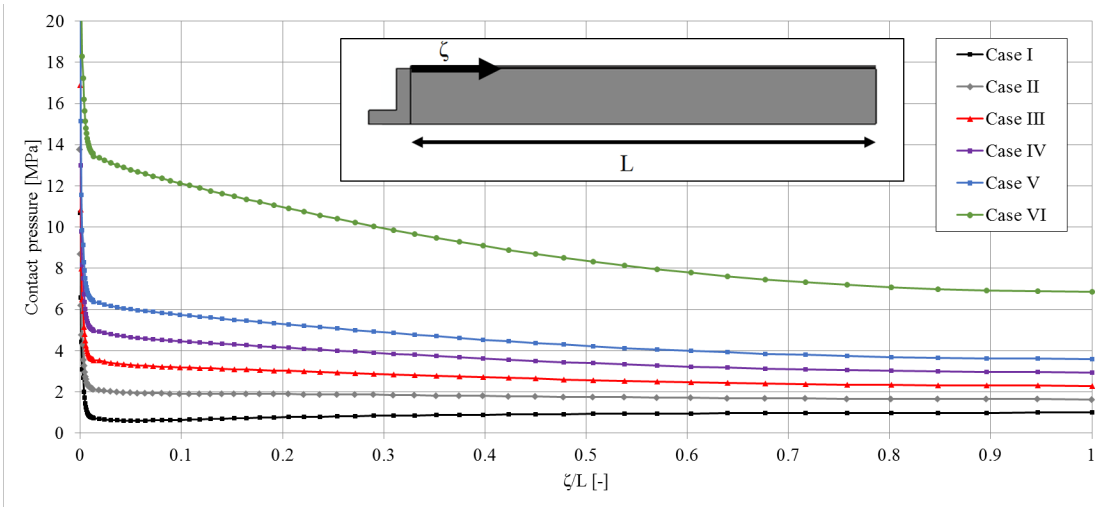


***Figure 6.18:*** *Contact pressure distributions along the contact line with the different nip roll pushing pressure cases.*

effect with black lines. SERR values due to residual stresses and rotational inertia are approximately constant through the circumference, but after the nip effect the values change near the contact area. With the longer crack the total SERR value increases from value 286 J/m$^2$ to value 317 J/m$^2$ in the contact area, but sharply decreases before leveling back to the original value when moved away from the contact area. With the shorther crack total SERR value decreases from value 478 J/m$^2$ to value 439 J/m$^2$ and then levels back to the original value. Figure 6.20 presents the behaviour of individual strain energy release rate components with nip effect. The nip roll presses the open coating edge back to a closed position, decreasing the mode I SERR value at the contact area with both crack lengths. However, with the longer crack length this effect is significantly stronger. With the shorter crack there is no notable difference in mode II component, but with

the longer crack mode II value increases at the contact area. Mode III components stay negligible small in all cases. Nip effect increases total strain energy values with the shorter edge crack in the studied case by 11% in the contact area. However, as typical $G_C$ values for pure mode II loading are significantly larger than in mixed mode loading cases, nip effect does not increase the criticality of the crack tip loading level. With the shorther crack $G_T$ decreases by 8%, and again the nip effect does not increase the crack tip loading criticality.

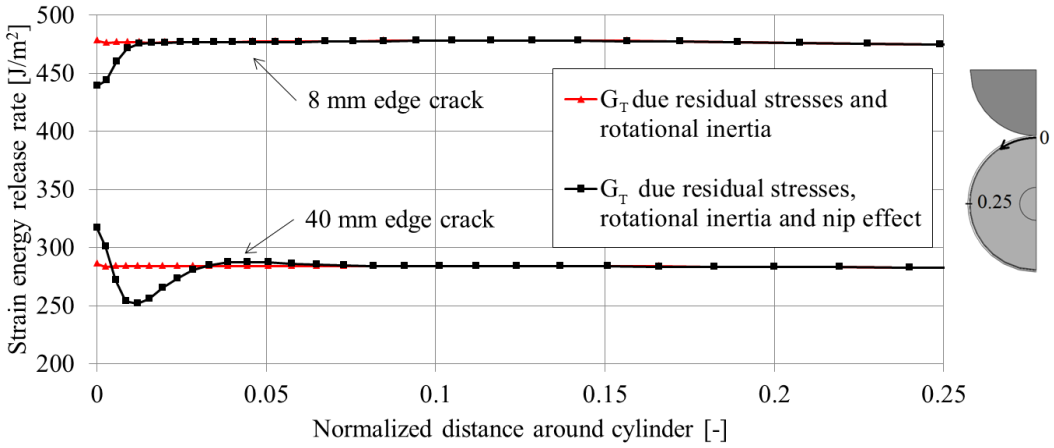


***Figure 6.19:*** *Nip effect with 8 mm and 40 mm edge cracks. Red lines describe SERR values due to residual stresses and rotational inertia and black lines after adding the nip roll effect.*

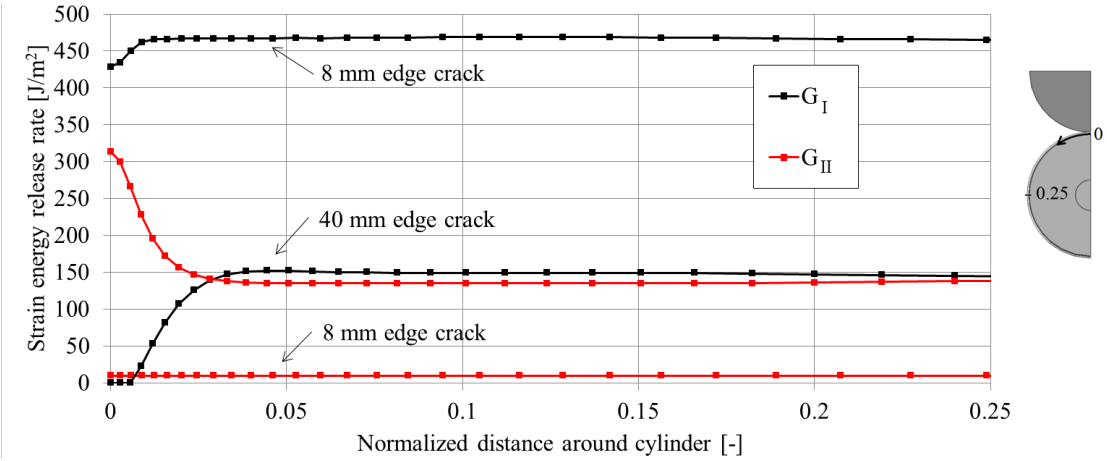


***Figure 6.20:*** *Strain energy release rate components $G_I$ and $G_{II}$ with 8 mm and 40 mm edge cracks due to residual stresses, rotational inertia and nip effect. $G_{III}$ values are negligible with both crack lengths.*

For an internal 200 mm crack the strain energy release rate total value and individual components after nip effect were also studied. Values due to residual stresses and inertial effect are negligible and nip roll contact did not significantly increase the total strain energy release rate value.

# 7 Conclusions

The aim of this thesis was to analyse the residual stress state and its criticality in a steel cylinder coated with composite surface layers. The literature study of the thesis presented the three main categories of residual stresses in polymer composites: thermal residual stresses, hygroscopic residual stresses and curing residual stresses. Based on the literature, especially thermal residual stresses are important when considering the total residual stress state after the manufacturing process of cylindrical composites bonded to another material.

In general, simulations of the residual stress formation can be divided according to the constitutive model used for the polymer material (elastic or viscoelastic model) or according to the scope of the simulation. Typical scope is the whole cure process including also curing residual stresses or only the cool-down phase including only thermal residual stresses. Linear elastic material models are typically used with a cool-down phase analysis and viscoelastic models for the whole cure cycle. Linear elastic simulation of the cool-down phase alone gave higher residual stress values than viscoelastic simulation of the cool-down phase alone or the full cure process for all cases found from the existing literature. Stress-relaxation due to the resin viscoelastic behaviour and resin curing shrinkage during the cure process counteracted the thermal residual stress formation in the reviewed cases. The final residual stress difference between the viscoelastic simulations for the whole cure cycle and linear elastic simulations of the cool-down alone varied between 8.6–110%. However, in most of the cases the difference was under 40%. The linear elastic simulation of the cool-down phase alone may be used to obtain an approximate of the residual stress state.

In this study, the obtained global residual stress components in the coated roll structure surface layers were not found to be critical. The mismatch between the surface layer and cylinder CTE values affected the emerging residual stress state. The cylinder and the bottom surface layer bond line shear stress was found to be close to the critical values for a straight and chamfered edge geometry, whereas clearly less critical value was obtained for a curved edge geometry. Thus, rounding should be used in the surface layer edge to reduce the shear stress in the bond near the coating edge.

The total strain energy release rate value between the cylinder and bottom surface layer reached the critical level for each studied edge geometry with specific edge crack lengths. The strain energy release rate values for an internal crack were negligible. Thus, edge cracks are more critical than internal cracks in the roll structure and an initial crack has potential to grow along the bond line. Rotational inertia with typical roll structure angular velocities did not significantly increase the crack tip strain energy release rate values, but the surface layer CTE value effect was substantial. CTE values of the surface layers should be tailored closer

to the cylinder CTE if both the residual stress state and strain energy release rate values with a cracked bond are to be reduced. A static nip effect was found to increase the total strain energy release rate values at the nip contact area with a 40 mm crack and to decrease the values with an 8 mm crack. Even though the total value is increased with the longer crack, mode mixity is simultaneously changed to pure mode II loading. Thus, the criticality of the crack tip loading level might not be increased due to the nip effect.

In order to assess the roll structure residual stress state more accurately, simulations for the whole cure process using viscoelastic constitutive models could be performed. However, extensive material characterisation (epoxy curing model, viscoelastic constitutive model, material property models) is essential for creating a solid base for these simulations. The linear elastic simulations could also be made more accurate by using temperature-dependant Young's modulus and coefficients of thermal expansion. Furthermore, the nip effect simulation models could be improved by including dynamic effects and paper and felt materials between the rolls. For future work, experimental studies could be performed to validate the obtained residual stress values and to gain more information about the residual stress formation process in the roll structure. In addition, the critical values of shear stress and strain energy release rate for the investigated materials could be determined experimentally.

# References


[1] Y. Yu, I.A. Ashcroft, and G. Swallowe. An experimental investigation of residual stresses in an epoxy-steel laminate. *International Journal of Adhesion and Adhesives*, 26(7):511–519, 2006.

[2] P.P. Parlevliet, H.E.N. Bersee, and A. Beukers. Residual stresses in thermoplastic composites - A study of the literature - Part I: Formation of residual stresses. *Composites Part A: Applied Science and Manufacturing*, 37(11): 1847–1857, 2006.

[3] J.A. Nairn and P. Zoller. Matrix solidification and the resulting residual thermal stresses in composites. *Journal of Materials Science*, 20(1):355–367, 1985.

[4] J.A. Barnes and G.E. Byerly. The formation of residual stresses in laminated thermoplastic composites. *Composites Science and Technology*, 51(4):479–494, 1994.

[5] J.-K. Kim and Y.-W. Mai. *Engineered interfaces in fiber reinforced composites*. Elsevier, 1998. ISBN 9780080426952.

[6] M.M. Shokrieh, editor. *Residual Stresses in Composite Materials*. Woodhead Publishing, 2014. ISBN 9780857092700.

[7] J.P. Favre. Residual thermal stresses in fibre reinforced composite materials - a review. *J Mech Behavior Mater*, 1(1-4):37–53, 1988.

[8] A. A. Johnston. *An integrated model of the development of process-induced deformation in autoclave processing of composite structures*. PhD thesis, The University of British Columbia, 1997.

[9] H.C. Park, N.S. Goo, K.J. Min, and K.J. Yoon. Three-dimensional cure simulation of composite structures by the finite element method. *Composite Structures*, 62(1):51–57, 2003.

[10] N. Rabearison, Ch. Jochum, and J.C. Grandidier. A FEM coupling model for properties prediction during the curing of an epoxy matrix. *Computational Materials Science*, 45(3):715–724, 2009.

[11] Ciba Polymers. Data sheet: Araldite LY5052 / Hardener HY5052, 1994.

[12] D. Hull and T. W. Clyne. *An introduction to composite materials*. Cambridge, 1996. ISBN 9780521388559.

[13] J.M. Svanberg and J.A. Holmberg. Prediction of shape distortions. Part II. Experimental validation and analysis of boundary conditions. *Composites Part A: Applied Science and Manufacturing*, 35(6):723–734, 2004.

[14] F.S. Jumbo, I.A. Ashcroft, A.D. Crocombe, and M.M Abdel Wahab. Thermal residual stress analysis of epoxy bi-material laminates and bonded joints. *International Journal of Adhesion and Adhesives*, 30(7):523 – 538, 2010.

[15] L. H. Sperling. *Introduction to Physical Polymer Science, 4th Edition.* John Wiley and Sons, 2005. ISBN 9780471706069.

[16] B. Tavakol, P. Roozbehjavan, A. Ahmed, R. Das, R. Joven, H. Koushyar, A. Rodriguez, and B. Minaie. Prediction of residual stresses and distortion in carbon fiber-epoxy composite parts due to curing process using finite element analysis. *Journal of Applied Polymer Science*, 128(2):941–950, 2013.

[17] D.U. Shah and P.J. Schubel. Evaluation of cure shrinkage measurement techniques for thermosetting resins. *Polymer Testing*, 29(6):629–639, 2010.

[18] T. Garstka, N. Ersoy, K.D. Potter, and M.R. Wisnom. In situ measurements of through-the-thickness strains during processing of AS4/8552 composite. *Composites Part A: Applied Science and Manufacturing*, 38(12):2517–2526, 2007.

[19] Lars A. Berglund and Jose M. Kenny. Processing science for high performance thermoset composites. *SAMPE Journal*, 27(2):27–37, 1991.

[20] D.A. Tilbrook, G.J. Pearson, M. Braden, and P.V. Coveney. Prediction of polymerization shrinkage using molecular modeling. *Journal of Polymer Science, Part B: Polymer Physics*, 41(5):528–548, 2003.

[21] Roger N. Rothon. *Particulate-Filled Polymer Composites (2nd Edition).* Smithers Rapra Technology, 2003. ISBN 9781859573822.

[22] C. Li, K. Potter, M.R. Wisnom, and G. Stringer. In-situ measurement of chemical shrinkage of MY750 epoxy resin by a novel gravimetric method. *Composites Science and Technology*, 64(1):55–64, 2004.

[23] C. Heinrich, M. Aldridge, A.S. Wineman, J. Kieffer, A.M. Waas, and K.W. Shahwan. Generation of heat and stress during the cure of polymers used in fiber composites. *International Journal of Engineering Science*, 53:85–111, 2012.

[24] W. Il Lee, A. C. Loos, and G. S. Springer. Heat of reaction, degree of cure, and viscosity of Hercules 3501-6 resin. *Journal of Composite Materials*, 16 (6):510–520, 1982.

[25] N. Rabearison, C. Jochum, and J.C. Grandidier. A cure kinetics, diffusion controlled and temperature dependent, identification of the Araldite LY556 epoxy. *Journal of Materials Science*, 46(3):787–796, 2011.

[26] M. Nishikawa, M. Hojo, and S. Goto. Finite element simulation of curing and adhesion process of epoxy resin to carbon fiber. In *Proceedings of Interface 21 - The International Conference on Composite Interfaces*, 2012.

[27] Ch. Jochum, J.C. Grandidier, and M. Smaali. Proposal for a long-fibre microbuckling scenario during the cure of a thermosetting matrix. *Composites Part A: Applied Science and Manufacturing*, 39(1):19–28, 2008.

[28] H.-B. Wang, Y.-G. Yang, H.-H. Yu, W.-M. Sun, Y.-H. Zhang, and H.-W. Zhou. Assessment of residual stresses during cure and cooling of epoxy resins. *Polymer Engineering and Science*, 35(23):1895–1898, 1995.

[29] Q. Zhu, P.H. Geubelle, M. Li, and C.L. Tucker III. Dimensional accuracy of thermoset composites: Simulation of process-induced residual stresses. *Journal of Composite Materials*, 35(24):2171–2205, 2001.

[30] J.-A. E. Manson and J. C. Seferis. Process simulated laminate (PSL). A methodology to internal stress characterization in advanced composite materials. *Journal of Composite Materials*, 26(3):405–431, 1992.

[31] T.J. Chapman, J.W. Gillespie, R.B. Pipes, J.-A.E. Manson, and J.C. Seferis. Prediction of process-induced residual stresses in thermoplastic composites. *Journal of Composite Materials*, 24(6):616–643, 1990.

[32] M.E. Adams, G.A. Campbell, and A. Cohen. Thermal-stress induced damage in a thermoplastic matrix material for advanced composites. *Polym Eng Sci*, 31(18):1337–1343, 1991.

[33] N. Ersoy, K. Potter, M. R. Wisnom, and M. J. Clegg. An experimental method to study the frictional processes during composites manufacturing. *Composites Part A: Applied Science and Manufacturing*, 36(11):1536 – 1544, 2005.

[34] J.M. Svanberg and J.A. Holmberg. Prediction of shape distortions Part I. FE-implementation of a path dependent constitutive model. *Composites Part A: Applied Science and Manufacturing*, 35(6):711–721, 2004.

[35] N. Zobeiry, R. Vaziri, and A. Poursartip. Computationally efficient pseudo-viscoelastic models for evaluation of residual stresses in thermoset polymer composites during cure. *Composites Part A: Applied Science and Manufacturing*, 41(2):247–256, 2010.

[36] S.R. White and Y. Kim. Process-induced residual stress analysis of AS4/3501-6 composite material. *Mechanics of Composite Materials and Structures*, 5 (2):153–186, 1998.

[37] Y.K. Kim and S.R. White. Cure-dependent viscoelastic residual stress analysis of filament-wound composite cylinders. *Mechanics of Composite Materials and Structures*, 5(4):327–354, 1998.

[38] H.Y. Hwang, Y.K. Kim, C. Kim, Y.-D. Kwon, and W. Choi. Thermo-viscoelastic residual stress analysis of metal liner-inserted composite cylinders. *KSME International Journal*, 17(2):171–180, 2003.

[39] N. Zobeiry, R. Vaziri, and A. Poursartip. Differential implementation of the viscoelastic response of a curing thermoset matrix for composites processing. *Journal of Engineering Materials and Technology, Transactions of the ASME*, 128(1):90–95, 2006.

[40] R.S. Lakes. *Viscoelastic Solids*. CRC Press, 1999. ISBN 9780849396588.

[41] J.D. Ferry. *Viscoelastic properties of polymers*. John Wiley and Sons, 1980. ISBN 9780471048947.

[42] R.A. Schapery. Viscoelastic behavior and analysis of composite materials. In G.P. Sendeckyj, editor, *Mechanics of Composite Materials*, volume 2 of *Composite Materials*, pages 85–168. Academic Press, 1974. ISBN 9780121365028.

[43] Y.K. Kim and S.R. White. Stress relaxation behavior of 3501-6 epoxy resin during cure. *Polymer Engineering and Science*, 36(23):2852–2862, 1996.

[44] N. Ersoy, T. Garstka, K. Potter, M.R. Wisnom, D. Porter, and G. Stringer. Modelling of the spring-in phenomenon in curved parts made of a thermosetting composite. *Composites Part A: Applied Science and Manufacturing*, 41 (3):410–418, 2010.

[45] M.-L. Sham and J.-K. Kim. Evolution of residual stresses in modified epoxy resins for electronic packaging applications. *Composites Part A: Applied Science and Manufacturing*, 35(5):537–546, 2004.

[46] H. Wang, J. Feng, Z. Guo, H. Hu, and J. Zhang. Influence of physical parameters on residual stresses of polymer composites during the cure process. In *Proceedings of SPIE - The International Society for Optical Engineering*, volume 8409, 2012.

[47] E. Ruiz and F. Trochu. Multi-criteria thermal optimization in liquid composite molding to reduce processing stresses and cycle time. *Composites Part A: Applied Science and Manufacturing*, 37(6 SPEC. ISS.):913–924, 2006.

[48] M.Y. Tsai and J. Morton. The stresses in a thermally loaded bimaterial interface. *International Journal of Solids and Structures*, 28(8):1053–1075, 1991.

[49] M.Y. Tsai and J. Morton. A stress analysis of a thermally loaded bimaterial interface: A localized hybrid analysis. *Mechanics of Materials*, 13(2):117–130, 1992.

[50] ASTM International. ASTM A36 A36M-12: Standard Specification for Carbon Structural Steel, 2012.

[51] H. Kettunen. Personal communication, August 25th 2014.

[52] Fran Cverna, editor. *ASM Ready Reference: Thermal Properties of Metals*. ASM International, 2002. ISBN 9780871707680.

[53] Dassault Systèmes. *Abaqus Documentation, version 6.13-3*, 2013.

[54] Claas Guss. Technical information - Grey lamellar graphite cast iron, 2006. Available: `http://www.claasguss.de/html_e/pdf/THBl1_engl.pdf`. Visited on 8.8.2014.

[55] Pierre J. Krueger, Ronald & Minguet. Skin-stiffener debond prediction based on computational fracture analysis. Technical report, Nasa, 2005.

[56] P. P. Camanho, C. G. Davila, and de Moura M. F. Numerical simulation of mixed-mode progressive delamination in composite materials. *Journal of Composite Materials*, 37(16):1415–1438, 2003.

[57] O. Saarela, I. Airasmaa, J. Kokko, M. Skrifvars, and V. Komppa. *Komposiittirakenteet*. Muoviyhdistys ry, 2007. ISBN 9789519271286.

[58] T. Hakala and A. Harlin. Simulation of a rapid nip pressure strike and its effect on press felt samples. *Autex Research Journal*, 8(3):84–91, 2008.

[59] A.B. Pereira and A.B. de Morais. Strength of adhesively bonded stainless steel joints. *International Journal of Adhesion and Adhesives*, 23(4):315 – 322, 2003. ISSN 0143-7496.

[60] M. Bordes, P. Davies, J.-Y. Cognard, L. Sohier, V. Sauvant-Moynot, and J. Galy. Prediction of long term strength of adhesively bonded steel/epoxy joints in sea water. *International Journal of Adhesion and Adhesives*, 29(6): 595 – 608, 2009. ISSN 0143-7496.

[61] X. J. Gong, F. Hernandez, and G. Verchery. Fracture toughness of adhesive bonded composite joints under mixed mode loading. In *Proceedings of ICCM12*, 1999.

# A Notes about simulation models

This appendix presents details about the used simulation models and special notes related to the simulation model creation.

## Simulation model presentation

Table A.1 presents an overview of the global residual stress simulation models including number of elements, element types, total number of unknown variables and relative calculation times. Solid elements used in the three-dimensional models are 8-node linear brick elements with reduced integration and hourglass control (Abaqus type C3D8R) and 6-node linear triangular prism elements (C3D6). Axisymmetric solid 4-node bilinear elements with reduced integration and hourglass control (CAX4R) are used in the axisymmetric model. [53] Figure A.1 presents these elements and in additon a 3-node linear element (CAX3), which is used in edge geometry simulation models.

***Table A.1:*** *Global residual simulation model details.*

| Model | Number of elements | Element types | Number of variables | Calculation time [%] |
|---|---|---|---|---|
| Full model | 77 920 | C3D8R (71120)<br>C3D6 (6800) | 269 838 | 100% |
| 1/8 model | 82 684 | C3D8R (79 909)<br>C3D6 (2775) | 285 912 | 65.8% |
| Axisymmetric model | 53 055 | CAX4R | 126 944 | 17.5% |

Mesh refinement study was performed with the axisymmetric model to make sure that the used amount of elements does not affect the calculated global residual stresses. Figure A.2 presents longitudinal stresses for different roll structure parts with models consisting of different amount of elements. Stress levels stay constant when element number exceeds 500, indicating that the number of elements used in the simulation models is adequate.

Table A.2 presents an overview of the three edge geometry simulation models used to study the cylinder and bottom surface layer bond shear stresses, strain energy release rate values with and without the inertia effect. Models consist mainly on 4-node bilinear elements with reduced integration and hourglass control (CAX4R).

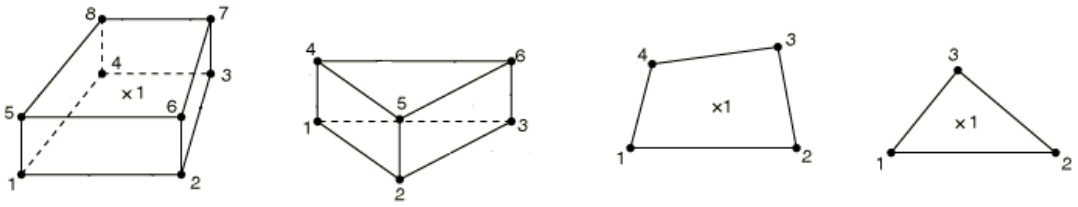


***Figure A.1:*** *Elements in three-dimensional and axisymmetric simulation models. From left to right: 8-node linear brick element with reduced integration and hourglass control (C3D8R), 6-node linear triangular prism element (C3D6), 4-node bilinear element with reduced integration and hourglass control (CAX4R) and 3-node linear element (CAX3). [53]*

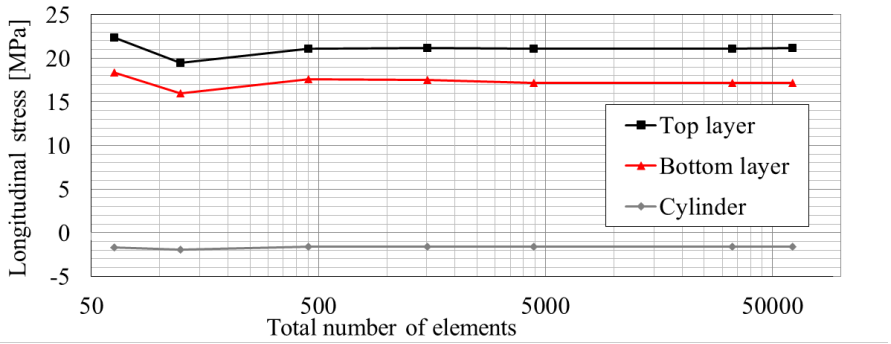


***Figure A.2:*** *Mesh refinement study results for longitudinal global residual stress component with axismmetric model using different number of elements.*

***Table A.2:*** *Edge geometry simulation model parameters.*

| Model | Number of elements | Element types | Number of variables |
|---|---|---|---|
| Straight edge | 68 261 | CAX4R (66 924)<br>CAX3 (1337) | 140 088 |
| Chamfered edge | 72 034 | CAX4R (70 689)<br>CAX3 (1345) | 147 628 |
| Curved edge | 78 689 | CAX4R (76 981)<br>CAX3 (1708) | 162 480 |

Table A.3 presents details about the three-dimensional chamfered-edge simulation model used to compare strain energy release rate values of two- and three dimensional models and the nip effect model. Same type of continuum elements as with global residual stress models are used in these models.

***Table A.3:*** *Three-dimensional chamfered edge and nip effect simulation model parameters.*

| Model | Number of elements | Element types | Number of variables |
|---|---|---|---|
| 3D chamfered edge | 61 960 | C3D8R (58 480)<br>C3D6 (3480) | 222 648 |
| 3D nip effect | 75 964 | C3D8R (63 490)<br>C3D6 (4045) | 263 376 |

# Special notes on model creation in Abaqus 6.13-3

Material orientation is defined in the Property-module. By using *user-defined discrete* method surface layer normal direction can be defined as the material normal direction and surface layer circumferential direction as the material primary axis direction in three-dimensional models. Material property values are then defined with *engineering constants*. In the axisymmetric model material directions cannot be defined freely: the out-of-plane direction in axisymmetric models is always material normal axis direction. Due to this, material normal and circumferential directions change places. Material property values are again defined with *engineering constants*, but special interest is to be directed to the correct material directions.

Composite surface layers are created as separate parts so that inconsistent meshes can be used in the cylinder and surface layers. This allows to use more refined mesh in the thin surface layers where changes in stress values are important. *Tie constraint* (created in the Interaction-module) is used to tie the surface layers and cylinder together. *Tie constraint* rules, that the displacements of slave surface nodes are equal to the displacements of master surface nodes. Now, between cylinder and bottom layer, cylinder surface was defined as master layer and between top and bottom layer the bottom layer outer surface was defined as the master surface.

The temperature change is defined using *predefined field* (created in the Load-module) and modifying this value in following analysis steps. Material expansion coefficients need to be defined. Inertial load is defined also in the Load-module by creating *rotational body force*. Material densities, angular velocity and rotation axis need to be defined.

Virtual crack closure technique is supported in version 6.13-3 of Abaqus CAE. Three parameters need to be defined in the Interaction-module to use VCCT in simulations:

1. An interaction for crack surfaces. The crack surfaces are defined by assigning contact interaction between them. The length of the initial crack is defined under *bonding* option, where the initially bonded nodes are defined as a

node-set. Nodes outside this set, but existing on crack surface, form the initial crack.

2. A crack. A new crack of type *debond using VCCT* need to be created. The initiation step of the crack and the created interaction for crack surfaces are selected.

3. A fracture criterion. Fracture criterion defines when the crack propagates (crack tip nodes are unbonded). Different mixed mode equations connecting individual SERR components as a total value can be chosen and critical values for individual SERR components can be defined. Now, very large critical SERR values are used to make sure that crack will not propagate in the performed simulations. When defining VCCT in Abaqus CAE, direction parameter for VCCT crack growth needs to be defined, even though this parameter is applicable only for enriched regions and not actually used in the simulations.